INFORMATION TO USERS

This manuscript has been reproduced from the microfilm master. UMI films the text directly from the original or copy submitted. Thus, some thesis and dissertation copies are in typewriter face, while others may be from any type of computer printer.

The quality of this reproduction is dependent upon the quality of the copy submitted. Broken or indistinct print, colored or poor quality illustrations and photographs, print bleedthrough, substandard margins, and improper alignment can adversely affect reproduction.

In the unlikely event that the author did not send UMI a complete manuscript and there are missing pages, these will be noted. Also, if unauthorized copyright material had to be removed, a note will indicate the deletion.

Oversize materials (e.g., maps, drawings, charts) are reproduced by sectioning the original, beginning at the upper left-hand corner and continuing from left to right in equal sections with small overlaps.

Photographs included in the original manuscript have been reproduced xerographically in this copy. Higher quality 6" x 9" black and white photographic prints are available for any photographs or illustrations appearing in this copy for an additional charge. Contact UMI directly to order.

Bell & Howell Information and Learning
300 North Zeeb Road, Ann Arbor, MI 48106-1346 USA
800-521-0600

Université d'Ottawa · University of Ottawa

NONLINEAR ELEASTIC MODELING OF PIPELINE IN SLOPING CLAY UNDER HIGH K_o

by

Hicham J. Salem

A thesis

submitted under the supervision of

Dr. Vinod K. Garga

in partial fulfillment of the

requirements for the degree of

Master of Applied Science

in

Civil Engineering

Department of Civil Engineering

University of Ottawa

Ottawa, Ontario, Canada, K1N 6N5

September, 1998

This Thesis is dedicated to my wife, Julie Anne

and my parents, Nawal and Joseph

ACKNOWLEDGEMENTS

Special appreciation is expressed to Dr. Vinod K. Garga for his valuable advice and assistance.

The author would also like to thank Dr. John Krahn and Ms. Carola Preusser of Geo-Slope International for providing the software and support.

Deep appreciation is felt for my wife, Julie Anne, for her continued support throughout this project. Many thanks to my sister Lena for her assistance.

Special thoughts for my mother, Nawal, and my late father Joseph, who kept our education as a first priority over the years.

ABSTRACT

Numerous cases of pipeline failures are documented every year, triggering new problems for research and the need for re-examination of already established design guidelines and standards. The problem of soil/pipeline interaction has been thoroughly researched over the years; however, further investigation is required in some areas.

This thesis presents an investigation, using numerical modeling to simulate the installation of a steel pipeline in overconsolidated clay. Some factors related to the site geometry (sloping ground) and construction methods (fill compaction), as well as the stiffness of the pipeline section, are also investigated.

This study shows that the reaction of the soil mass to the trench excavation continued for as long as four years after backfilling. In addition, the following conclusions can be drawn from the results presented in this thesis:

- When the pipeline is installed in a trench, at the base of a v-shaped depression, a higher total stress acts at the base and crown of the pipeline with level ground and smaller ground slopes causing more deformation in the pipeline section than with steep ground slopes

- A static, surcharge-type compaction for a reasonable duration is found to reduce damaging stresses at the base and crown of the pipeline, during and after surcharge loading

- A less rigid pipeline section would carry less of the weight of overlying fill material and will cause more of the load to be carried by the fill material on either side of the pipeline. This results in higher lateral pressure on the pipeline section and slower dissipation of pore water pressure around the pipeline.

TABLE OF CONTENTS

Section **Page**

TABLE OF CONTENTS (Continued)

Section **Page**

TABLE OF CONTENTS (Continued)

Section **Page**

LIST OF TABLES

Table **Page**

LIST OF FIGURES

Figure **Page**

LIST OF FIGURES (Continued)

Figure **Page**

LIST OF FIGURES (Continued)

Figure **Page**

LIST OF FIGURES (Continued)

Figure **Page**

LIST OF FIGURES (Continued)

Figure **Page**

CHAPTER 1

INTRODUCTION

CHAPTER 1

INTRODUCTION

1.1. BACKGROUND

In the future, as the move is made into new frontiers to exploit natural resources, the use of pipeline networks will continue to play an increasingly significant role as a viable mode of transport. Presently, it is the most efficient mode of inland oil and gas transportation between remote sources and the ports of distribution and shipping. To illustrate the magnitude of Canada's pipeline infrastructure, the amount of oil currently transported daily from Calgary to Toronto by the nation's pipeline system is equivalent to over 39,000 trailer truck loads.

Despite being one of the most economical ways of energy transport, the initial cost of building pipeline networks is very high. Millions of kilometers of pipelines, vital to the North American economy are currently aging underground. In 1978, there were an estimated 1.6 million kilometers of pipeline for crude oil alone in the US, which were reported to have cost over $650,000 US per kilometer (Paulin, 1998).

Pipelines are laid across vast terrain, with diverse geology and landscape profiles along their paths. This reality made pipeline construction one of the most researched topics in the history of geotechnical engineering. There are still, however, many areas which require further investigation. Pipeline failures are constantly reported in the literature (Cowherd & Corda, 1994; Heger & Selig, 1994; Seed & Raines, 1988, etc...), many of them during or immediately after construction. This shows that more effort is needed to better understand the mechanisms involved in soil/pipeline interaction.

In today's cash-strained economy, it is necessary to eliminate the staggering cost of pipeline failures due to unexpected interaction behavior or even the unnecessary cost of overdesigned pipelines due to the unknown elements of soil/pipeline interaction. There is an imminent need for proper evaluation of the current construction methods under different site conditions to avoid both, pipeline failures and the tremendous cost of pipeline repair and replacement.

1.2. STATEMENT OF THE PROBLEM

Numerous cases of pipeline failures are documented every year, triggering new problems for research and the need for re-examination of already established design guidelines and standards. The problem of soil/pipeline interaction has been thoroughly researched over the years; however, further investigation is required in some areas.

When installing pipelines in overconsolidated clay zones, significant horizontal stresses, locked in the soil mass, are released upon trench excavation. This unloading effect is observed as movements and deformations in the vicinity of the trench following the excavation. The reaction of the soil mass, further away from the trench, may not be noticeable over a short time period; however, its long-term effect on the buried pipeline may be critical. Some factors related to the site geometry (sloping ground) and construction methods (fill compaction) may have a direct bearing on the unloading effect, and should be addressed as well.

Most of the research involving buried conduits, considered the stress-deformation relationships of embankment or backfill soils to evaluate the stresses imposed on the conduit. Little was done, however, on investigating the long-lasting effect of disturbing the equilibrium in the native soil mass by excavating and backfilling.

It is practically impossible to cover all aspects of soil/pipeline interaction through laboratory or full-scale modeling due to high cost, technical difficulties associated with scaling, and time limitation, especially when modeling in soils with low hydraulic conductivity. Computer modeling with finite element methods can be used to simulate actual geotechnical problems and to predict long-term behavior of soil and structures.

1.3. OBJECTIVES OF THE RESEARCH

Research using finite element analysis applied to specific cases and aspects of soil/pipeline interaction can be found in the literature (see chapter 2). The main objective of this research is to develop a better understanding of the mechanics involved in soil/pipeline interaction in overconsolidated soils with low hydraulic conductivity. This interaction behavior is investigated from the time the soil mass, in equilibrium under high K_o conditions, is excavated, through several years after the excavation is backfilled.

Four aspects of soil/pipeline interaction are investigated in this research:

- The delayed effect on buried pipelines of trench excavation in London clay soils under high K_o conditions, long after installation
- The effect of sloping ground on pipelines installed in a v-shaped depression
- The effect of backfill compaction
- The effect of pipeline stiffness.

The complete construction sequence is modeled for accurate simulation of actual conditions: In-situ conditions followed by excavation then pipeline installation and backfilling.

It is not the objective of this research to study the characteristic behavior of overconsolidated London Clay. This specific soil is merely used for illustration while the main objective, as mentioned earlier, is to study the mechanics involved in pipeline installation under the various conditions mentioned above.

1.4. SCOPE OF RESEARCH

This research involves the modeling of a pipeline segment buried in a trench excavated in overconsolidated stiff clay such as London clay. The same clay soil is used to model the backfill material. Finite element analysis using the hyperbolic soil model is utilized to conduct the study.

The first step in the research scope is to determine the hyperbolic model parameters of London clay soil using laboratory test results by Som, 1968

A preliminary analysis using the fitted soil model is performed to simulate an excavation with different in-situ conditions and different boundary conditions. This analysis uses a simple finite element mesh to investigate the feasibility of the intended construction in London clay and the limitations on in-situ stresses and boundary conditions.

After the modeling limitations and boundary conditions are validated, a more elaborate finite element mesh is used to simulate a staged installation of a circular steel pipeline, 0.95 m diameter and 25 mm wall thickness, in V-shaped depressions with various sloping angles (0.0°, 5.7°, 11.3°, and 20° are investigated). The upper bound slope approaches the internal friction angle of

London clay. The simulated installation involves excavating a 2 m deep by 1.5 m wide trench, installing the pipeline, and backfilling, about 40 minutes after the excavation with the same clay material. The fill at this stage will be consolidating under its own weight only.

Once the effect of site geometry is determined, the analysis case with 20° slopes is repeated with three different compaction methods applied to the clay backfill. This is done to determine the effect of backfill compaction on the soil/pipeline interaction.

The case with 20° slopes is again repeated with different values of the pipeline's wall thickness. This is done to study the effect of pipeline stiffness and deformation on the interaction behavior.

1.5. LIMITATIONS OF THE HYPERBOLIC SOIL MODEL

The hyperbolic model is widely used in the industry because of its simplicity and convenience for most applications. There are however some limitations inherent in this model, as outlined below:

- The model is based on the generalized Hooke's law for isotropic behavior and does not have provisions for anisotropic, either inherent or stress induced, responses. In this study, however, the model parameters were determined from triaxial tests performed on horizontal and vertical samples. In the author's opinion, considering tests in both directions would minimize the error induced by anisotropy.

- Shear dilatancy is not modeled. It is also only capable of modeling the pre-peak response, whereas the strain-softening behavior is not represented.

- The parameters that are used to characterize the model in the equations are determined by fitting the model to triaxial test data, and if the loading path deviates greatly from that of triaxial compression, the strains predicted by the model may not be accurate. In this study, since tests on samples in both, the vertical and the horizontal directions are fitted, a more accurate modeling of extension problems can be expected. It is conceivable that the model can be fitted for triaxial extension conditions to further improve the accuracy; however, this was not within the scope of this research.

1.6. OUTLINE OF THE THESIS

The thesis is presented in eight chapters outlined as follows:

Ch 1 Introduction

Ch 2 Literature review

Ch 3 Finite element application, soil model, and parameters

Ch 4 Preliminary excavation analysis

Ch 5 Pipeline installation in v-shaped depression

Ch 6 Effect of compaction on soil/pipeline interaction

Ch 7 Effect of pipeline stiffness on soil/pipeline interaction

Ch 8 Conclusions and recommendations for further research

CHAPTER 2

LITERATURE REVIEW

CHAPTER 2

LITERATURE REVIEW

2.1. GENERAL

Pipelines and buried conduits have been some of the most researched topics in the history of Geotechnical Engineering. There are, however, many aspects of pipeline design and pipeline/soil interaction that are still candidates for further research to better understand the mechanics involved in buried conduits. Numerical methods were introduced recently to pipeline geotechniques and are still in the development stage. The use of conventional methods and theories, based on simplifications and assumptions, are still the norm in the industry. A selection of publications related to the subject of this research are briefly presented below. These publications relate to buried conduits and pipeline design and analysis using conventional analytical methods and numerical methods, as well as case histories of conduit failures and instrumented buried structures.

2.2. RELATED LITERATURE

MARSTON-SPANGLER THEORY

The Marston-Spangler theory is the most commonly used design method to determine earth loads on buried culverts and conduits. It was developed in Iowa State University by Marston, Shlick, and Spangler in 1920. The method is described in many references (Spangler 1951 and 1962) and it considers four different simplified classes of conduit installation as shown in Illustration 2.1 below. The method utilizes the equations of equilibrium for the prism of fill which is considered to be supported by the buried conduit, and the friction on either side with the adjacent soil prisms. Illustration 2.2 shows the free body diagram of the soil prism assumed in Marston-Spangler theory.

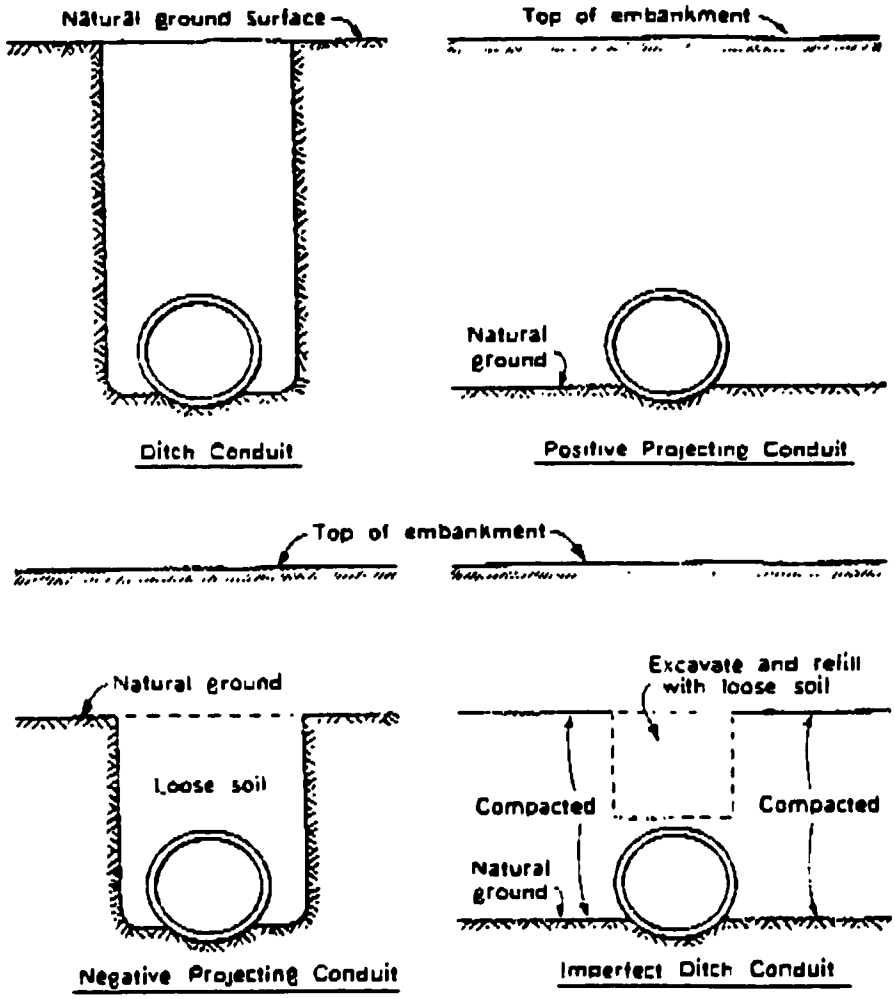

Illustration 2.1 Classes of conduit installation, Marston-Spangler theory (Spangler, 1962)

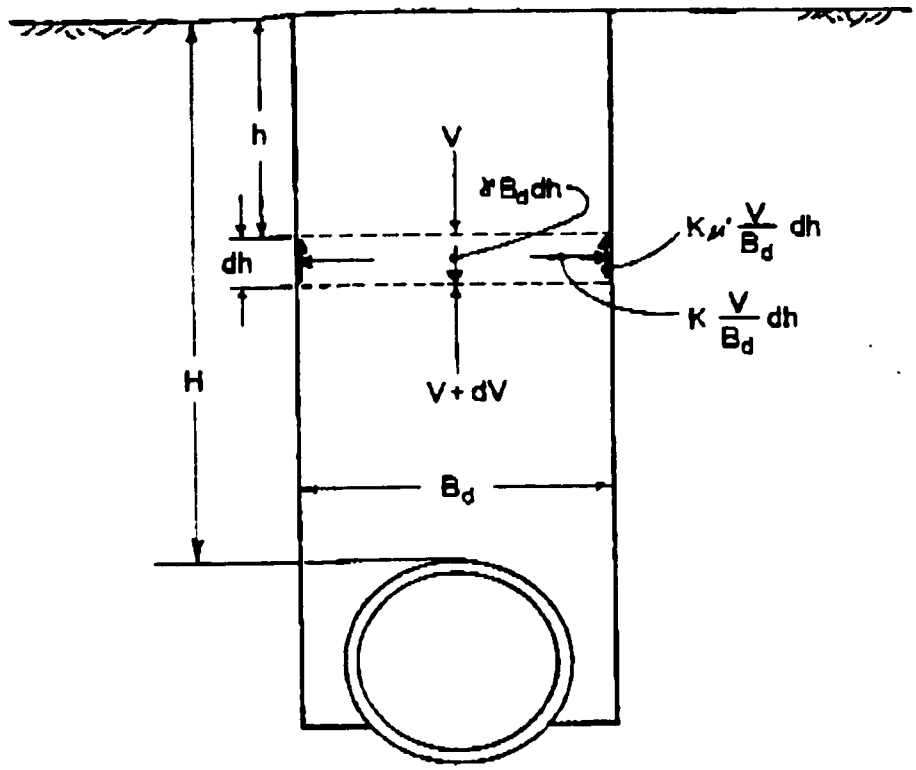

γ = unit weight of fill material, pcf

V = vertical pressure on any horizontal plane, plf

B_d = width of ditch at top of conduit, ft

H = height of fill above top of conduit, ft

h = distance from natural ground surface to horizontal plane, ft

μ' = tan $\emptyset'$ = coefficient of friction between fill material and sides of ditch

K = ratio of active lateral pressure to vertical pressure

Illustration 2.2 Free-body diagram, Marston-Spangler theory (Spangler, 1962)

The resulting formulae can be used to compute the total vertical load on the conduit and are of the form:

$$F_y = C\gamma B^2$$

Where:

F_y = Vertical load on top of the conduit

γ = unit weight of fill

B = Width of trench or conduit, depending upon the class of installation

C = load coefficient

Values of C can be obtained from figures given in the appropriate references.

Although this method is the most widely used in designing buried conduits, it relies on numerous assumptions and it is limited to four theoretical pipeline layout schemes. An important assumption on which this theory is based is that the soil acts as a solid prism resting on top of the conduit. This is certainly not the case in real soil backfill where a multi-dimensional flow of soil around the conduit section results in a complex redistribution of the applied forces, which cannot be described by simple equilibrium equations. Various researchers have attempted to overcome the limitations of the Marston-Spangler theory using theory of elasticity solutions. These solutions however were restricted to circular conduits buried deeply in weightless, linearly elastic soil where loads were simulated by application of surface pressure.

DESIGN METHODS USING FINITE ELEMENT ANALYSIS

In 1978, Donald W. Quigly and J. M. Duncan performed a series of finite element analyses for various conduit shapes under different installation schemes and compared the results with available data from instrumented conduits in operation. The work was part a contract between the U. S. Army Engineer Waterways Experiment Station (WES) and the University of California at Berkeley. The main objective of the study was to provide improved design guidance for the structural analysis of cast-in-place concrete conduits, however, it also provided more general information with respect to earth pressure distribution on buried conduits. In their research, the authors simulated the installation of reinforced concrete conduits of circular, oblong, and

rectangular shapes. Embankment height over the conduits was varied, as well as the soil base under the conduit and the placement details (shallow placement, rock foundation, shallow trench placement, ...). The effect of embankment soil type was also examined. As a result of the study, the authors presented simplified diagrams of earth pressure distribution and analytical formulae that approximate the finite element findings. The study, however, does not consider the time dependant response associated with low permeability soils or the delayed response of the cohesive soil mass to trench excavation prior to conduit installation. These effects are especially important when dealing with overconsolidated low-permeability native soil.

BACKFILL PRESSURES WITHIN A REINSTATED TRENCH: THE GATINEAU FIELD PROJECT

Crawford (1997) presented the results of a research project undertaken by the National Research Council (NRC) and the City of Gatineau, QC, supervised by Dr. Erman Evgin, University of Ottawa, ON.

The research objective was to provide a better understanding of backfill mechanics in a reinstated trench with a buried water pipe, and to quantify the forces acting through the trench and on the buried pipe.

A reinstated trench, with a buried 200 mm diameter ductile iron water pipe, was instrumented with thermocouples and pressure cells. Thermocouples were installed in the backfill at various depths, and the pressure cells were installed over the pipe crown and a bit higher into the backfill material.

Temperature and pressure data were collected over a one year period and analyzed to establish a correlation between frost depth and backfill pressures.

The data showed a complex behavior of the trench-native soil structure under frost action. A crucial role was attributed to differential frost heave between the native soil and the trench material. A more pronounced heave in the native soil was found to relieve the pressure in the backfill by uplift action; hence, an inverse relationship was found between frost depth and backfill pressure.

LESSONS LEARNED FROM CULVERT FAILURES AND NONFAILURES

Cowherd and Corda (1994) evaluated the stability of corrugated metal culverts on the basis of their degree of "flattening" under earth pressure. Their study included failure and non failure case histories where they measured and analyzed the movement of midordinates of circular arcs that form the pipe arch section and the position at which the failure occurred.

The authors divided the arch section into several circular arcs defined by the change in curvature along the arch perimeter. The midordinate of each arc, in particular the top midordinate labeled as "K" in Illustration 2.1 below, was monitored for several structures that failed, and others that did not fail, in order to develop recommendations. The authors used two computer programs in their study. One program was used to quickly compute the midordinates from measured deformations. The other program uses analytical equations to estimate culvert deformations based on soil data, compaction data, and culvert stiffness.

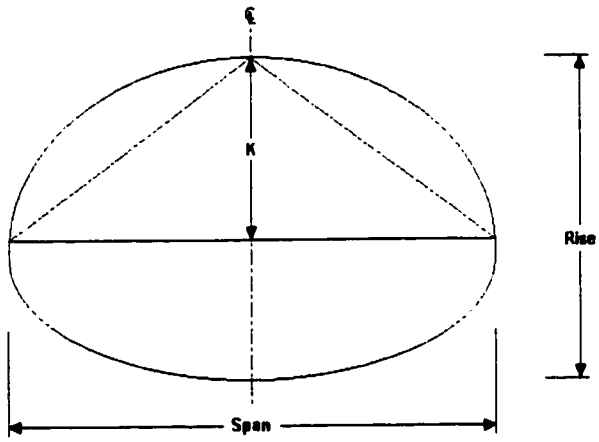

Illustration 2.3 Top midordinate of pipe arch structure

Computed vertical movement of pipe crown for five different structures were compared to measured ones. Subsequently, the computer program was used to perform a parametric study with estimated input parameters for different types of backfill soil and different degrees of compaction. The computed "degree of flattening", or the change in top midordinate dimension, was used as a criterion for recommended remedial action.

It should be noted that the measurements used to validate the computed deformations were mostly (except in one case) from culverts installed in stable rocky ground where no movement of the foundation was involved.

The closed-form analytical solutions for backfill pressure on the structure produces a prismatic pressure on the top and sides of the culvert which may not be the case in the field, especially with clay backfill where the flow of soil and the short-term pore water pressure that develop upon backfilling may result in redistribution of pressure and stress concentrations. These time dependant effects cannot be evaluated using analytical equations, and without a thorough consolidation-type analysis.

PREDICTING PERFORMANCE OF BURIED METAL CONDUITS

Leonards et al. (1985) used the modified finite-element program Culvert Analysis and Design (CANDE) to predict the performance of buried metal conduits. Their analysis focused on the effect of using different soil models and the importance of: the sequence in placing soil layers, the effect of soil-conduit interface, yielding and buckling of the conduit wall, and some applications to practice. In this paper buckling of buried metal conduits was shown to be an important failure mode while yielding without buckling can result in a favorable redistribution of soil pressures.

The analyses showed a significant difference in the results using various soil models. Linear elastic soil models were found inadequate to simulate soil/pipeline interaction problems. Among the soil models investigated, the hyperbolic model by Duncan and Chang gave a good representation of soil response when compared with actual field measurements.

The authors also presented proposed design guidelines as a diagram for estimating the maximum thrust in circular and elliptical conduits.

This investigation was limited to granular backfill which does not warrant the study of long-term behavior, including pore water pressure build-up and dissipation.

PREDICTING PERFORMANCE OF BURIED METAL PIPE ARCHES

Leonards and Juang (1985) used the finite element analyses to present the deflected shape of a metal pipe arch conduit and the distributions of thrust, bending moment, and soil pressure on the

conduit wall. The effect of compacting the soil backfill and of inclusions around the pipe haunches on the fundamental response characteristics of closed pipe arches was investigated.

The results of the study showed the pipe arch to be an efficient structural shape for buried conduits supporting overburden loads. The study also showed the importance of soil densification around the pipe arch in terms of improved performance. Only granular backfills were considered in this study (loose and dense sand)

PIPE FAILURE CAUSED BY IMPROPER GROUNDWATER CONTROL

Selig and McGrath (1994) explained the failure of a pipeline, a short time after installation, as a result of inadequate control of the groundwater during construction.

A groundwater level above the trench base resulted in water washing into the trench through open sheeting joints carrying native sand with it and creating cavities behind the sheeting. Gaps behind the sheeting as large as 1 m^3 were reported. The contractor tried to fill some of the voids with crushed stone before removing the sheeting. When the sheeting was removed, lateral support of crushed stone fill was lost and severe deflection of the pipeline crown was observed. The use of vibratory equipment to remove the sheeting accelerated the problem. This caused failures of pipeline segments and subsequently the collapse of the roadway.

BACKFILL PLACEMENT METHODS LEAD TO FLEXIBLE PIPE DISTORTION

McGrath and Selig (1994) presented the case of a nuclear power plant construction on a site with a high water table to emphasize the importance of construction stresses on pipeline integrity. In order to achieve the required density, large vibratory rollers were used for compaction of the backfill leading to severe distortion and delamination of joints in flexible fiberglass buried pipes. The paper focuses on the importance of construction methods in terms of matching the pipe, backfill material, and compaction equipment. High upward deflections of the pipe during compaction were ignored until the construction was completed, which resulted in a very expensive case history.

CENTRIFUGE MODELING OF LATERALLY LOADED PIPELINES

Poorooshasb et al. (1994) and Paulin et al. (1995 and 1996) presented the results of a series of centrifuge tests on lateral pipeline/soil interaction. The main objective of the multiple-phased testing program was to study the lateral force induced by landslides or slow lateral earth

movement on pipelines anchored in stable soil outside the slide zone. The tests consisted of model pipeline segments (1:50 scale) installed in trenches excavated in simulated cohesive soil (Kaolin clay was used in the centrifuge model). The pipeline trenches were backfilled with cohesive soil as well. Many test set-ups were prepared differing by trench width, depth of trench cover, native material properties, backfill material properties, boundary conditions (depth to solid base, distance between the trench and the wall of the centrifuge strong box, ...), or any combination thereof. The model pipeline segments were connected to a variable speed motor via tension wires at each end of the segment. Under centrifuge effect at 50 g acceleration, the instrumented model pipeline sections were pulled at a constant rate through the backfill material and the trench wall. The authors presented the measured interaction force per unit length of pipeline versus the pipeline displacement into the surrounding soil. Peak interaction forces and corresponding movements were used to compute interaction factors. The results were compared to those developed for lateral resistance of foundation piles, found in the literature.

OVERSTRESSED PRECAST CONCRETE PIPE ARCH AND ITS REDESIGN

Hill and Laumann (1994) presented the case of a large precast concrete pipe arch that cracked at the pipe haunches after a heavy rainfall. The authors suggested that the underestimated stresses were due to the saturation of the soil surrounding the arch. The soil saturation was believed to have caused a loss in lateral support, and subsequently, excessive vertical compression under the high embankment load was responsible for the observed damage. The authors proceeded with a structural analysis of the conduit and presented recommendations for modified reinforcement details. No further efforts were made to investigate the cause of underestimating the backfill pressure on the conduit.

RIGID PIPE DISTRESS IN HIGH EMBANKMENTS OVER SOFT SOIL STRATA

Heger and Selig (1994) examined two case histories where severe cracking and shear and tension failures were observed in rigid concrete pipe culverts. Reported loads on the pipe culverts exceeded those calculated by Marston-Spangler theories. In the study, the excessive loads were attributed to the soft soil supporting the embankment adjacent to the pipe, which cannot be accounted for in traditional design methods. This leads to underestimating the earth load on the pipe.

The authors used finite element analyses to model both cases with and with soft and firm bedding. The main conclusion was that the differential stiffness between the pipe and the

adjacent soft soil causes in increase in earth load on the pipe from the embankment. In addition, the authors concluded that this was not the only reason for the observed failures since they found the design pipe section inadequate for the intended embankment height, regardless of the bedding stiffness.

FINITE ELEMENT ANALYSIS APPLIED TO THE RESPONSE OF BURIED FRP PIPE UNDER VARIOUS INSTALLATION CONDITIONS

Sharp et al. (1885) applied the finite-element analysis to flexible pipes. Conventional finite element programs are not designed to model large deflections. In their study they developed new features to the program to consider large deflections of pipes, sensitivity of the pipe, and the soil response to compaction loading. The main modification in the program was to eliminate the iteration to conversion process when large deflections are involved and replace it with an approximation routine. Numerical results were compared with measured pipe responses and were reported to be in good agreement.

COMPUTER MODELING OF THE CROSS CANYON CULVERT

Lawrence C. Rude (1983) used the finite element computer program to determine the effectiveness of three different soil models in predicting the behavior of an underdesigned reinforced concrete culvert installed under a deep fill. Dummy culvert sections were installed in the same embankment as a functional culvert in Cross Canyon, California. The dummy sections were 2.133 m inside diameter reinforced concrete pipes and were grossly underdesigned for the 55 m overfill. The sections were instrumented with contact stressmeters on the outer surface to measure normal and tangential pressure. Weldable strain gages were placed on the pipe reinforcement (eight gages distributed around the perimeter) to measure stresses and strains within the structure. An Extensometer was used to determine interior wall displacements by measuring chord distances between steel balls fastened to the interior perimeter. Several different types of soil models were used in the analyses for comparison with actual behavior. The hyperbolic model recommended by Duncan predicted the actual behavior with the least error.

FIELD TESTING OF A CONCRETE BOX CULVERT

In 1989, Tadros et al. studied the construction of a concrete box culvert, they recorded measurements of soil pressures, strains, deflections, and settlements both during and after

construction; reported soil pressures observed resulting from soil and truck loading and compared measurements, theory, and AASHTO specifications.

FAILURE OF FLEXIBLE LONG-SPAN CULVERTS UNDER EXCEPTIONAL LIVE LOADS

In 1988, Seed and Raines presented three case studies to evaluate the accuracy and reliability of the finite element analysis method. their analyses involved culvert failure under exceptional live loads where live loads only barely exceeded the structural capacities of the culvert. their results provides a good support for the accuracy and reliability of analytical procedures.

DEFLECTION AND STRAINS IN BURIED FRP PIPES SUBJECTED TO VARIOUS INSTALLATION CONDITIONS

In 1985, Moser et al. defined the performance of fiberglass reinforced plastic (FRP) pipe in relation to loads induced strains and deflections. They based their study on discussing effects due to soil density, pipe stiffness, soil type, and installation techniques.

EFFECT OF HEAVY LOADS ON BURIED CORRUGATED POLYETHYLENE PIPE

In 1983, Watkins et al. investigated the structural performance and performance limits of large-diameter corrugated polyethylene pipes when subjected to external soil pressures. These pipes were originally used in only 4-12in diameter size for land drainage. In this paper, test were conducted on pipes with 15-18- and 24in inner diameter.

FINITE-ELEMENT MODELING OF BURIED CONCRETE PIPE INSTALLATIONS

In 1982, Selig et al. developed a finite-element computer program, Soil-Pipe Interaction Design and Analysis (SPIDA) for buried concrete pipe. The program is based on the Marston-Spangler approach to update the current concrete pipe design methods with expectation of reducing the cost of the installation and providing a more accurate representation of field conditions.

DESIGN METHOD FOR CONCRETE PIPE UNDER HIGH FILLS

In 1982, Kay and Hain performed a series of finite element analyses to model the stresses in concrete conduits induced by high overlaying fill. The analyses were performed using simple linear elastic model for the concrete pipe and the surrounding soil, among other simplifying assumptions. The authors then produced design charts that relate the height and specific weight

of the fill to induced pressure on the conduit for a range of fill to native soil modulus ratios and conduit diameter to thickness ratios.

2.3. SUMMARY OF LITERATURE REVIEW

Literature regarding conventional closed form solutions to pipeline/soil interaction problems reveal a significant number of assumptions and simplifications which may or may not apply to actual field conditions. Furthermore, most of the conventional methods are directed towards the "most common" situations and designs, which may be more adapted to urban areas and controlled sites. Pipeline construction, however, is a more random problem due to the size of the geographical areas that constitute the sites for pipeline construction. More flexible design tools that can adapt to new situations are therefore in demand.

The use of finite element methods in the literature is now more frequently encountered. However, in most of the available literature, numerical analyses are directed towards resolving specific problems encountered during a conduit failure, or in evaluating the behavior of a specific type of conduit, or to simulate a case history involving instrumented full scale buried conduit.

Some published research involves the use of numerical methods in developing design guidelines in terms of stress distribution resulting from different loading scenarios. Most of these publications address the immediate stress-deformation relationships upon installation of the structures. The time dependant behavior is rarely addressed.

CHAPTER 3

FINITE ELEMENT APPLICATION, SOIL MODEL, AND PARAMETERS

CHAPTER 3

FINITE ELEMENT APPLICATION, SOIL MODEL AND PARAMETERS

3.1. Introduction

The finite element software selected to conduct this research is SIGMA/W by Geo-Slope International. The software is selected because of its proven strength in modeling soil/structure interaction and staged construction, and its powerful pre-processing and post-processing capabilities. Coupled with SEEP/W (by Geo-Slope International), SIGMA/W is used to perform fully coupled stress-deformation and consolidation analyses to model long term conditions.

For realistic soil deformation analyses, it is important that the stress-strain characteristics of the soil be adequately represented. At the same time, any meaningful representation of soil behavior has to be simple enough to be applicable in practice using available laboratory test data and resources.

The soil model selection for the purpose of this research is based on the following criteria:

1. Suitable to model excavation and backfilling in overconsolidated clay
2. Simple to apply using commercial finite element software
3. Sufficient data available to adequately determine the required model parameters

SIGMA/W incorporates several constitutive soil models ranging from simple linear elastic model to complex Cam-clay and Modified Cam-clay plasticity models.

One of the main objectives of this research is to investigate the effect of soil overconsolidation on pipeline construction. Cam-clay plasticity models are originally designed for "wet" clays that are normally or lightly overconsolidated. These models have not been successfully applied to highly overconsolidated clays and therefore were not selected for the purpose of this study. The Hyperbolic model, formulated by Duncan and Chang, 1970, was selected instead for a better representation of highly overconsolidated soil behavior.

The hyperbolic stress-strain relationship provides a simple framework encompassing the most important characteristics of soil stress-strain behavior using the data available from conventional laboratory tests. This relationship has been used in finite element analyses of a number of static soil mechanics problems.

A brief description of the Hyperbolic soil model, its parameters, and its application within SIGMA/W finite element software are presented in the following sections.

The step by step determination of the model parameters is discussed in the following sections and applied to determine the parameters for the London clay (High Ongar clay) used throughout this research as the native and backfill soil.

3.2. THE HYPERBOLIC SOIL MODEL AND SIGMA/W (SIGMA/W docs.)

The stress-strain behavior of soil becomes nonlinear, particularly as failure conditions are approached (see Illustration 3.1). A procedure for modeling this soil behavior by varying the soil modulus is addressed in the following subsections.

SIGMA/W uses the formulation presented by Duncan and Chang (1970) to compute the soil modulus. In this formulation, the stress-strain curve is hyperbolic and the soil modulus is a function of the confining stress and the shear stress that a soil is experiencing. This nonlinear material model is attractive since the required soil properties can be readily obtained from triaxial tests or the literature (for example, Duncan et al., 1980).

Duncan and Chang's non-linear stress-strain curve is a hyperbola in the shear stress, $\sigma_1 - \sigma_3$, versus axial strain space. Depending on the stress state and stress path, three soil moduli are required; namely, the initial modulus, E_i the tangential modulus, E_t, and the unloading-reloading modulus, E_{ur} (see Illustration 3.1).

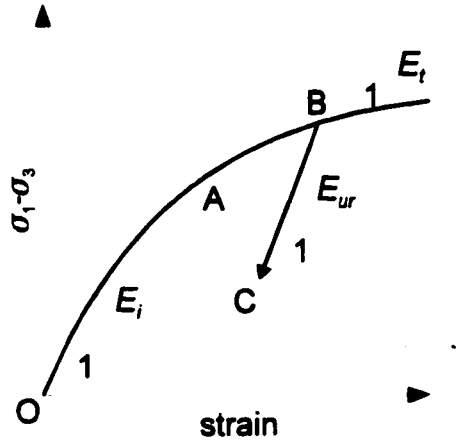

Illustration 3.1 Non-Linear Stress-Strain Behavior

3.2.1. Initial Modulus

When a soil is subjected to zero shear stress (i.e. when $(\sigma_1 - \sigma_3) = 0$), its stress-strain behavior is modeled using the initial modulus, E_i. This initial tangent modulus is controlled by the confining stress, σ_3 and is calculated as follows:

$$E_i = K_L P_a \left(\frac{\sigma_3}{p_a} \right)^n \tag{3.1}$$

where:

E_i = initial tangent modulus as a function of confining stress, σ_3
K_L = loading modulus number
p_a = atmospheric pressure (used as a normalizing parameter)
σ_3 = confining stress
n = exponent for defining the influence of the confining pressure on the initial modulus

When the exponent n is equal to 1.0, the initial tangent modulus, E_i, is directly proportional to the confining stress. When n is equal to 0, E_i is independent of the confining stress.

Two different methods are used in SIGMA/W to calculate the initial soil modulus. When K_L is equal to zero (i.e., not defined by the user), the initial tangent modulus, E_i, is set to the user-

specified value for E and remain constant throughout an analysis. If K_L is nonzero (i.e., defined by the user), E_i is computed using Equation 3.1.

When the confining stress is zero or negative (i.e., the soil is in a state of tension), it is possible for the initial modulus, E_i, to become zero or negative. In order to avoid this problem when computing E_i, SIGMA/W imposes a lower limit of $(0.01 p_a)$ on the confining stress, σ_3.

3.2.2. Tangent Modulus

A soil is said to be following a loading path when it is subjected to a shear stress higher than it has previously experienced, for example, from point O to point A in Illustration 3.1. Along this loading path, its constitutive behavior is governed by the tangent modulus, E_t. This tangent modulus is defined in Duncan and Chang model as a function of soil properties, triaxial stress difference (deviator stress), $(\sigma_1 - \sigma_3)$, and confining stress, σ_3 using the following equation:

$$E_t = \left[1 - \frac{R_f(\sigma_1 - \sigma_3)(1-\sin\phi)}{2c(\cos\phi) + 2\sigma_3 \sin\phi}\right]^2 E_i \tag{3.2}$$

where:

E_i = initial tangent modulus
E_t = tangent modulus
ϕ = friction angle of soil
c = cohesive strength of soil
R_f = ratio between the asymptote to the hyperbolic curve and the maximum shear strength.
σ_1 = major principal stress
σ_3 = minor principal stress

In SIGMA/W, the [ ] bracketed term is arbitrarily limited to a minimum value of 0.0001, implying that R_f is limited to 0.99.

3.2.3. Determination of Parameters *K* and *n*

The modulus and exponent values for the Nonlinear-Elastic model can be determined by plotting triaxial test results on a log vs. log plot, as shown in Illustration 3.2. The stiffness values E/P_a and B_m/P_a are plotted versus σ_3 / P_a. The slope of a straight line through the data points gives the exponent. The modulus number K is equal to the value on the vertical scale, where σ_3 / P_a is equal to 1.0

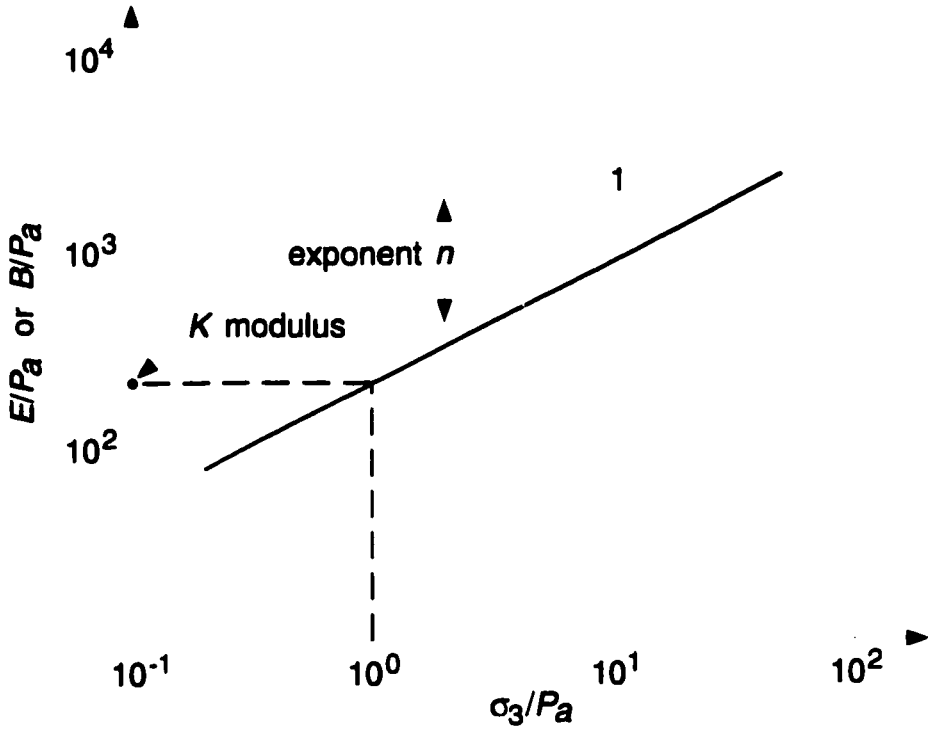

Illustration 3.2 Determination of Nonlinear-Elastic Soil Properties

The bulk modulus B_m is defined as,

$$B_m = \frac{(\Delta\sigma_1 + \Delta\sigma_2 + \Delta\sigma_3)/3}{\Delta\varepsilon_v} \tag{3.3}$$

where:

$\Delta\sigma_1$, $\Delta\sigma_2$, $\Delta\sigma_3$ = change in principal stress values

$\Delta\varepsilon_v$ = change in volumetric strain

Further details of the hyperbolic model can be found in a report by Duncan et al. (1980) This report also contains a list of hyperbolic parameters for some 135 different soils.

3.2.4. Unloading-Reloading Modulus

When a soil is unloaded from a higher shear stress state, (for example, going from point B to point C in Illustration 3.1), the non-linear model uses the unload-reloading modulus, E_{ur}.

The unload-reloading modulus, E_{ur}, is computed in a manner similar to the computation of the initial modulus, E_i except that the unloading-reloading modulus number, K_{ur} replaces K_L in Equation 3.1. Thus, the unloading-reloading modulus is calculated as:

$$E_{ur} = K_{ur} p_a \left(\frac{\sigma_3}{p_a} \right)^n \tag{3.4}$$

Unlike the tangent modulus, this unloading-reloading modulus is unaffected by the shear stress level.

If the unloading-reloading modulus number, K_{ur}, is not defined by a user, it is assigned the value of the loading modulus number, K_L, and the soil will unload or reload along the hyperbolic curve.

3.2.5. Poisson's Ratio

The Poisson's ratio of the non-linear elastic model can either be specified as a constant which is independent of stress state, or it can be computed from the soil bulk modulus, which depends on the confining stress. For the latter case, the bulk modulus is given by:

$$B_m = K_b p_a \left(\frac{\sigma_3}{p_a} \right)^m \tag{3.5}$$

where:

B_m = bulk modulus
K_b = modulus number
p_a = atmospheric pressure
m = bulk modulus exponent

The relationship of the bulk modulus to the Poisson's ratio can be defined as follows from theory of elasticity.

$$B_m = \frac{E}{3(1-2\nu)} \tag{3.6}$$

Letting the Poisson's ratio, ν, equal to zero in the above equation gives a bulk modulus, B_m, equal to $E/3$. When letting the Poisson's ratio, ν, equal to 0.49, B_m has a value of $17E$. SIGMA/W imposes both upper and lower limits on the computed value of Poisson's ratio. The upper limit is 0.49. The lower limit is either the user-defined constant value or 0.01.

If K_b is not defined (i.e. zero), SIGMA/W assigns the user input constant value to the Poisson's ratio. Otherwise it is calculated using Equation 3.5.

3.2.6. Yield Zones

From a theoretical standpoint, yield conditions cannot be defined when using a non-linear elastic model. In order to show high shear stress zones in a non-linear elastic material, SIGMA/W identifies such zones as "yielded" when the following criterion is satisfied:

$$\frac{\sigma_1 - \sigma_3}{2} - \frac{\sigma_1 + \sigma_3}{2}\sin\phi \geq R_f c\cos\phi. \tag{3.7}$$

In Duncan and Chang's formulation of the hyperbolic model, R_f, the failure ratio, is used in the following manner:

$$(\sigma_1 - \sigma_3)_f = R_f(\sigma_1 - \sigma_3)_{ult} \tag{3.8}$$

The ultimate strength term, $(\sigma_1 - \sigma_3)_{ult}$, represents the asymptote which the hyperbolic stress-strain curve will approach at large strains. The $(\sigma_1 - \sigma_3)_f$ is the deviator stress at failure. From a Mohr's diagram, it can be seen that:

$$\frac{(\sigma_1 - \sigma_3)_{ult}}{2} - \frac{(\sigma_1 + \sigma_3)_{ult}}{2}\sin\phi = c\cos\phi \tag{3.9}$$

When multiplied by R_f and substituting in Equation 3.8, this equation can be written as follows.

$$\frac{(\sigma_1 - \sigma_3)_f}{2} - \frac{(\sigma_1 + \sigma_3)_f}{2}\sin\phi = R_f c\cos\phi \tag{3.10}$$

Comparing the Equation 3.10 with Equation 3.7, it is seen that the inequality given in Equation 3.7 provides an indicator to how close the stress state is to the failure state.

3.3. Parameters for London Clay (High Ongar)

Hyperbolic model parameters for a typical overconsolidated clay are determined for London clay based on extensive triaxial testing results by Som, 1968. Average values of solid density, bulk density, natural water content, and Atterberg limits of London clay (Ongar) as determined by Som, 1968, are as follows:

Average properties of London clay (Som, 1968):

Solid density = 2.7

Bulk density = 19.6 kN/m^3

Natural water content = 27 %

Atterberg limits: Liquid Limit = 67.5 Plastic Limit = 26.5 Plasticity Index = 41

The degree of saturation measured from various samples was about 100 %.

Selected triaxial test results used to determine the model parameters are presented in the following subsections. Table 3-1 lists the triaxial tests that will be used in this study.

Table 3-1: Summary of triaxial tests (Som, 1968)

Test #	Sample #	Test description	Sampling Direction	Confinement Stress * kPa
DC1	T HO 25	Drained triaxial compression to failure	Vertical	550
DC2	T HO 24	Drained triaxial compression to failure	Vertical	655
DC3	T HO 26	Drained triaxial compression to failure	Vertical	827
DC4	T HO 34	Drained triaxial compression to failure	Horizontal	414
DC5	T HO 35	Drained triaxial compression to failure	Horizontal	690
DC6	T HO 36	Drained triaxial compression to failure	Horizontal	690
UEC1	T HO 6	Undrained extension followed by compression	Vertical	690
UEC2	T HO 7	Undrained extension followed by compression	Vertical	690
IC1	T HO 8	Isotropic consolidation, single drainage	Vertical	403
IC2	T HO 9	Isotropic consolidation, single drainage	Vertical	386
IC3	T HO 21-1	Isotropic consolidation, double drainage	Vertical	484
IC4	T HO 21-2	Isotropic consolidation, double drainage	Vertical	690
IC5	T HO 24-1	Isotropic consolidation, double drainage	Vertical	455
IC6	T HO 26-1	Isotropic consolidation, double drainage	Vertical	400
IC7	T HO 26-2	Isotropic consolidation, double drainage	Vertical	483
IC8	T HO 33-1	Isotropic consolidation, double drainage	Vertical	407
IC9	T HO 35-1	Isotropic consolidation, double drainage	Horizontal	427
IC10	T HO 36-1	Isotropic consolidation, double drainage	Horizontal	459

* Initial stress for isotropic consolidation

3.3.1. Initial tangent modulus, E_i and the R_f ratio

Data of Tests DC1, DC2, and DC3 (vertical samples) are presented in Figure 3-1 as axial strain versus stress difference and volumetric strain. A similar presentation is provided for Tests DC4, DC5, and DC6 (horizontal samples) in Figure 3-2. A hyperbolic curve is fitted to the data of all six compression tests. The transformed equation of the fitted stress-strain hyperbola (Duncan and Chang, 1970) can be written as:

$$\frac{\varepsilon}{\sigma_1 - \sigma_3} = a + b\varepsilon \tag{3.11}$$

which is the equation of a straight line with intercept a and slope b. Parameters a and b can be determined by plotting the transformed stress-strain data as axial strain (ε_a) versus axial strain / stress difference ($\varepsilon_a/(\sigma_1-\sigma_3)$). A straight line is then fitted to the data points. From the hyperbolic curve properties, the intercept of the fitted line (a) is the inverse of the initial tangent modulus E_i and the slope (b) is the inverse of the asymptote value, which in the case of stress-strain relationship can be termed as the ultimate stress difference $(\sigma_1-\sigma_3)_{ult}$. The parameter R_f can be determined as the ratio of stress difference at failure from test data to the ultimate stress difference ($R_f = (\sigma_1-\sigma_3)_f / (\sigma_1-\sigma_3)_{ult}$). Illustration 3.3 depicts the hyperbolic stress-strain representation.

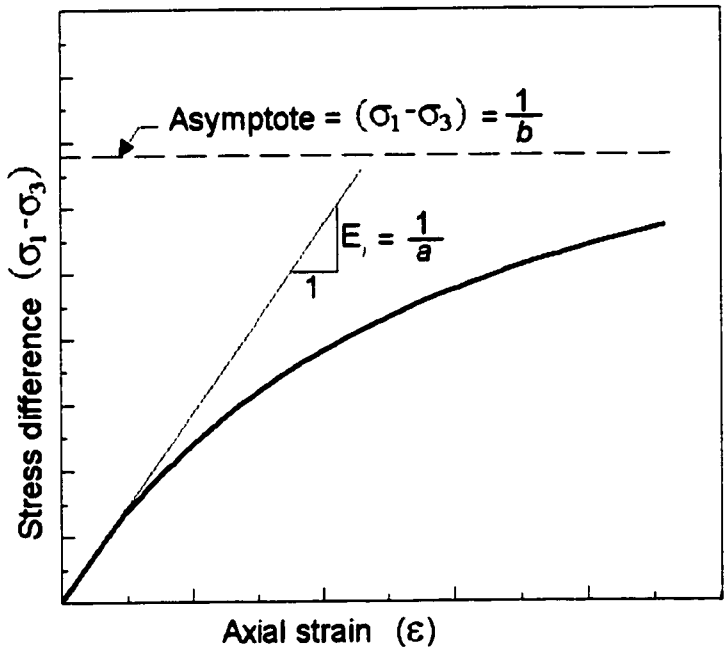

Illustration 3.3 Hyperbolic stress-strain curve

Transformed stress strain data of all six drained conventional compression tests are used to determine E_i and $(\sigma_1-\sigma_3)_{ult}$.at different confinement pressures. The transformed data as well as the fitted hyperbolic stress-strain curve for Tests DC1 through DC6 are presented in Figures 3-3 through 3-8. Table 3-2 presents the computed initial moduli and R_f parameters for the six tests.

Table 3-2: Summary of computed Initial moduli and R_f parameters

Sample #	Sampling Direction	Confinement Stress (σ_3) kPa	Stress difference at failure (max.) $(\sigma_1-\sigma_3)_f$, kPa	Ultimate Stress Difference $(\sigma_1-\sigma_3)_{ult}$, kPa	Initial Tangent Modulus, E_i kPa	R_f $(\sigma_1-\sigma_3)_f / (\sigma_1-\sigma_3)_{ult}$
T HO 25	Vertical	550	516	934	32,279	0.55
T HO 24	Vertical	655	738	1297	42,846	0.57
T HO 26	Vertical	827	924	1665	48,821	0.55
T HO 34	Horizontal	414	545	980	29,391	0.56
T HO 35	Horizontal	690	896	1520	39,412	0.59
T HO 36	Horizontal	690	779	1344	35,350	0.58
					Average R_f value ⇒	**0.57**

The average R_f value of 0.57 will be used for the hyperbolic model representation of London clay in this study. The computed E_i values with different confining pressures will be used in subsequent sections to determine the loading modulus (K_L) and exponent (n) which define the influence of confining pressure on the initial modulus.

3.3.2. Loading modulus number, K_L and exponent, n

As described in Section 3.2, the initial tangent modulus is controlled by the confining stress, σ_3 and is calculated as follows (Equation 3.1):

$$E_i = K_L P_a \left(\frac{\sigma_3}{p_a}\right)^n$$

This equation can be rewritten as:

$$\log\left(\frac{E_i}{P_a}\right) = \log(K_L) + n\log\left(\frac{\sigma_3}{p_a}\right) \tag{3.12}$$

Considering $\left(\frac{E_i}{p_a}\right)$ and $\left(\frac{\sigma_3}{p_a}\right)$ as the dependant and independent variables (y and x), respectively, Equation 3.12 represents a straight line in a log-log scale plot with K_L being the intercept ($K_L = y$ for $x = 10^0$), and n being the slope.

Figure 3-9 shows the plot of $\left(\frac{E_i}{P_a}\right)$ versus $\left(\frac{\sigma_3}{P_a}\right)$ for the six initial moduli computed in the previous section including the fitted line and the measured intercept and slope. Details of the calculations are presented in Table 3-3.

Table 3-3: Detailed computation of parameters K_L and n

Sample #	Confinement (σ_3) kPa	E_i kPa	σ_3/P_a	E_i/P_a	log(σ_3/P_a) Regression X	log(E_i/P_a) Regression Y
T HO 25	550	32279	5.43	318.65	0.735	2.503
T HO 24	655	42846	6.47	422.96	0.811	2.626
T HO 26	827	48821	8.16	481.95	0.912	2.683
T HO 34	414	29391	4.09	290.14	0.611	2.463
T HO 35	690	39412	6.81	389.06	0.833	2.590
T HO 36	690	35350	6.81	348.96	0.833	2.543

Regression Output:		
Intercept = log (K_L) =		2.020
	=> $K_L = 10^{2.020} =$	**105**
Std Err of Y Est		0.042
R Squared		0.788
No. of Observations		6
Degrees of Freedom		4
	Slope = n =	**0.69**
Std Err of Coef.		0.180

Fitted line	
σ_3/P_a	E_i/P_a
1	104.71
10	518.08

3.3.2. Unloading-reloading modulus number, K_{ur}

As described in Section 3.2, the unloading-reloading tangent modulus, like the initial modulus, is controlled by the confining stress, σ_3 and is calculated as follows (see Equation 3.4):

$$E_{ur} = K_{ur} P_a \left(\frac{\sigma_3}{p_a}\right)^n$$

The value of K_{ur} is usually determined assuming that the value of the modulus exponent, n, is the same as for primary loading. This assumption simplifies the determination of K_{ur}. Based on

Equation 3.3, once the value of n is determined, a value of E_{ur} from a single unloading curve is sufficient to determine K_{ur} as:

$$K_{ur} = E_{ur} \Big/ P_a \left(\frac{\sigma_3}{p_a} \right)^n \tag{3.13}$$

No unloading-reloading was performed for the London clay during the triaxial compression testing. The initial modulus from the triaxial extension tests (UEC1 and UEC2) will be used instead, since those tests were performed by unloading in the vertical direction. Since the confinement is almost the same for both tests, average values of the extension modulus and confinement will be used for more accuracy in representing the soil behavior. Figure 3-10 shows the extension data for Tests UEC1 and UEC2 and the line fitted to the beginning of unloading. The following values are used to determine K_{ur} as per Equation 3.13:

Average E_{ur} = 33,500 kPa (slope of the fitted line)
Modulus exponent, n = 0.69
Average confinement, σ_3 = 380.5 kPa
Atmospheric pressure, P_a = 101.3 kPa
The calculated K_{ur} is evaluated at 136

3.3.3. Bulk modulus number, K_b and exponent, m

As described in Section 3.2, a stress-dependant Poisson's ratio can be related to the bulk modulus B_m as in Equation 3.5. Bulk modulus, like the initial modulus, is controlled by the confining stress, σ_3 and is calculated as follows (see Equation 3.5):

$$B_m = K_b p_a \left(\frac{\sigma_3}{p_a} \right)^m$$

The determination of K_b and m is similar to that of K_L and n for initial loading. The determination of these parameters involves two steps. The first step is to determine the bulk modulus (B_m) for each test (drained triaxial compression Tests DC1 through DC6). For conventional triaxial tests,

where the stress difference $(\sigma_1-\sigma_3)$ increases while the confining pressure is held constant, Equation 3.11 can be expressed as:

$$B_m = \frac{(\sigma_1 - \sigma_3)}{3\varepsilon_v} \tag{3.14}$$

The value of B_m can be computed using Equation 3.14 at 70 % stress level (Duncan et al., 1980). Table 3-4 summarizes the calculation of B_m for Tests DC1 through DC6.

Table 3-4: Summary of computed bulk moduli

Sample #	Sampling Direction	Confinement Stress, σ_3 kPa	Stress difference at 70% stress level $(\sigma_1-\sigma_3)_{70}$, kPa	Volumetric strain at 70% stress level ε_{v70}	Bulk Modulus, Bm $(\sigma_1-\sigma_3)_{70} / (3\,\varepsilon_{v70})$ kPa
T HO 25	Vertical	550	361	0.0108	11,143
T HO 24	Vertical	655	516	0.0135	12,751
T HO 26	Vertical	827	647	0.0156	13,819
T HO 34	Horizontal	414	381	0.0094	13,521
T HO 35	Horizontal	690	627	0.0120	17,429
T HO 36	Horizontal	690	545	0.0135	13,467

The second step is to plot $\left(\frac{B_m}{p_a}\right)$ versus $\left(\frac{\sigma_3}{p_a}\right)$ on a log-log scale, similar to the determination of K_L and n. A straight line fitted to the data points would have K_b as the intercept ($K_b = y$ for $x = 10^0$), and m as the slope.

Figure 3-11 shows the plot of $\left(\frac{B_m}{p_a}\right)$ versus $\left(\frac{\sigma_3}{p_a}\right)$ for the six bulk moduli including the fitted line and the measured intercept and slope. Details of the calculations are presented in Table 3-5.

Table 3-5: Detailed computation of parameters K_b and m

Sample #	Confinement (σ_3) kPa	B_m kPa	σ_3/P_a	B_m/P_a	log(σ_3/P_a) Regression X	log(B_m/P_a) Regression Y
T HO 25	550	11143	5.43	110.00	0.735	2.041
T HO 24	655	12751	6.47	125.88	0.811	2.100
T HO 26	827	13819	8.16	136.42	0.912	2.135
T HO 34	414	13521	4.09	133.48	0.611	2.125
T HO 35	690	17429	6.81	172.05	0.833	2.236
T HO 36	690	13467	6.81	132.94	0.833	2.124

Regression Output:		
Intercept = log (K_b) =		1.981
	=> $K_b = 10^{1.981}$ =	**96**
Std Err of Y Est		0.067
R Squared		0.092
No. of Observations		6
Degrees of Freedom		4
	Slope = m =	**0.18**
Std Err of Coef.		0.290

Fitted line	
σ_3/P_a	B_m/P_a
1	95.72
10	146.48

3.3.4. Strength parameters, c' and ϕ'

Strength parameters c' and ϕ' can be determined in different ways. In this study, the slope, ψ' and intercept, α' of the failure stress ratio line (K_f-line) will be used. Stress paths of Tests DC1 through DC6 are shown in Figure 3-12, along with the K_f-line fitted to the failure points. The following values can be computed from the plot:

$$\tan(\psi') = 0.36$$

$$\alpha' = 19.33 \text{ kPa}$$

Parameters c' and ϕ' can be determined as follows:

$$\phi' = \sin^{-1}(\tan(\psi')) = 21°$$

$$c' = \alpha' / \cos(\phi') = 20.7 \text{ kPa}$$

3.3.5. Coefficient of permeability, k

The permeability of ten London clay (Ongar) samples, eight vertical and two horizontal, subjected to isotropic consolidation (Tests IC1 through IC 10), was also determined by Som, 1968. Table 3-6 presents a summary of the isotropic consolidation tests and the determined coefficient of permeability for each sample.

Table 3-6: Coefficient of permeability (Som, 1968)

Sample #	Drainage Condition	Initial confinement kPa	Change in stress kPa	Axial strain %	Volumetric strain %	k 10^{-11} m/s
Vertical Samples						
T HO 8	S	403	262	0.66	1.58	**1.146**
T HO 9	S	386	214	0.59	1.36	**1.206**
T HO 21-1	D	484	205	0.48	0.98	**0.730**
T HO 21-2	D	690	207	0.37	0.78	**0.465**
T HO 24-1	D	455	200	0.44	1.02	**1.158**
T HO 26-1	D	400	83	0.2	0.5	**1.414**
T HO 26-2	D	483	345	0.78	1.78	**1.334**
T HO 33-1	D	407	283	0.87	1.79	**0.965**
Horizontal Samples						
T HO 35-1	D	427	193	0.6	1.4	**2.240**
T HO 36-1	D	459	231	0.62	1.63	**2.567**

The following coefficients of permeability, obtained by averaging from test results, will be used to model the London clay soil:

Vertical direction:	$k_v = 1.25 \times 10^{-11}$ m/s
Horizontal direction:	$k_h = 2.40 \times 10^{-11}$ m/s

3.3.6. Summary of hyperbolic model parameters for London clay

In the previous subsections, all parameters required to model the London clay soil using the hyperbolic model were determined from triaxial testing data by Nitindra Nath Som, 1968. Following is a summary of the determined parameters which will be used in finite element analysis throughout this research:

Ratio of failure stress difference to ultimate stress difference	$R_f = 0.57$
Loading modulus number	$K_L = 105$
Loading modulus exponent	$n = 0.69$
Unloading-reloading modulus number	$K_{ur} = 136$
Bulk modulus number	$K_b = 96$
Bulk modulus exponent	$m = 0.18$
Angle of internal friction	$\phi' = 21°$
Cohesion strength	$c' = 20.7$ kPa
Coefficient of earth pressure at rest	$K_o = 2$
Coefficient of permeability - Vertical direction	$k_v = 1.25 \times 10^{-11}$ m/s
Coefficient of permeability - Horizontal direction	$k_h = 2.40 \times 10^{-11}$ m/s
Ratio of vertical to horizontal permeability (k_v/k_h)	k-ratio = 0.53

FIGURES

CHAPTER 3

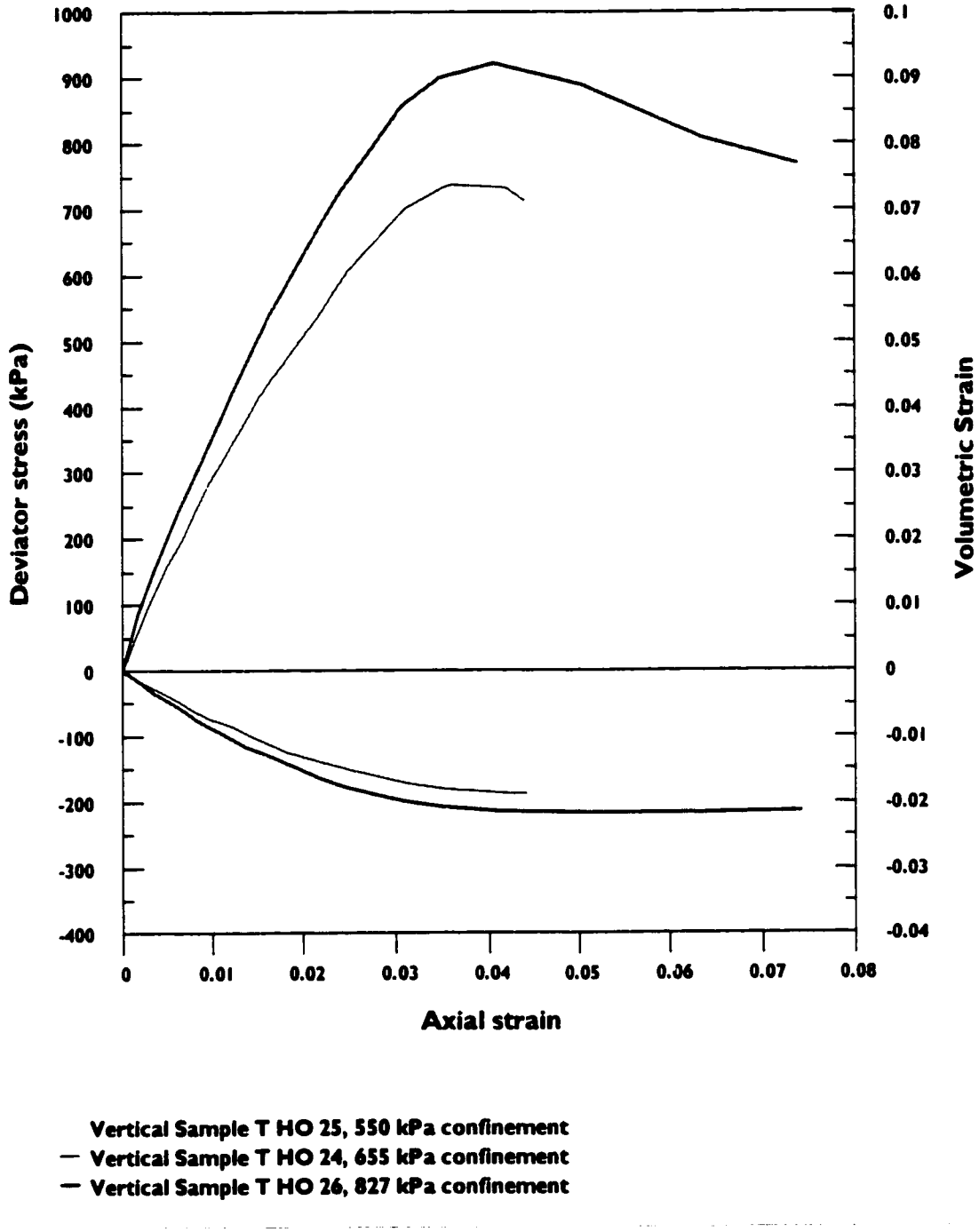

Figure 3-1: Drained triaxial compression - vertical samples (Som, 1968)

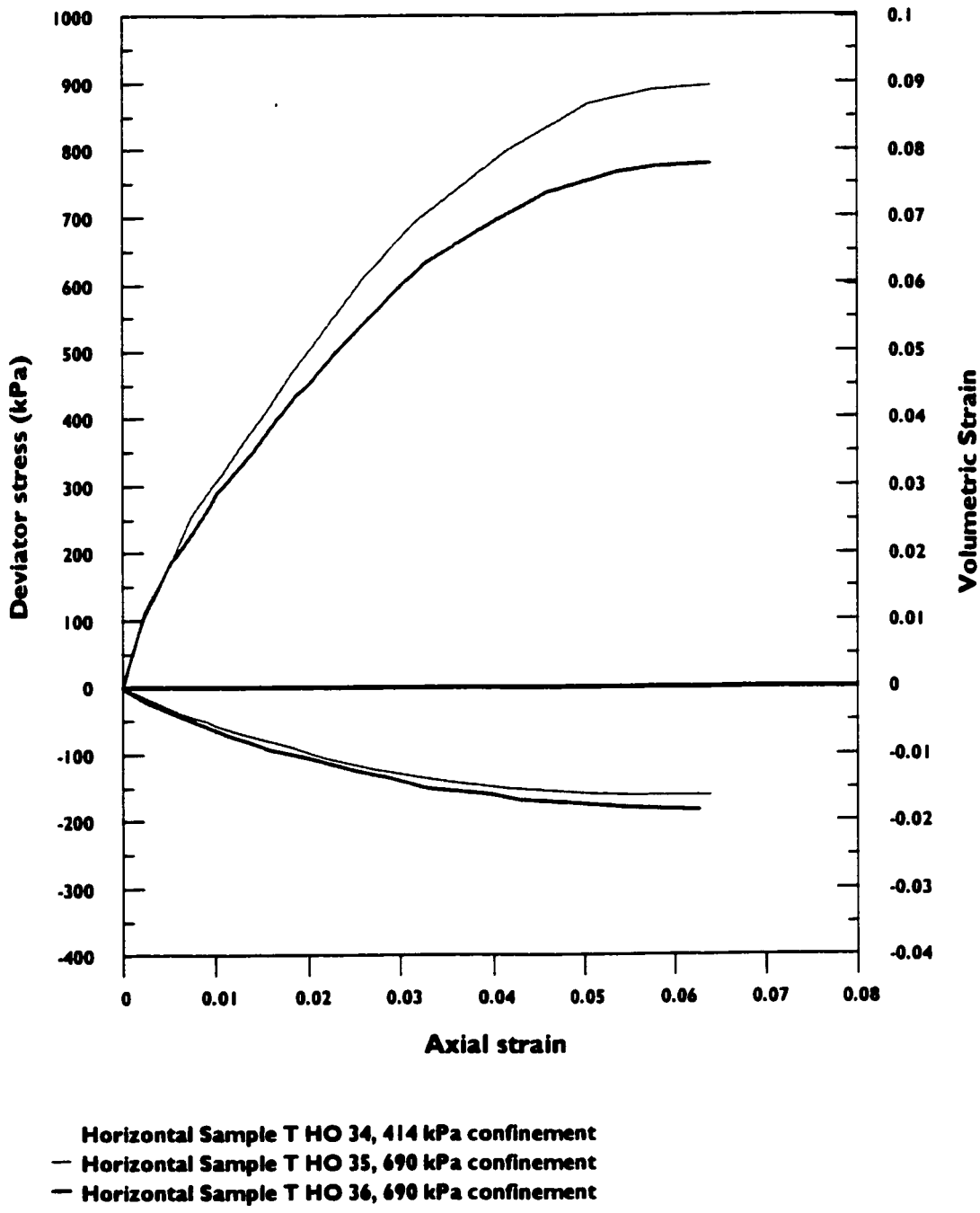

Figure 3-2: Drained triaxial compression - horizontal samples (Som, 1968)

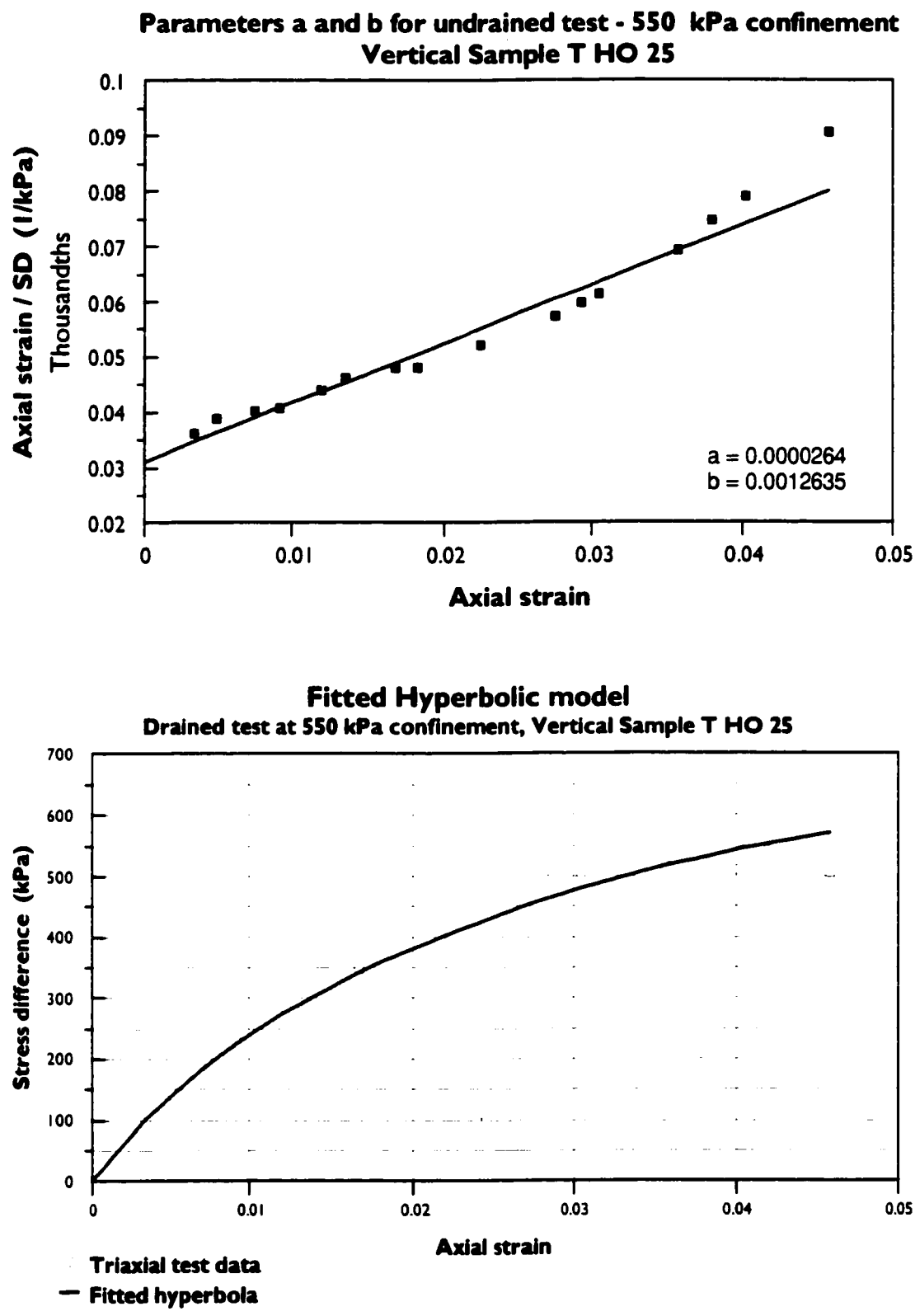

Figure 3-3: Hyperbolic stress-strain representation - Sample T HO 25

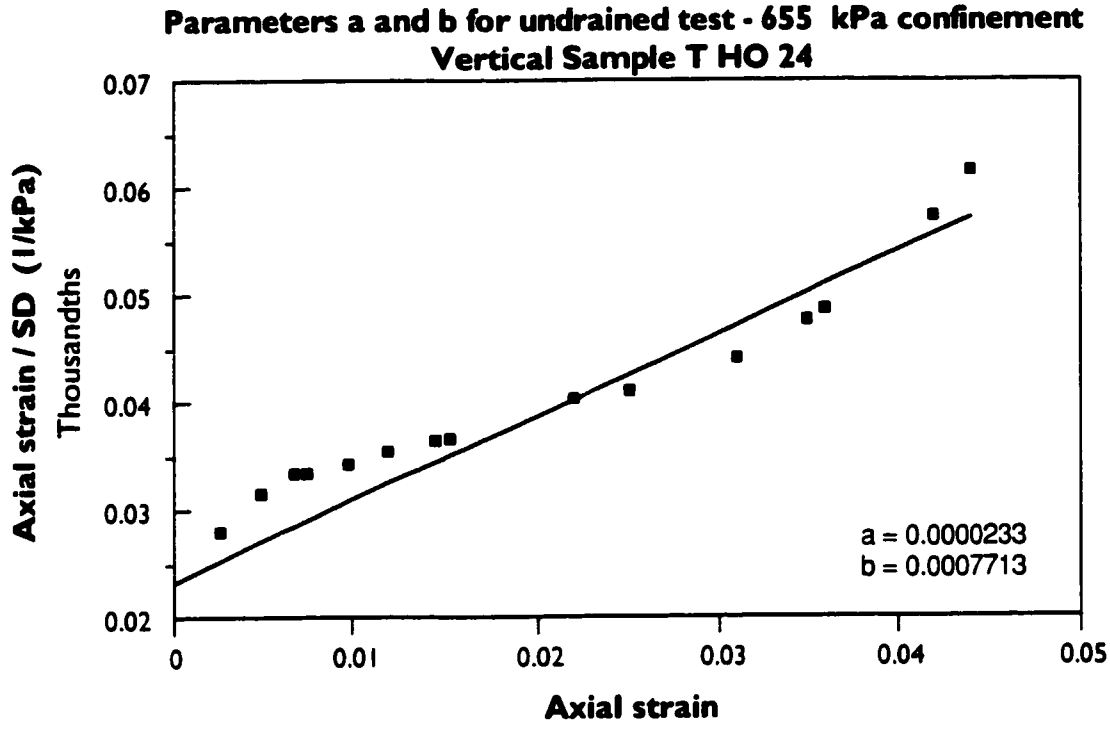

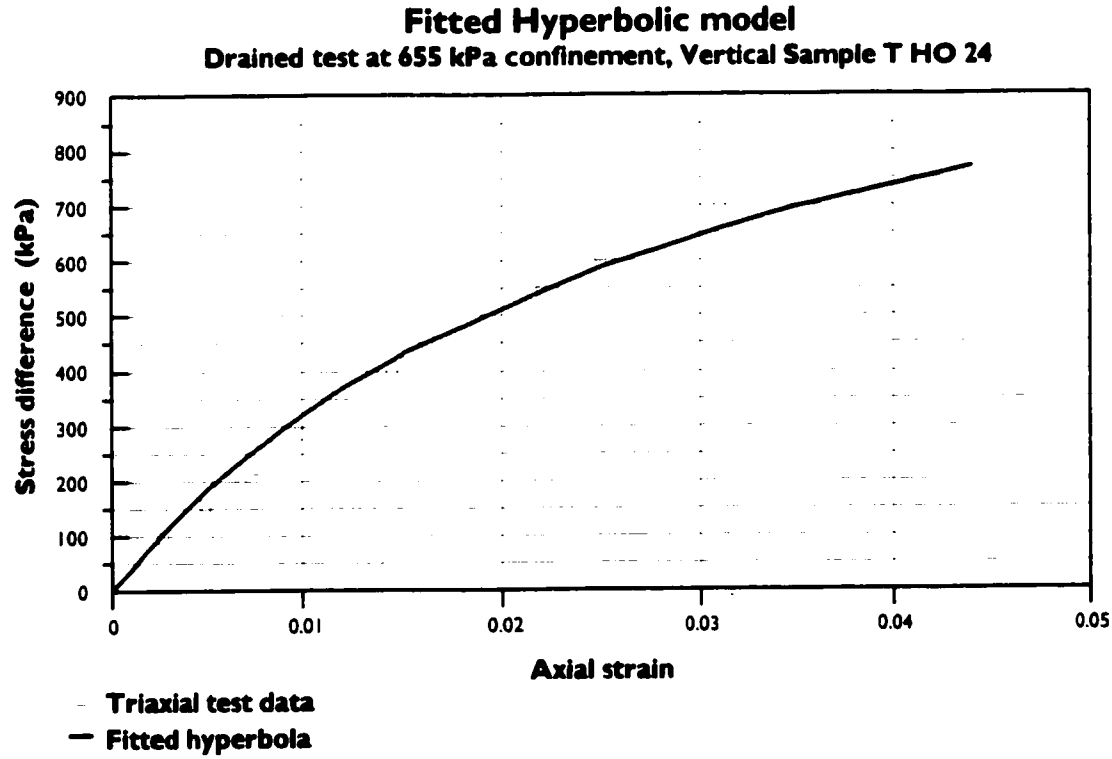

Figure 3-4: Hyperbolic stress-strain representation - Sample T HO 24

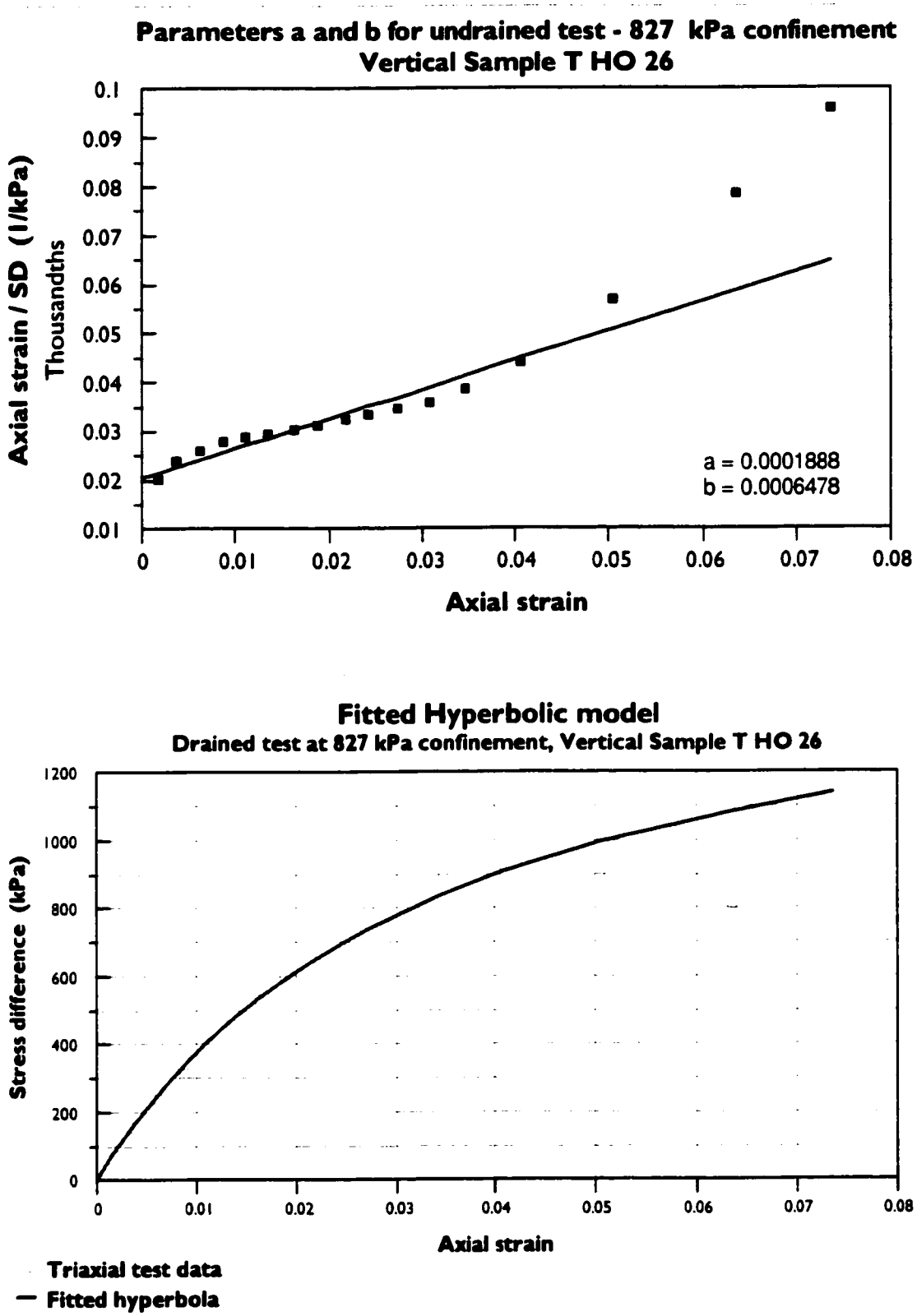

Figure 3-5: Hyperbolic stress-strain representation - Sample T HO 26

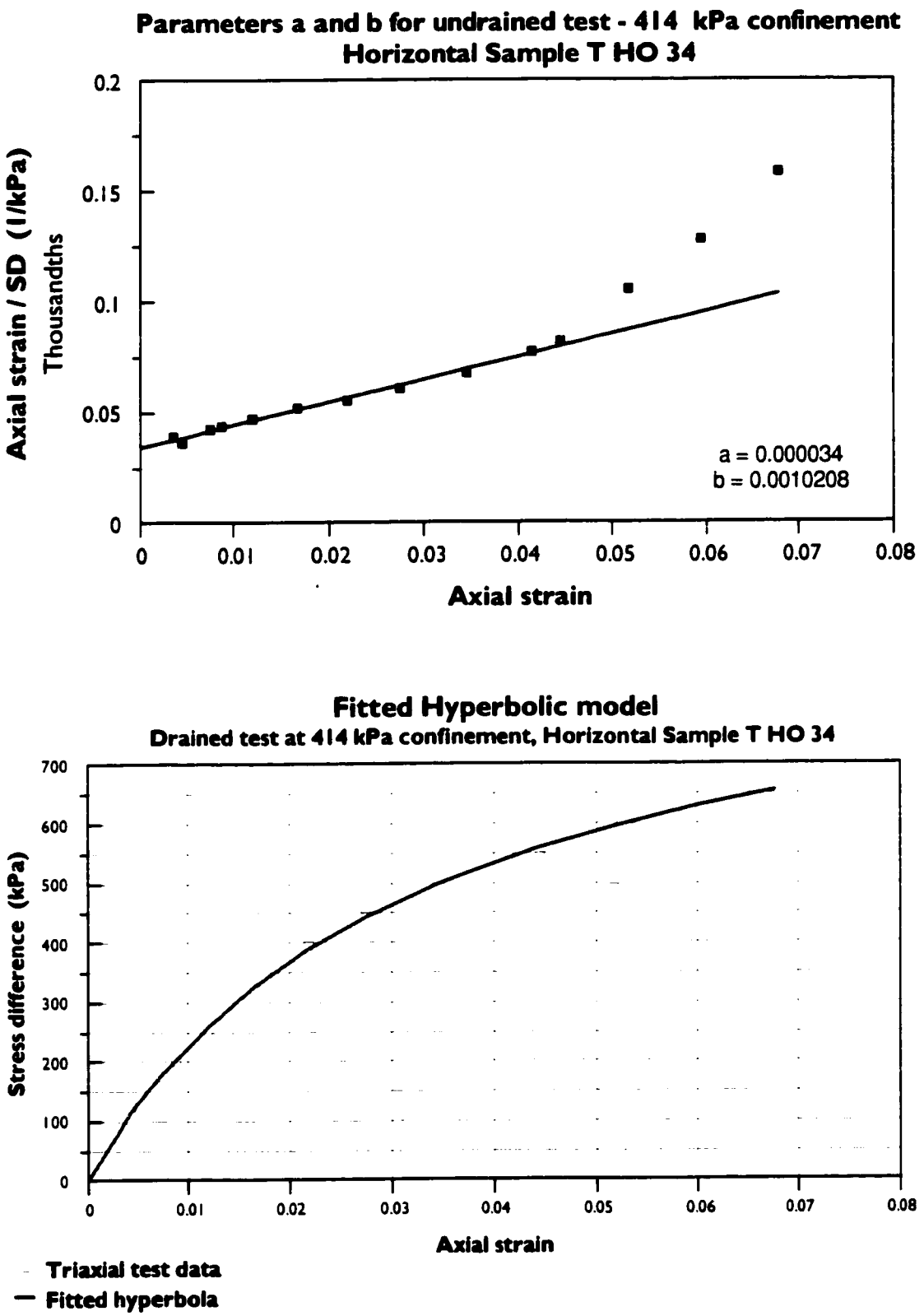

Figure 3-6: Hyperbolic stress-strain representation - Sample T HO 34

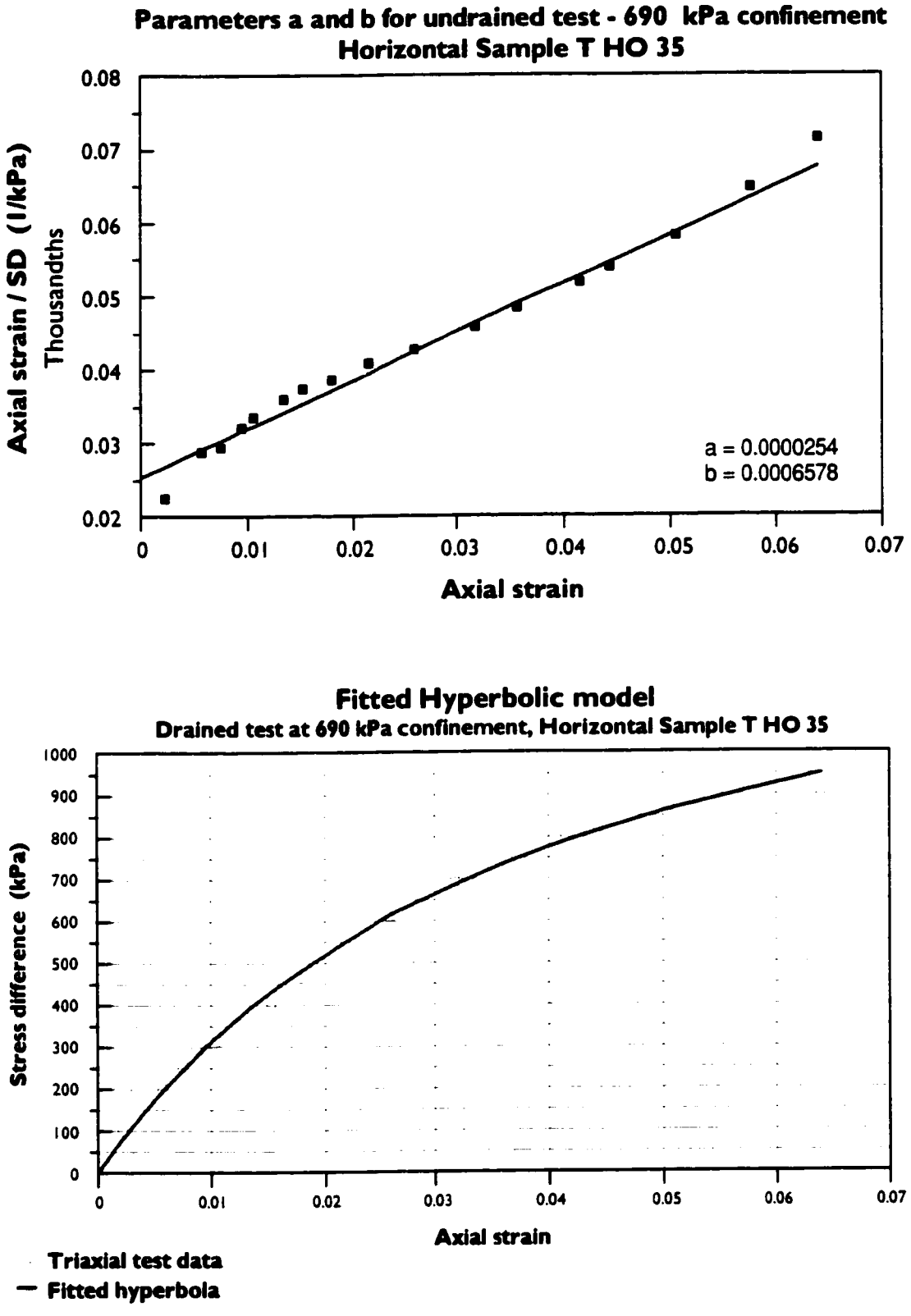

Figure 3-7: Hyperbolic stress-strain representation - Sample T HO 35

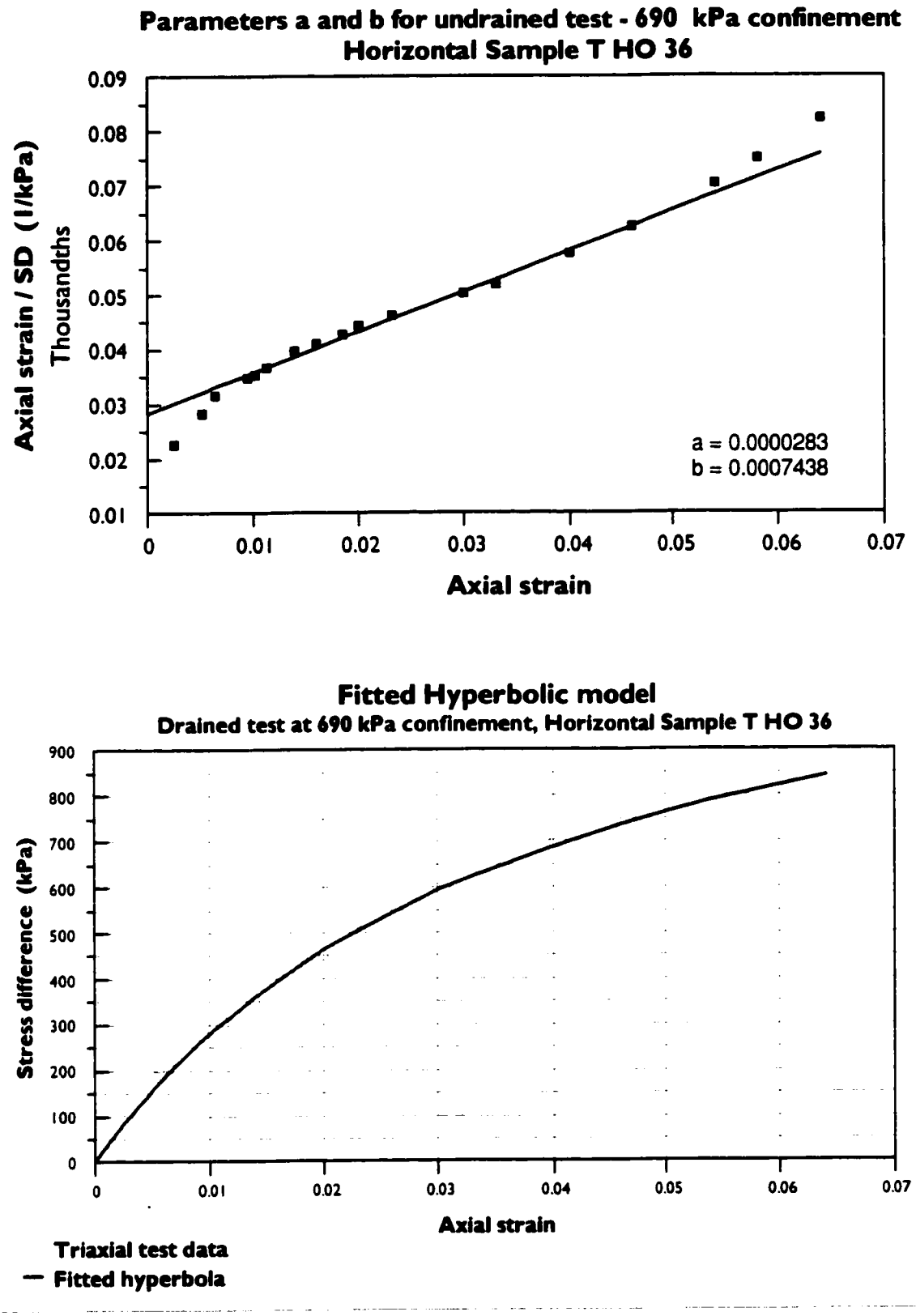

Figure 3-8: Hyperbolic stress-strain representation - Sample T HO 36

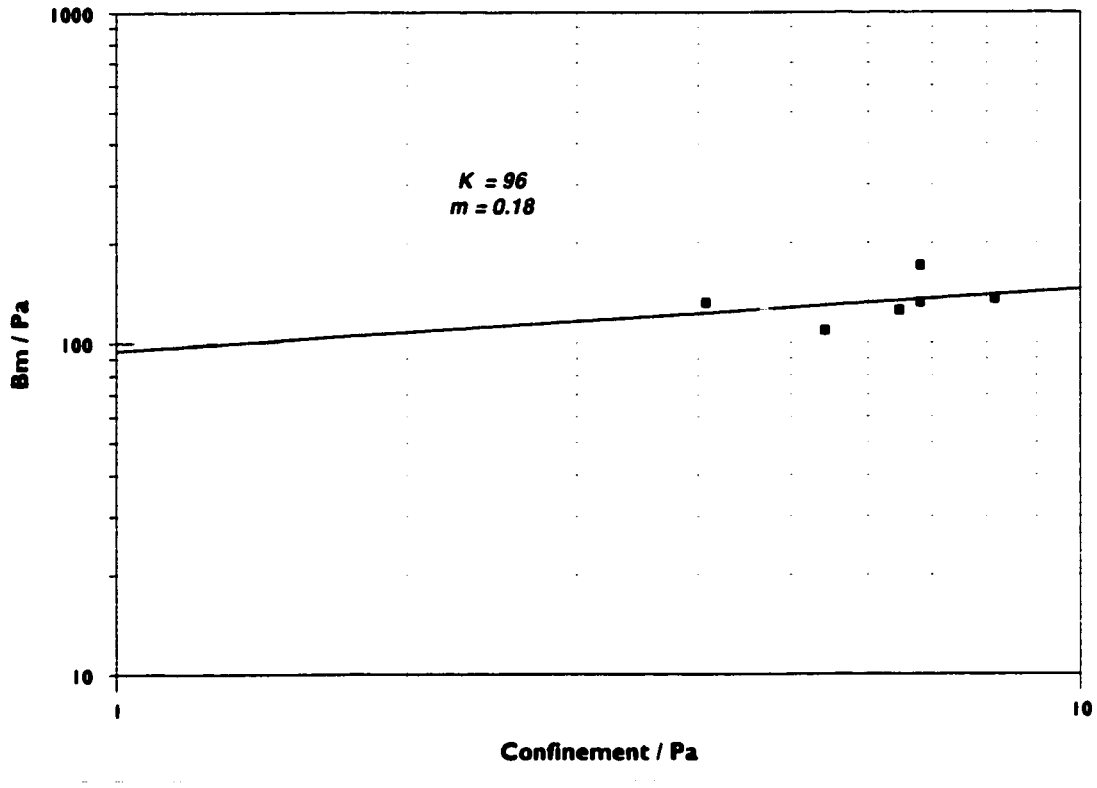

Figure 3-9: Bulk modulus number and exponent

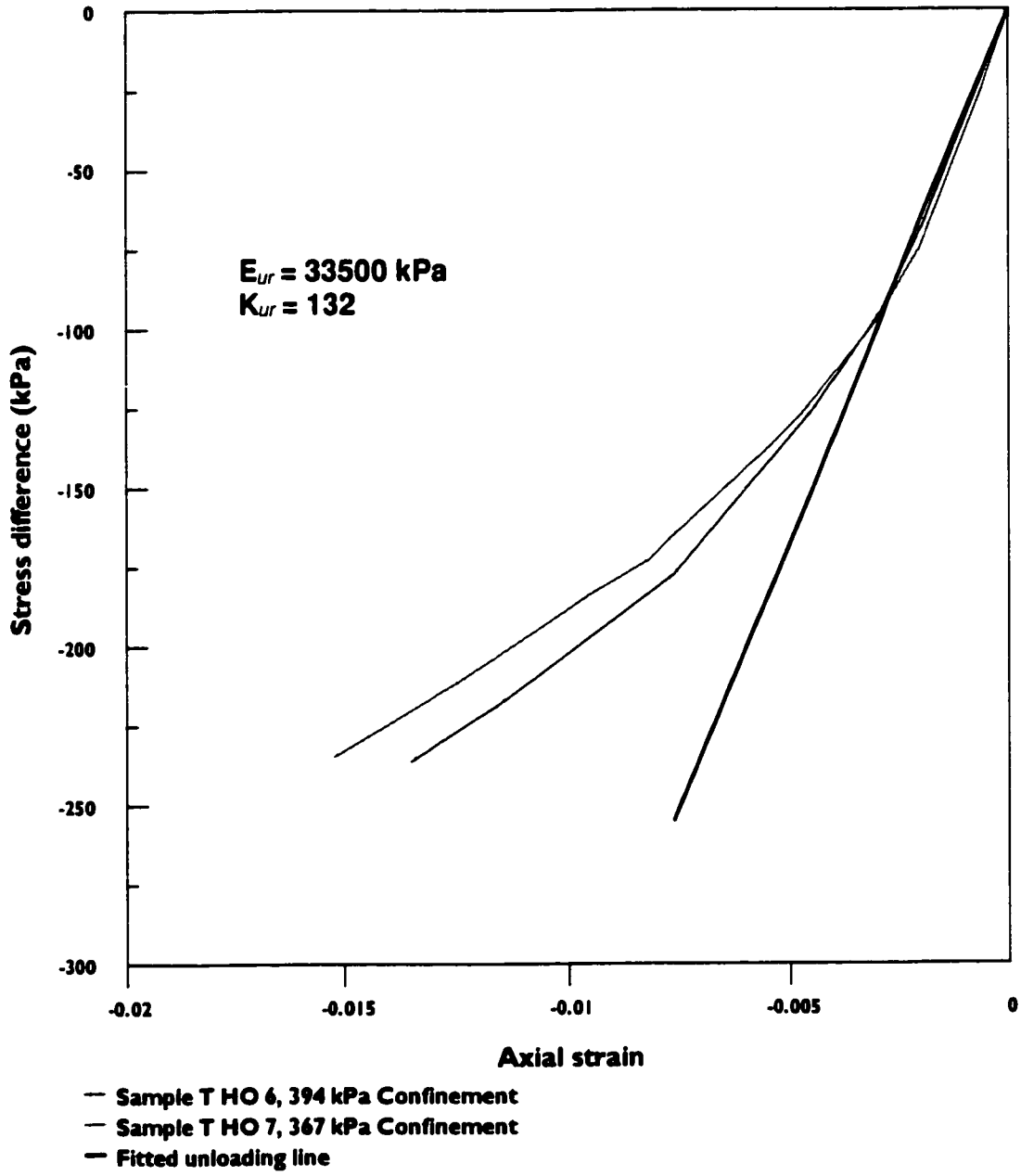

Figure 3-10: Unloading-reloading modulus number

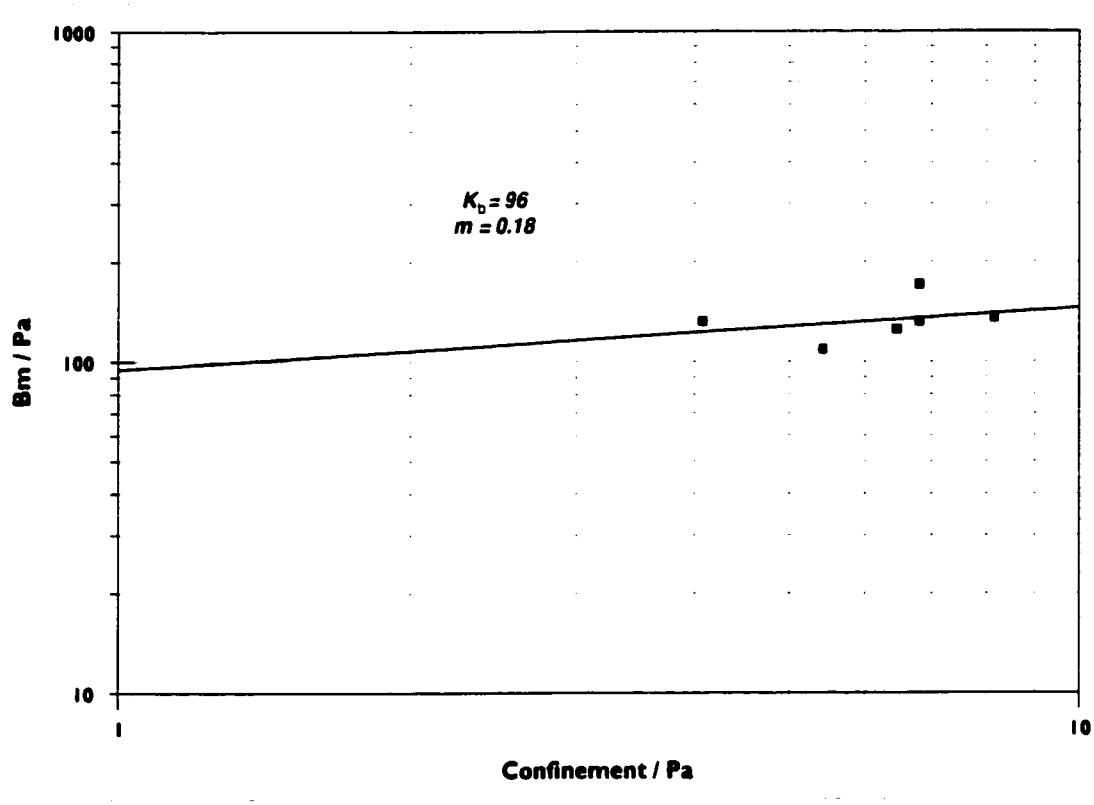

Figure 3-11: Bulk modulus number and exponent

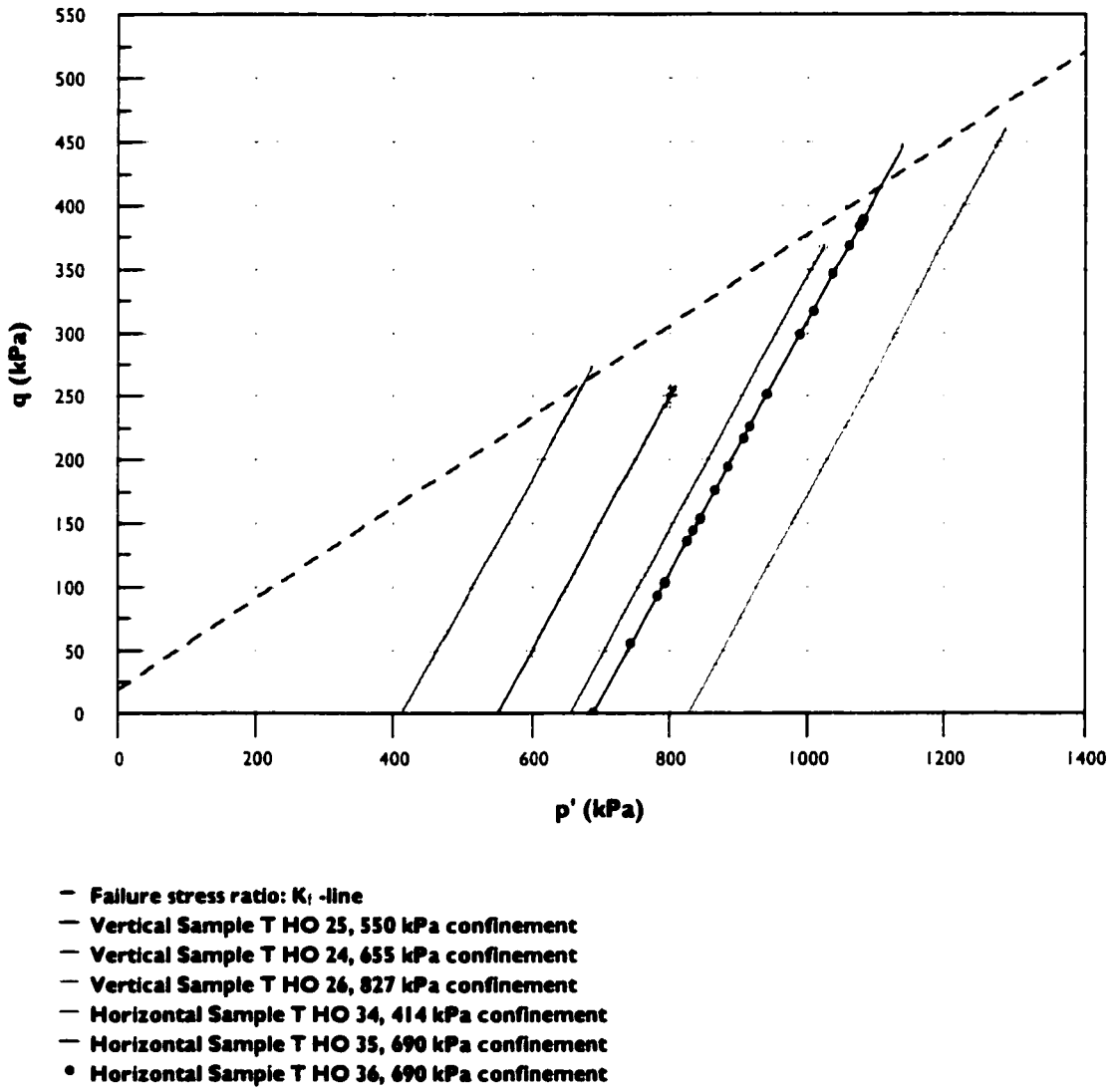

Figure 3-12: Stress paths - Drained triaxial compression tests (Som, 1968)

CHAPTER 4

PRELIMINARY EXCAVATION ANALYSIS

CHAPTER 4

PRELIMINARY EXCAVATION ANALYSIS

4.1. INTRODUCTION

Subsequent to the determination of soil parameters in the preceding chapter, it is necessary to investigate the feasibility, in this model soil (London Clay), of construction procedures intended for this research.

The analyses to be performed in this research involve simulating a trench excavation in overconsolidated London clay soil, as a first step. Subsequent analyses simulating the installation of a steel pipeline section and backfilling in the excavated trench will be carried out. These are coupled stress-deformation and consolidation analyses that will be extended to represent a significant period time after construction (as long as four years).

At this stage, some of the analysis limiting conditions can be established using a simple finite element model to avoid time consuming trial and error procedures. A coarse finite element mesh with a limited number of nodes is created to simulate the trench excavation. The main objectives of this preliminary analysis are:

- Establish adequate boundary conditions in terms of the distance between the construction zone and the physical boundaries with fixity
- Establish the level of clay overconsolidation (K_o value) that can be modeled while a stable unsupported trench is excavated
- Evaluate the sensitivity of the problem to the time duration between excavation and backfilling. This is necessary for selecting an adequate duration to avoid unnecessary computing time

4.2. THE FINITE ELEMENT MODEL

The intended trench excavation is 1.5 m wide by 2 m in depth. Figure 4-1 shows a simple two-dimensional finite element mesh with quadrilateral and triangular elements all with secondary nodes at the center of each side. Vertical boundaries with restricted horizontal displacement are imposed 10.5 m left of the intended trench centerline and 15.5 m to the right of the centerline. A horizontal boundary with restricted horizontal and vertical movement is imposed at 10 m depth below ground surface.

The water table is assumed to be at the level of the trench bottom (2 m below surface). A thickness of 1 m is given to the finite elements in this plane strain problem. The model cross-section extends 10.5 m to the left of the excavation centerline and 15.5 m to the right of the excavation centerline. Since the excavation problem is symmetrical, the effect of the cross-section extents boundary can be evaluated by comparing the results computed on either side of the trench.

Also indicated in Figure 4-1 are eight nodes at which the analysis results will be reported.

4.3. ANALYSIS PROCEDURE AND RESULTS

In–situ conditions are obtained with different K_o values varying from 0.5 through 4.0. The simulated excavation was then performed in three stages assuming fast soil removal (about 7 minutes to end of excavation).

With the in–situ conditions corresponding to $K_o = 3$, a numerical instability was encountered at the end of excavation. This indicates that the resulting trench is unstable without shoring or other support. A Ko value of 2.0 was then selected for the remainder of the study.

From in–situ initial conditions corresponding to $K_o = 2$, the analysis was continued for about 27 hours after the excavation to investigate the evolution of stresses, strains, movements, and pore water pressure surrounding the trench and to evaluate the effect of boundary conditions.

4.3.1. Conditions across the analyzed section

Contours of pore water pressure throughout the analyzed cross-section, immediately after the end of excavation, as well as 1 hour and 27 hours after the end of excavation are presented in Figures 4-2, 4-3, and 4-4, respectively. As shown in Figure 4-2, significant negative pore water pressures are generated on each side of the trench, up to a distance of about 5 m from the trench wall, as well as within 0.5 m below the trench base. Also, an increase in pore water pressure from hydrostatic steady state conditions is computed beyond 0.5 m below the trench base. This increase in pore water pressure tapers down as we move horizontally away from the trench centerline, reaches the initial hydrostatic level at about 2 m from the trench centerline and reverses to a gradual reduction from hydrostatic conditions beyond that point This is due to sudden expansion of the surrounding soil as a result of relieving the locked-in horizontal stresses. Figure 4-3 shows that most of the negative pore water pressures have dissipated within an hour after the excavation, however, the pore water pressure fluctuations below the level of the trench base remain almost unchanged even after 27 hours as shown in Figure 4-4.

Contours of horizontal and vertical displacement throughout the modeled cross-section, 27 hours after the excavation, are presented in Figures 4-5 and 4-6, respectively. Negative horizontal displacement is in the direction of decreasing x-axis, while negative vertical displacement is in the direction of decreasing y-axis.

The distribution of horizontal and vertical effective stresses, 27 hours after the excavation, are presented in Figures 4-7 and 4-8 respectively.

4.3.2. Reference points

As mentioned earlier, eight control points corresponding to nodes on the finite element mesh are selected to view the computed conditions with time during and after the simulated excavation.

These nodes are shown in Figure 4-1 and are located as follows:

Node #	Depth m	Distance from trench wall m
960	1	0.75
1127	1	1.75
1282	1	4.75
1387	1	9.75
952	2	0.75
1123	2	1.75
1278	2	4.75
1348	2	9.75

Figures 4-9 and 4-10 show the change in pore water pressure at the reference points during the staged excavation and a short time after during the early recovery. At the mid-height level of the trench (Figure 4-9), all four points, initially under negative pore water pressure of about -10 kPa, show an increase in pore water pressure during the removal of the top soil layer followed by a gradual reduction starting about half way into the soil removal. By the end of the excavation, the pore water pressure at 4.75 m from the trench wall was back to about the initial pressure while the closer points went below initial level and the further point retained a good increase in pressure. A fast rebound is observed at all four points immediately after the excavation end, within about 10 minutes, where the pressure increased to about 3 to 5 kPa above initial conditions. A much slower rate of change in pore water pressure was observed beyond that point.

At the level of the trench bottom (Figure 4-10), initially at 0 kPa pore water pressure, a significant amount of negative pore water pressure (about –30 kPa) is computed at 1.75 m from the trench wall at the end of excavation. A similar behavior but to a lesser degree is observed at 4.75 m. A fast recovery within about 10 minutes from the end of excavation is observed at both locations. Minor fluctuations in pore water pressure are observed at 0.75 m and 9.75 m from the trench wall throughout the excavation and afterwards. A minor change from initial conditions (slight reduction to negative pore water pressure) is computed at all four reference points, beyond 10 minutes from the end of excavation; further pressure changes are rather slow.

Pore water pressure computed at the reference points up to about 8.5 hours after excavation are presented in Figures 4-11 and 4-12. The figures show the rather slow rate of change in pressure.

Horizontal displacements at the reference points are shown in Figures 4-13 and 4-14, from the start of excavation until about 4 hours after excavation. During the excavation, all displacements are towards the trench (negative displacements). After the end of excavation, however, a slight rebound is observed at 4.75 m and 9.75 m from the trench wall. This rebound away from the trench continues at a slow rate while a movement towards the trench continues at 0.75 m and 1.75 m from the wall, also at a slow rate.

4.4. CONCLUSIONS

Although the analyzed problem is symmetrical, the finite element model of the cross-section was extended to a longer distance away from the trench on the right side. This uneven section (10.5 m from trench centerline on the left and 15.5 m on the right) was intentional to confirm adequate boundary conditions to be used for the continuation of this research. In general, it can be seen from plotted contours of the analysis results that a 30% shorter cross-section span left of the trench centerline had no significant effect on the analysis results around the trench zone in terms of violating the problem symmetry. A vertical boundary located at 15.5 m on either side of the trench centerline is therefore deemed adequate for further analysis. A horizontal boundary at 10 m depth is deemed adequate since no significant movement or stress changes are computed beyond the depth of 5 m below ground surface.

The results reported across the analysis section and at the reference points show that any changes in pore water pressure or any displacement occurring beyond 0.5 hour from the end of excavation, proceed at a very slow rate. Therefore, a delay of one day or less between the excavation and any backfilling activity or pipeline placement will not have a significant effect on pipeline soil interaction behavior. A modeled pipeline placement beyond 30 minutes from the end of excavation is deemed representative of actual pipeline construction.

Further details of soil behavior as a result of trench excavation are not in the scope of this research. The next chapter will present a modeling of trench excavation in a V-shaped depression, followed by pipeline placement and backfilling. The effect of the depression slopes and the pipeline section stiffness on the pipeline-soil interaction will be investigated.

FIGURES

CHAPTER 4

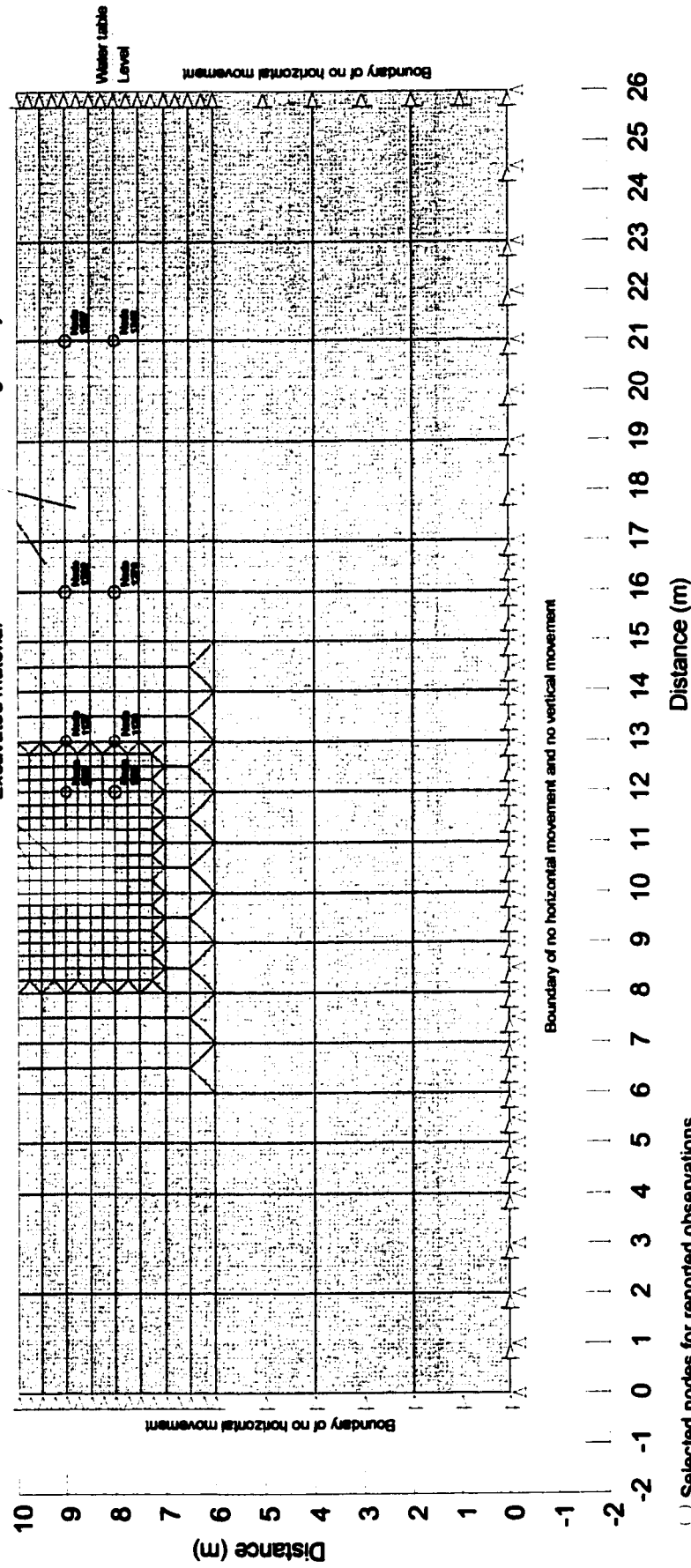

Figure 4-1: Finite element model for the preliminary excavation analysis

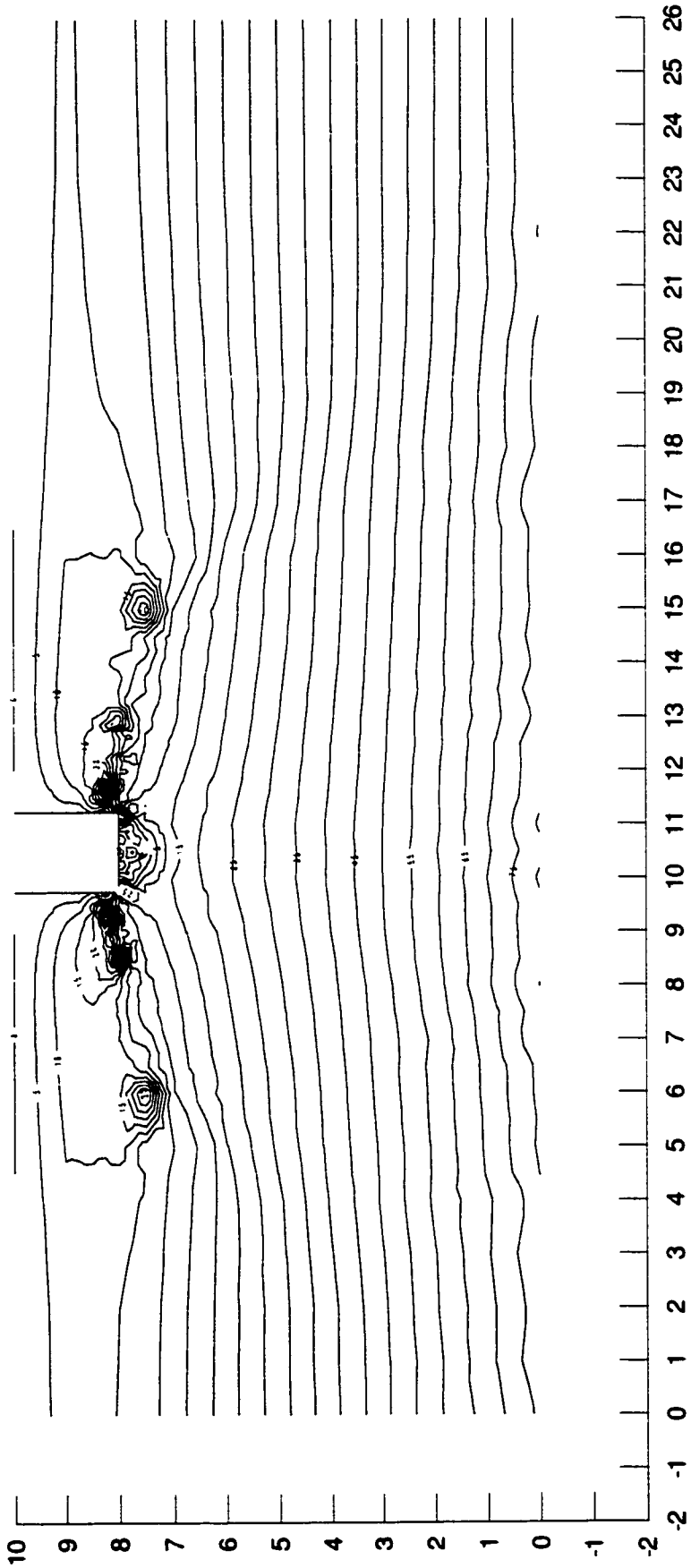

Figure 4-2: Pore water pressure contours (kPa), Immediately after the end of excavation

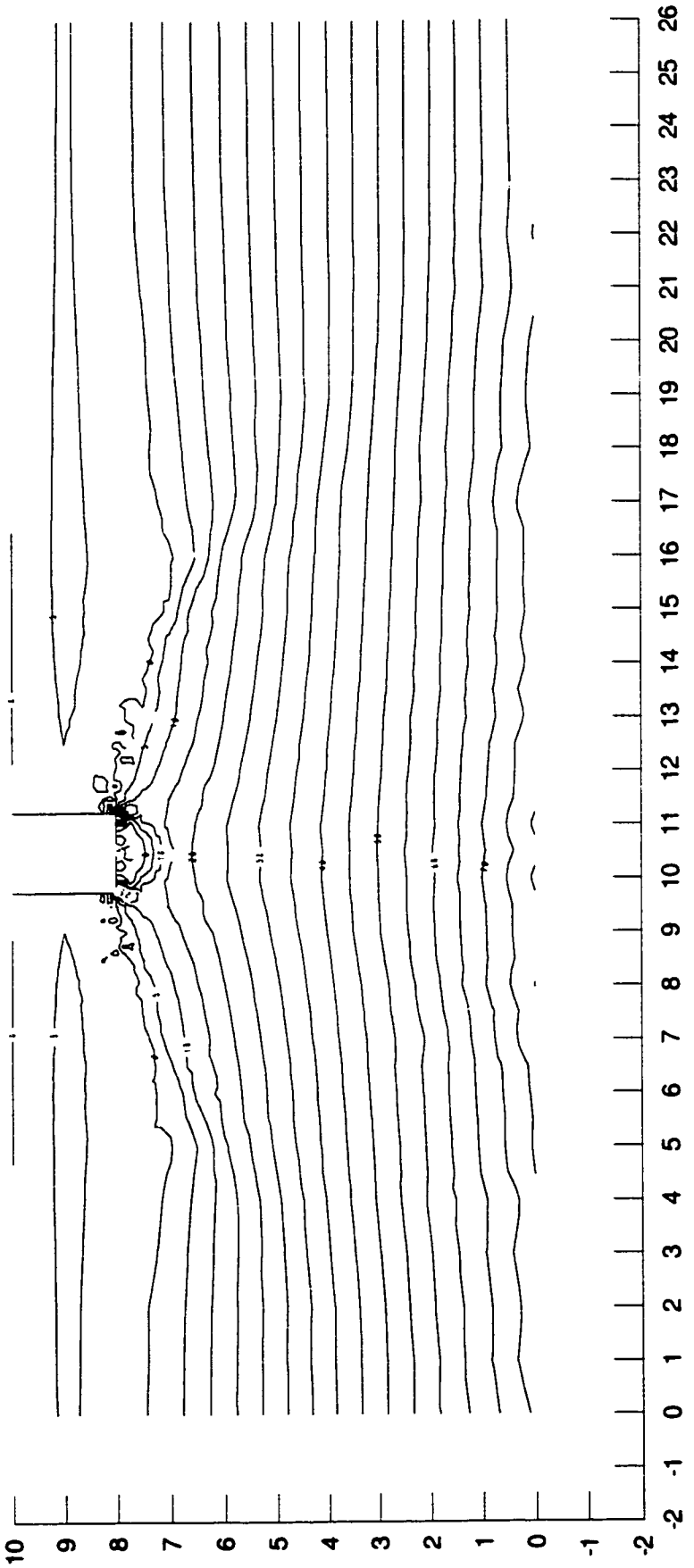

Figure 4-3: Pore water pressure contours (kPa), 1 hour after excavation

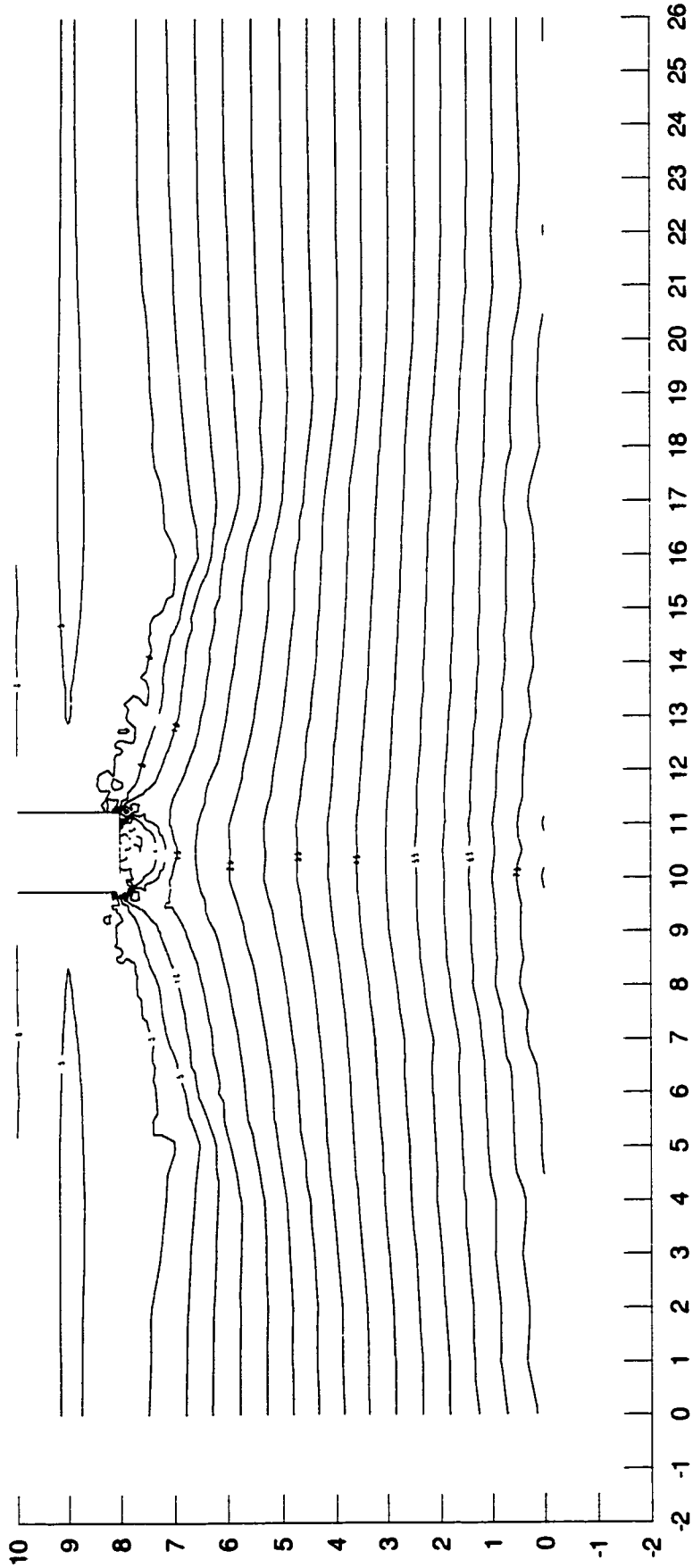

Figure 4-4: Pore water pressure contours (kPa), 27 hours after excavation

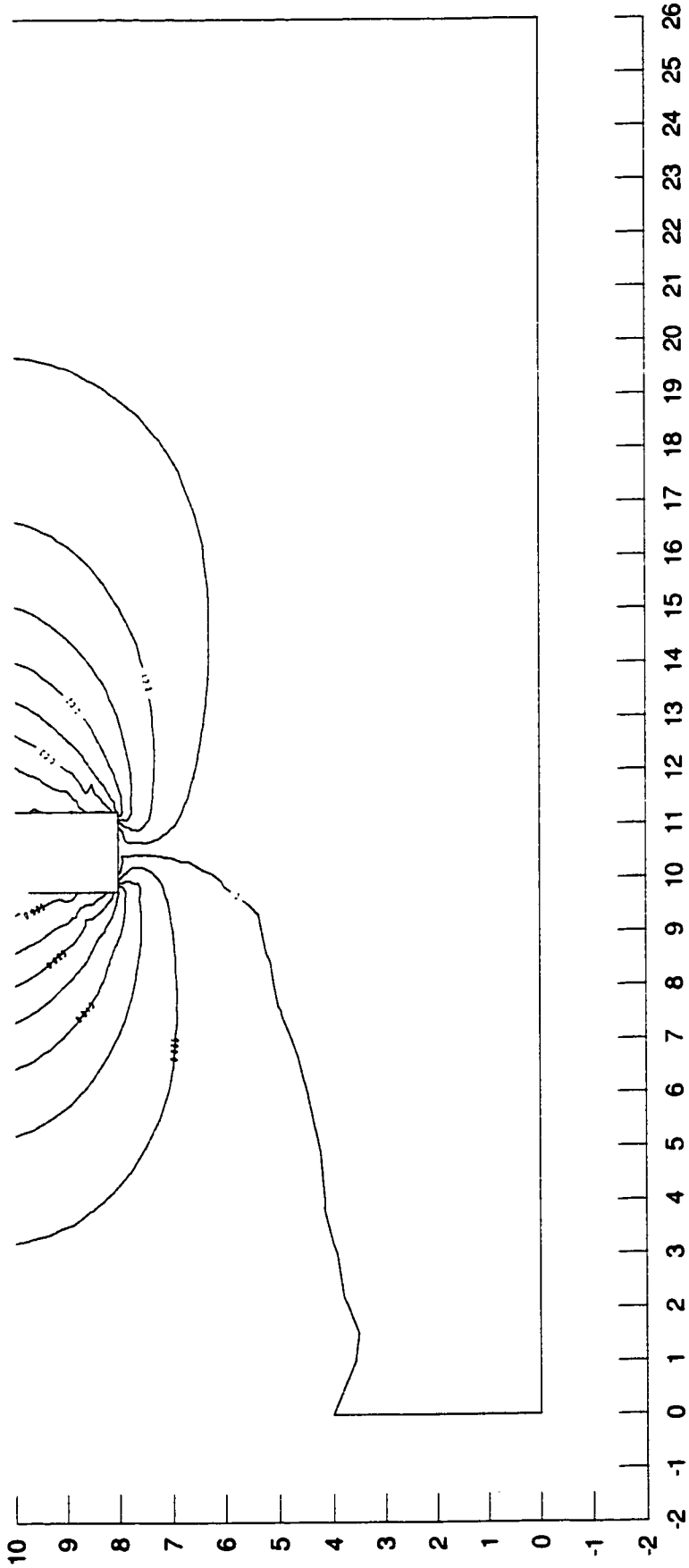

Figure 4-5: Horizontal displacement contours (m), 27 hours after excavation

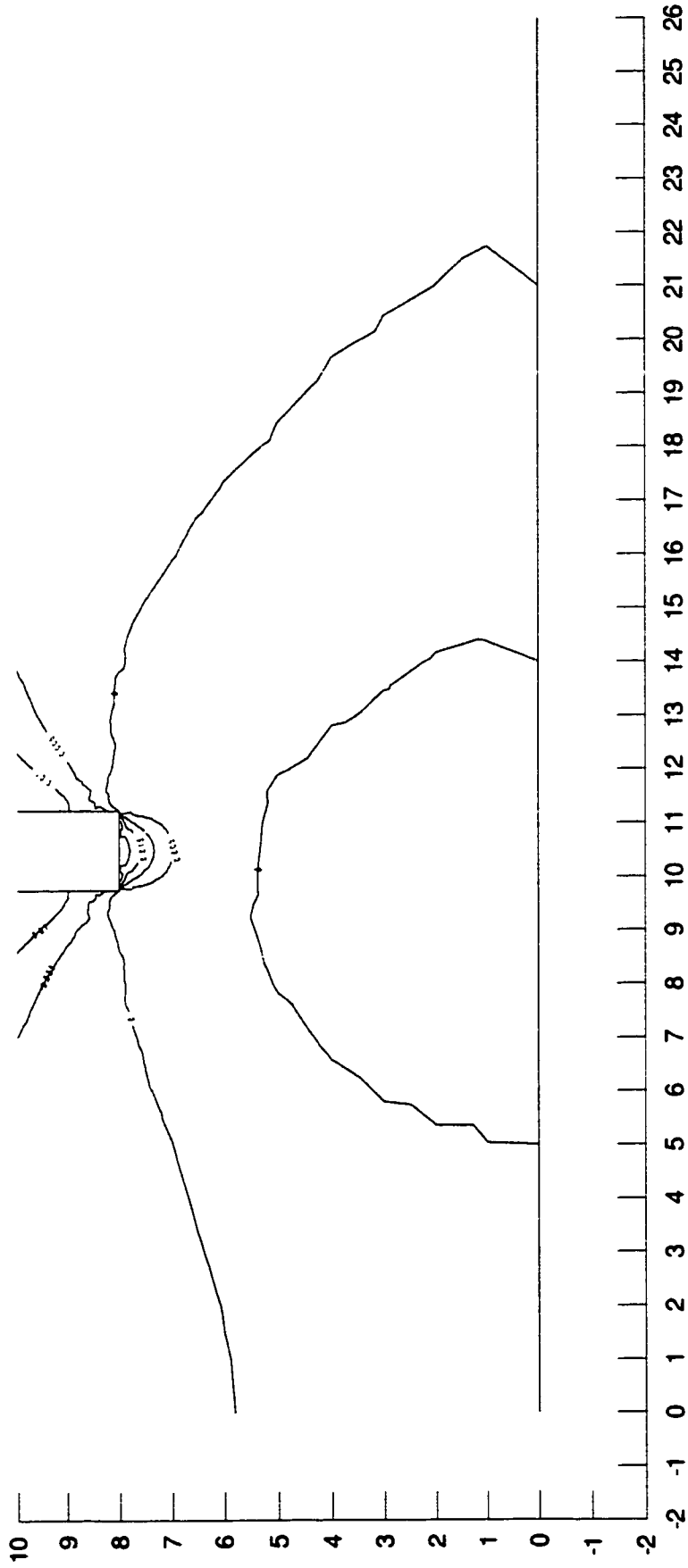

Figure 4-6: Vertical displacement contours (m), 27 hours after excavation

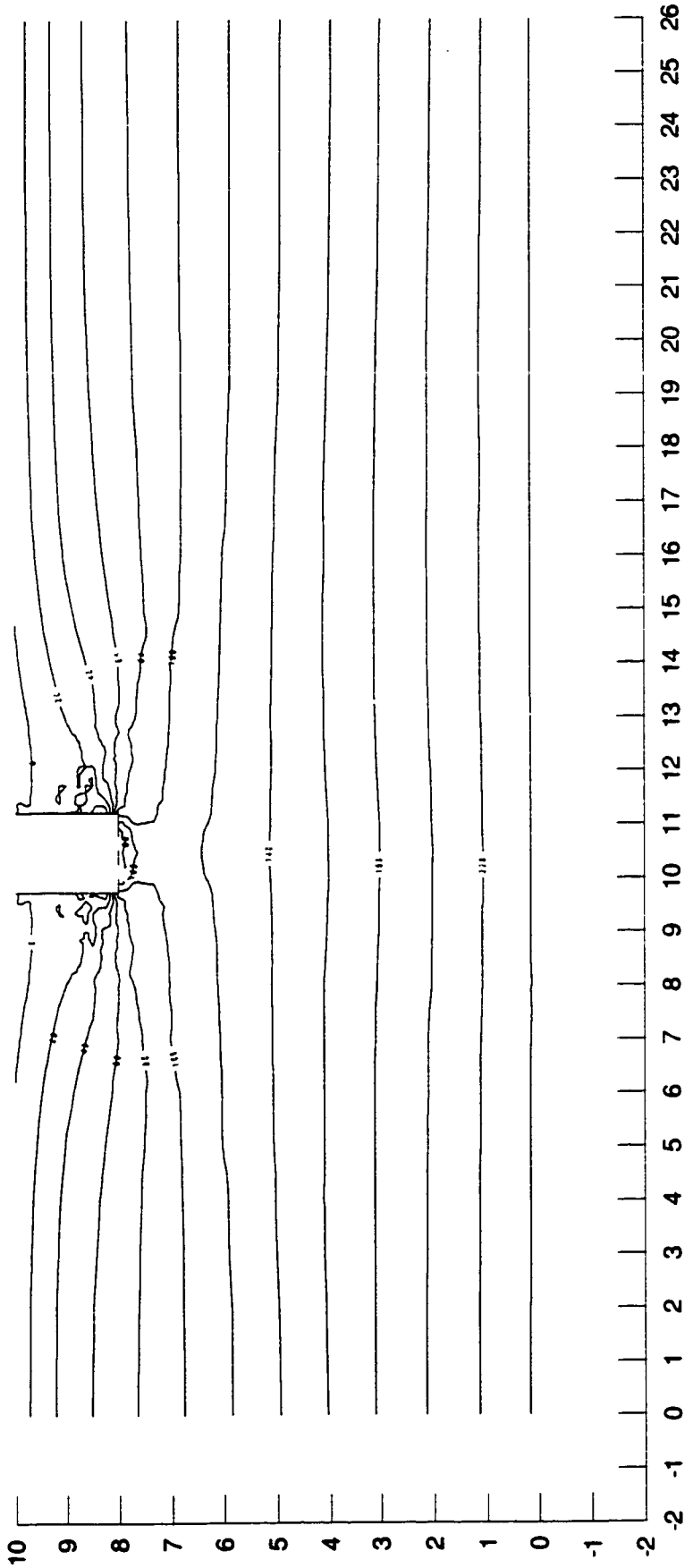

Figure 4-7: Horizontal effective stress contours (kPa), 27 hours after excavation

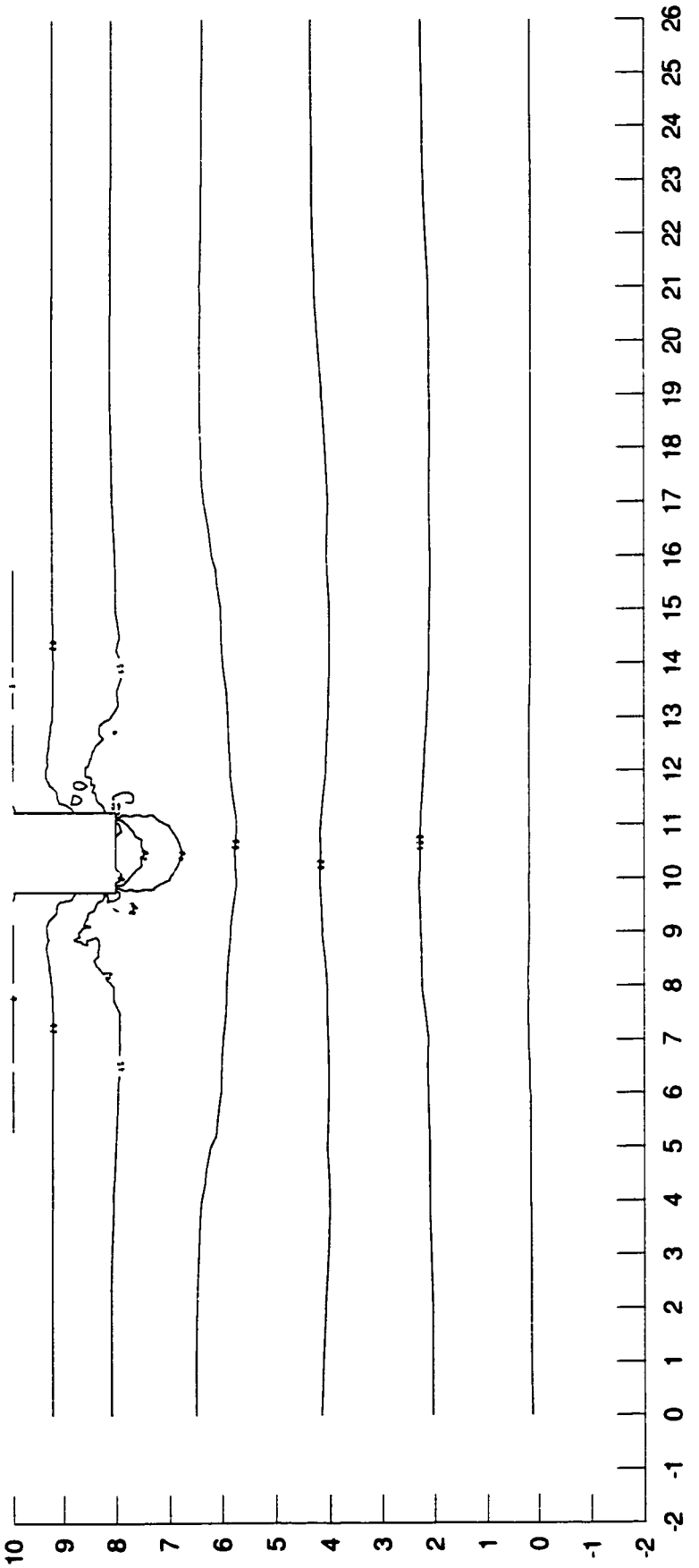

Figure 4-8: Vertical effective stress contours (kPa), 27 hours after excavation

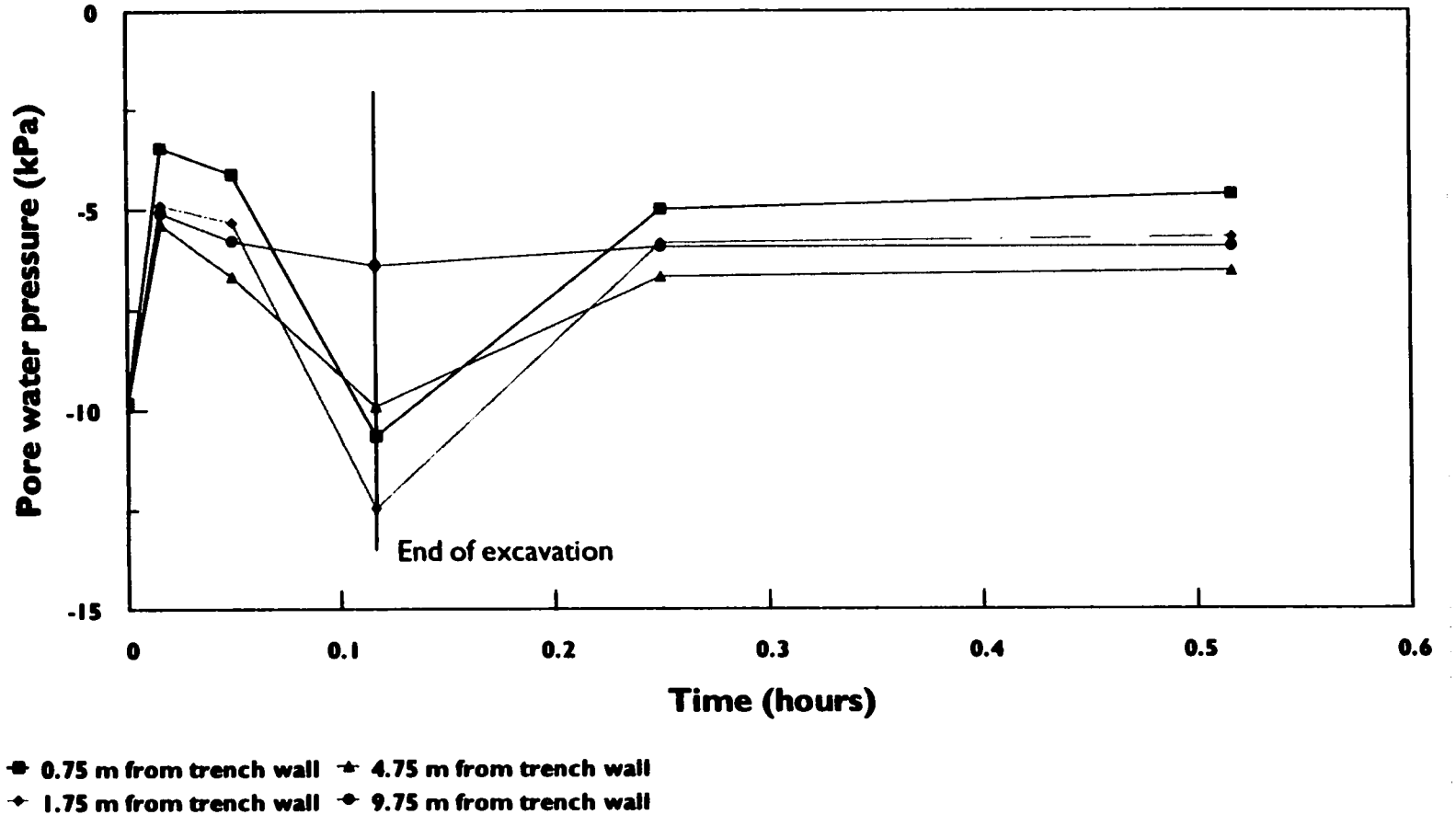

Figure 4-9: Pore water pressure during and immediately after excavation (within 0.5 hour, at the level of trench mid-height)

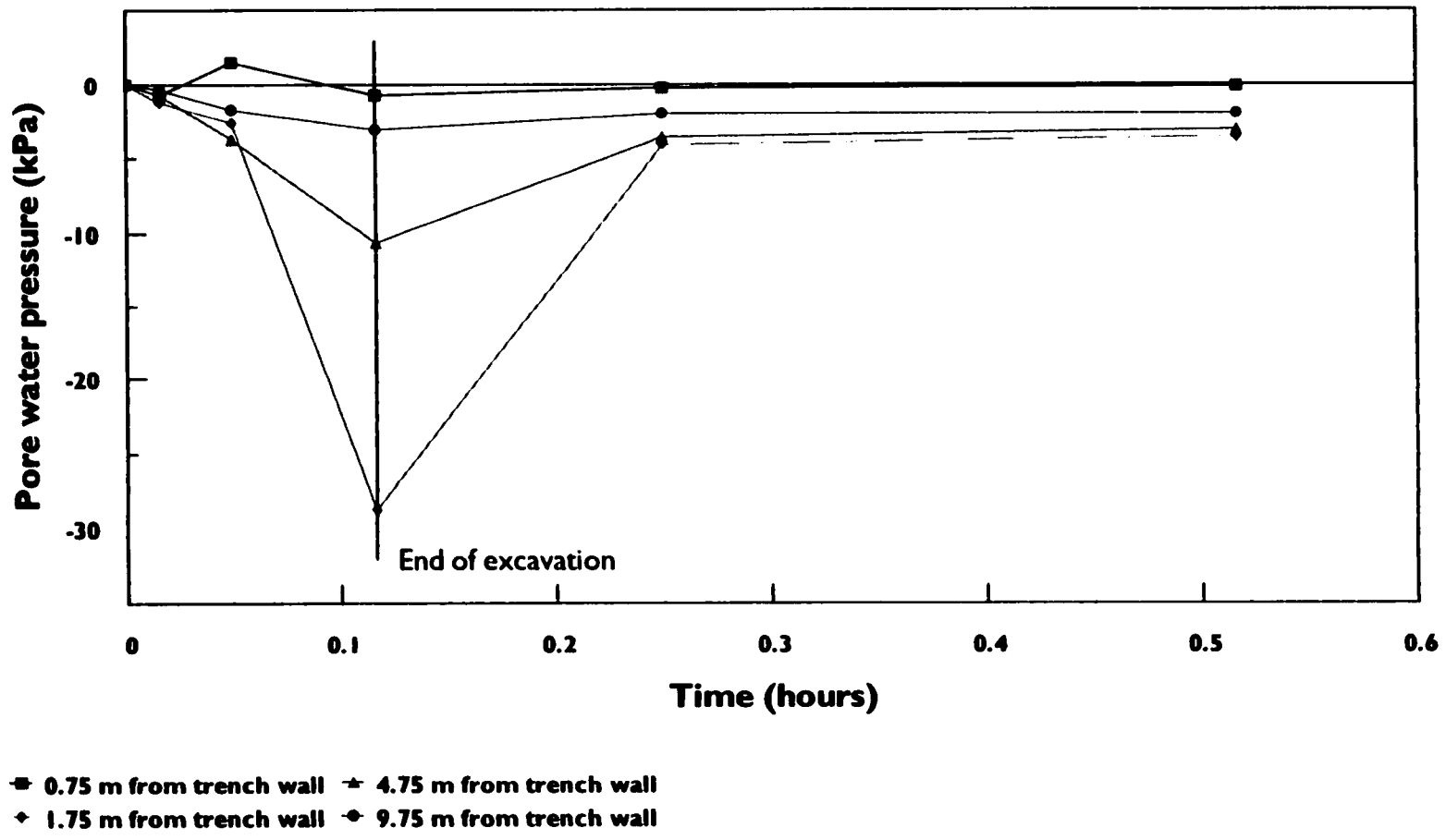

Figure 4-10: Pore water pressure during and immediately after excavation (within 0.5 hour, at the level of trench bottom)

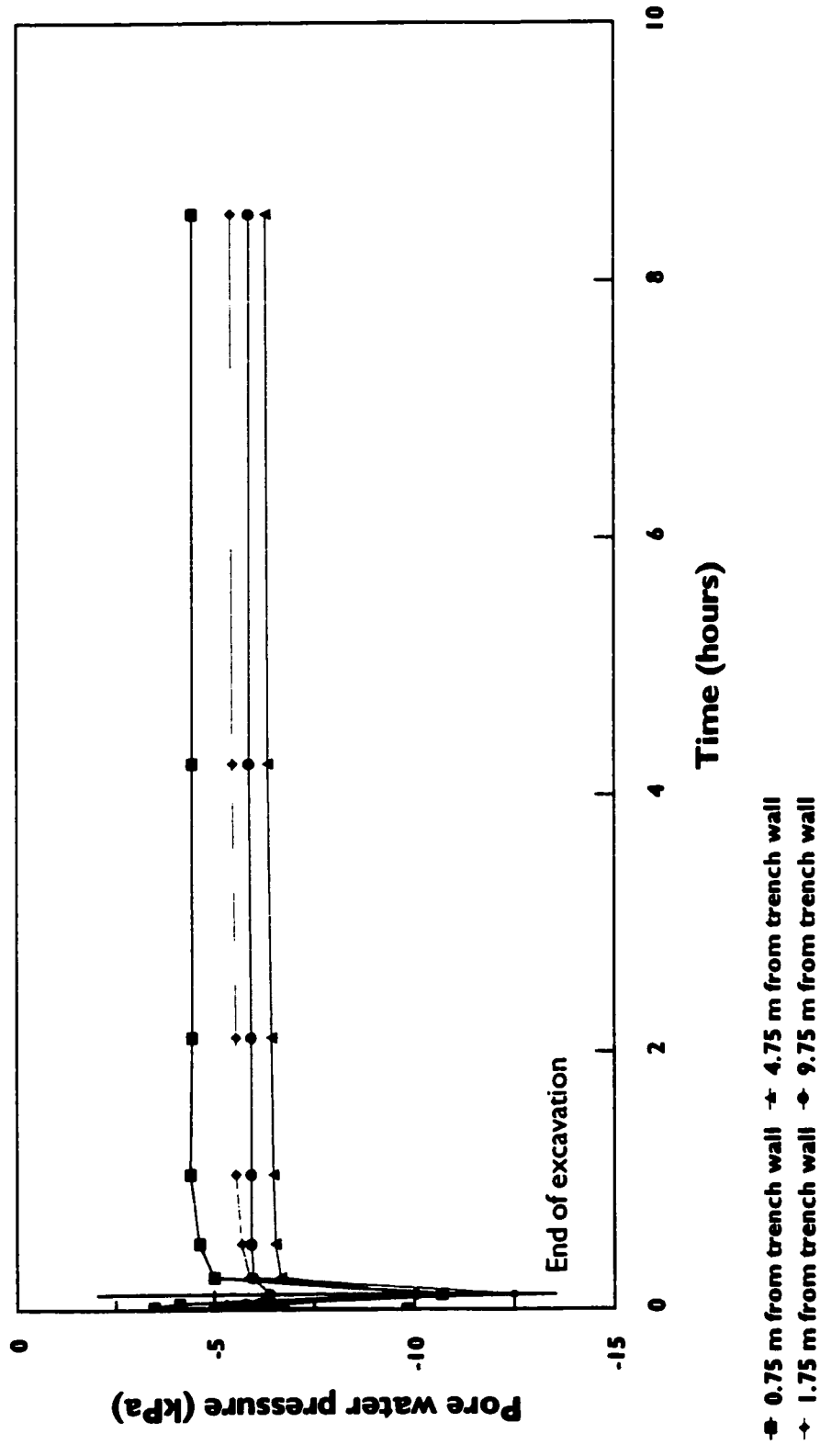

Figure 4-11: Pore water pressure during and after excavation (within 9 hours, at the level of trench mid-height)

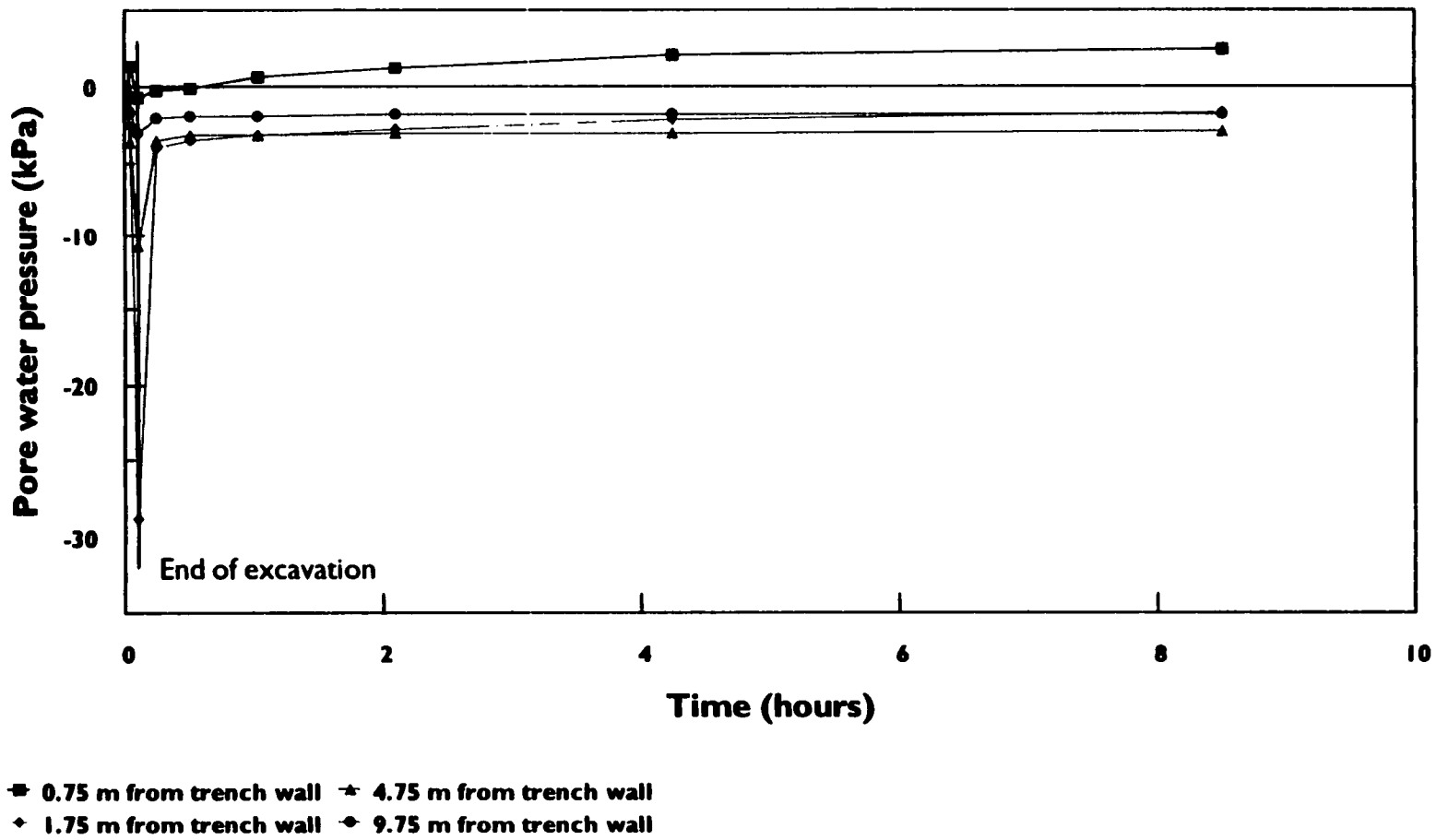

Figure 4-12: Pore water pressure during and after excavation (within 9 hours, at the level of trench bottom)

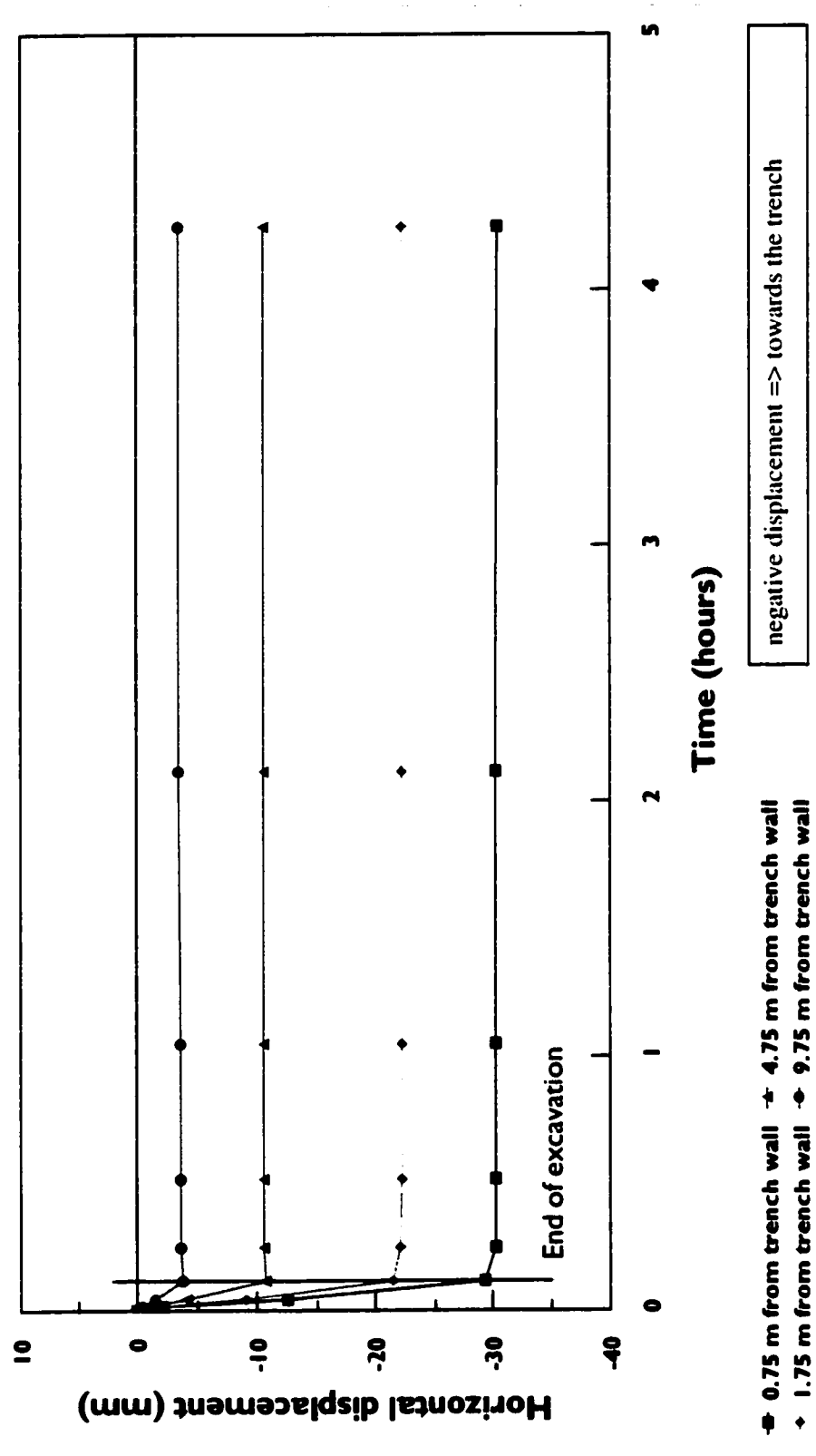

Figure 4-13: Horizontal displacement during and after excavation (at the level of trench mid-height)

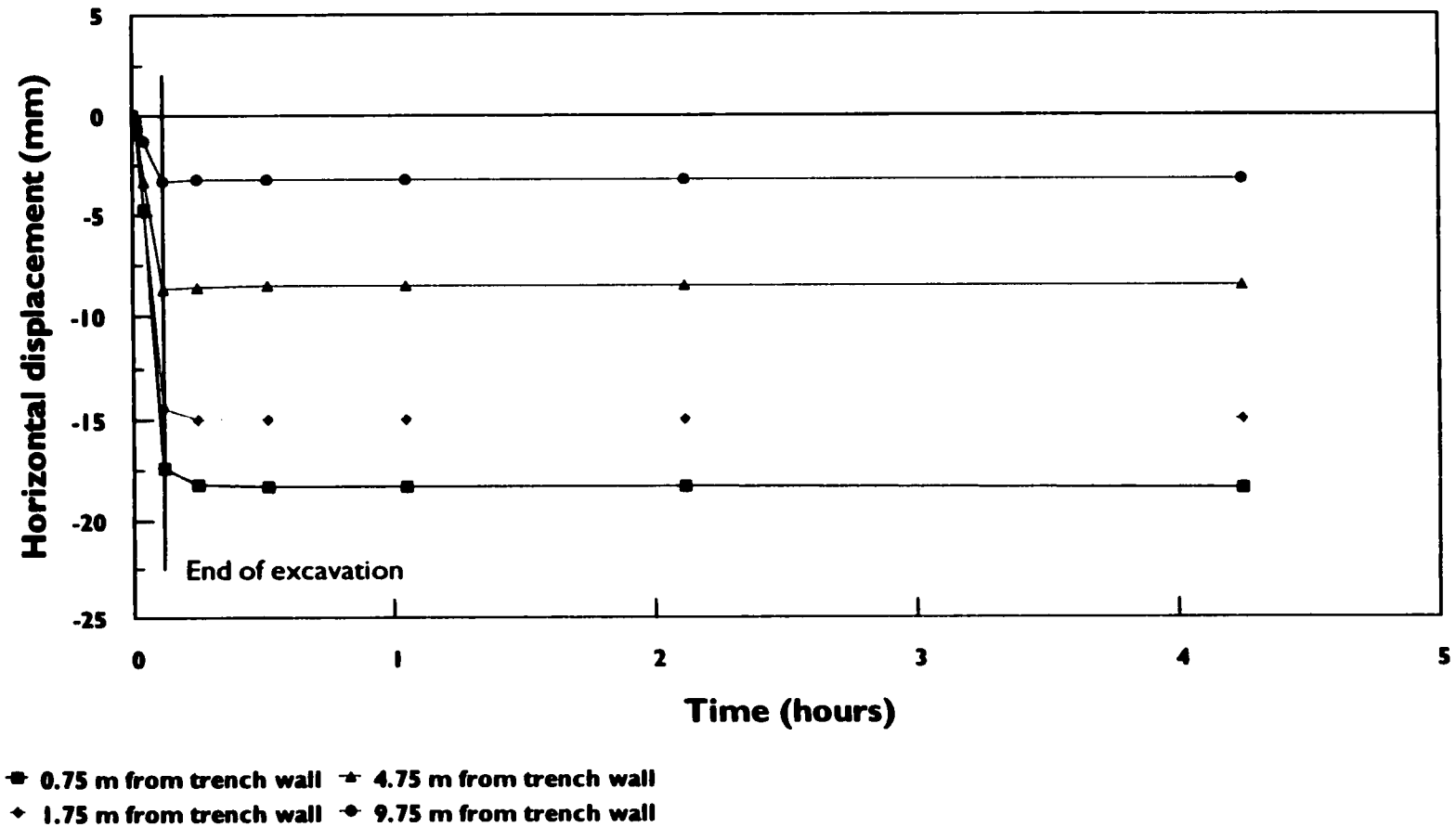

Figure 4-14: Horizontal displacement during and after excavation (at the level of trench bottom)

CHAPTER 5

PIPELINE INSTALLATION IN V-SHAPED DEPRESSION

CHAPTER 5

PIPELINE INSTALLATION IN V-SHAPED DEPRESSION

5.1. INTRODUCTION

Following the investigation presented in Chapter 4, it was established that a 2 m deep by 1.5 m wide trench can be excavated without support in overconsolidated London clay soil with $K_o = 2$ for placing pre-assembled pipeline sections and backfilling. Suitable boundary conditions were also verified for use in further analyses.

In this chapter, a more elaborate finite element model is used to simulate the sequence of excavating the trench, installing the pipeline segment, and backfilling, at the bottom of a V-shaped depression. The simulation is performed with three different magnitudes of the ground surface slopes toward the trench to investigate their effect on the pipeline/soil interaction.

The simulation performed in the following analyses considers the long term effects of construction procedures (excavation and backfilling). The change in pore water pressure, stresses, and strains, are evaluated for a period of about four years after the construction of the pipeline.

5.2. THE FINITE ELEMENT MODEL

As mentioned earlier, the analysis to be performed using this finite element model consists of simulating an unshored trench excavation and subsequent pipeline placement and backfilling operation. The same finite element mesh is used for all construction stages. Four analysis cases are presented in this chapter, studying the effect of level ground surface, as well as three different slopes for the sides of the v-shaped depression: 5.7° (10H:1V), 11.3° (5H:1V), and 20° (2.7H:1V) which is close to the internal friction angle of the London clay. Figure 5-1 shows the two-dimensional finite element mesh with 11.3° slopes. Quadrilateral and triangular elements all with secondary nodes at the center of each side were used in the mesh. The zone with the darker shade at the top center of the mesh represents the trench cross-section (2 m deep by 1.5 m wide). Vertical boundaries with restricted horizontal displacement are imposed 15.5 m from the trench

centerline. A horizontal boundary with restricted horizontal and vertical displacement is imposed at 10 m depth below ground surface at the trench centerline (8 m below the trench base).

The water table is assumed to be at the level of the trench base (2 m below surface). A thickness of 1 m is given to the finite elements in this plane-strain problem. Also indicated in Figure 5-1 are two nodes at which some results from the excavation analysis are reported. These nodes are located 0.75 m from the trench wall at the level of pipeline centerline and 0.75 m below the trench base under the pipeline centerline.

The pipeline indicated in Figure 5-1 is a steel pipeline of circular cross-section, 0.95 m in diameter and 25 mm wall thickness. The pipeline cross-section is simulated using a series of structural elements of the same dimensions and stiffness.

The hyperbolic model fitted to the London clay soil in previous sections is used in this study. Model parameters are summarized in Chapter 3.

5.3. ANALYSIS PROCEDURE

In–situ conditions are obtained with $K_o = 2$ for each of the four study cases (the various ground slopes). The timing and duration of construction stages are chosen to reflect actual field construction schedules. The simulated excavation is performed in two stages: The top 0.75 m of soil is removed over a duration of 10 minutes, then another 10 minutes is assumed for the rest of the trench to be excavated. The total duration of complete soil removal within the trench cross-section is therefore 20 minutes. The trench is kept open for another 40 minutes until the placement of the pipeline segment and backfill with the same London clay. The trench is therefore backfilled about 1 hour from the start of excavation. The stress-deformation-consolidation analysis is continued to simulate the time dependant effects of excavation, pipeline placement, and backfilling over the following 1440 days (about four years).

For this part of the study, uncompacted London clay backfill is considered. Compaction effects will be examined later in this study.

The same analysis sequence is repeated for each of the four cases which differ by the sloping angle of the ground on either side of the trench. The following notation will be used hereafter to refer to the analysis cases:

- Case 1: Level ground around the trench
- Case 2: 5.7° side slopes
- Case 3: 11.3° side slopes
- Case 4: 20.0° side slopes

Results of the four analysis cases are compared to evaluate the effect of sloping ground on induced pipeline stress level and pipeline/soil interaction.

5.4. RESULTS OF ANALYSIS CASES

5.4.1. EXCAVATION

Soil conditions across the model section are examined at one hour after the start of excavation. This would be the state of the soil surrounding the trench, just before the pipeline installation and backfilling. Pore water pressures, one hour after the start of excavation, are presented as contour lines across the model section in Figures 5-2 through 5-5, for each of the four cases. In all cases, high pore water pressure develops at the base corners of the trench. It is evident, however, from the contour lines that the excavation in level ground results in significantly higher pore water pressures than in the cases of sloping ground. In addition, the concentration of high pore water pressure in the level ground case is not just limited to the corners of the trench, in fact it extends as high as mid trench height. Once in a sloping ground case, the contour lines show that the developed pore water pressure drops significantly, but further change with increasing slope is not as appreciable.

Contours of accumulated horizontal displacement throughout the modeled cross-section, one hour after the start of excavation, are presented in Figures 5-6 through 5-9, for each of the four cases. The figures show that the horizontal displacement near the trench walls decreases with the increasing ground slope. Also, the zone subjected to noticeable horizontal movement, extends further away from the trench with smaller slope of surrounding ground. Negative horizontal displacement is in the direction of decreasing x-axis.

A vertical reference section through the model cross-section, 0.75 m from the trench wall, is used to examine the horizontal movement with depth during and after the excavation of the trench, until the time of backfilling (one hour from the start of excavation). Figure 5-10 shows the

evolution of horizontal displacement with time in the case of level ground. Similar results are presented for each of the three other cases in Figures 5-11 through 5-13. Figure 5-14 shows a compilation of the accumulated horizontal displacement for all four cases, one hour after the start of excavation. By examining Figures 5-10 through 5-14, the following observations can be made:

- Most of the resulting horizontal movement occurs during the removal of soil. Further movement beyond one hour from the start of excavation is very slow.
- The zone affected by horizontal displacement extends to a depth of twice the trench height, below the trench base.
- The point which exhibits the maximum horizontal movement in the case of level ground is at the ground surface. This point of maximum movement is deeper, the higher the ground slope around the trench.
- From Figure 5-14, it is obvious that the magnitude of horizontal movement around the trench, one hour after the start of excavation is higher with smaller slope of adjacent ground and particularly higher when the adjacent ground is level. This order is practically reversed at higher depth, starting about one meter below the trench base, however, the magnitude and variation in horizontal displacement between the four cases becomes less pronounced at this depth.

The evolution of horizontal effective stress at the observation points (see Figure 5-1), during and after the excavation, are presented in Figure 5-15. At the observation point located 0.75 m below the trench base, an increase in horizontal effective stress of about 20 kPa is observed in all four cases towards the end of excavation. Further changes beyond the end of excavation are very slow. At the observation point located 0.75 m away from the trench wall, the horizontal effective stress in the three cases with sloping ground drops to about 20 kPa towards the end of excavation and proceed with very slow changes. In level ground, however, a somewhat different behavior is observed whereby the horizontal effective stress reduces slowly during excavation (about 5 kPa reduction), then continues to drop at an accelerated rate after the end of excavation for about 20 minutes (an additional drop of about 25 kPa). Further reduction is observed beyond that point, however, at a very slow rate.

Accumulated horizontal strain at the observation point located 0.75 m away from the trench wall are shown in Figure 5-16. Expansion strains of about 1 % are computed in all cases towards the end of excavation. Further expansion after the end of excavation proceeds at a very slow rate

with the exception that in the case of level ground, the rate of expansion after the end of excavation continues to be noticeable whereby an additional expansion strain of about 0.5 % is accumulated in the 40 minutes after the excavation.

5.4.2. PIPELINE PLACEMENT AND BACKFILLING

As mentioned earlier, the initial conditions for this analysis stage are the computed conditions of the section with excavated trench, one hour after the start of excavation (i.e. 40 minutes after the end of excavation).

5.4.2.1. Pipeline deformation

The first effect to examine is the pipeline deformation with time. Pipeline compression is defined as the relative displacement between two edges of the same diameter line. The computed vertical compression for all cases are presented in Figure 5-17. The magnitude of the compression is very small (less than 1 mm) due to the relatively high stiffness of the pipeline; however, the effect of the sloping ground is obvious. The results for all cases show an immediate compression after backfilling followed by a gradual rebound over the following 50 to 100 days. The rebound that follows backfilling is expected due to consolidation and flow of the soil underlying the pipeline, which is a time dependant process. The immediate compression after backfilling and the initial rebound is a behavior observed in all cases since it is mostly related to the fast backfilling and the soil's reaction to the new imposed loading. After 50 to 100 days, the rebound of the pipeline section gradually ceases, with the exception of Case 2 (5.7° slopes) in which it proceeds at a slow rate. In Case 1 (level ground), the rebound ceases completely about 50 days after backfilling and the pipeline reverses back to a gradual compression which stabilizes about 600 days after, around the same level computed before the first rebound. In Case 2, as mentioned earlier, the rebound from the initial compression continues past the first 50 days and throughout the analyzed duration of 1440 days, although at a much slower rate. In Cases 3 and 4, the initial rebound gradually stabilizes over about 200 days, a slight recompression of the section is observed over the following 200 days, then reverses back to a slow rate rebound which continues throughout the analysis period. The observed recompression is more noticeable in Case 4.

It is obvious from the results shown in Figures 5-17 and 5-18 that the behavior observed past the initial compression and rebound is directly associated with the long term effect of the excavation.

The soil mass further away from the trench continues to unload locked-in overconsolidation stresses for a long time, even if the trench is backfilled.

In all four cases, the compression computed in the horizontal direction, presented in Figure 5-18, show a lateral expansion of the pipeline section resulting from the pipeline spring action due to vertical compression.

5.4.2.2. Stress and pore water pressure around the pipeline

The results of the four analysis cases in terms of stresses and pore water pressure with time after pipeline installation and backfilling are reported at three points around the pipeline section. Vertical total stress, pore water pressure, and vertical effective stress, are reported at the base (lowest point of the pipeline cross-section) in Figures 5-19 through 5-21, and at the crown (highest point of the pipeline cross-section) in Figures 5-22 through 5-24, respectively. In the same manner, horizontal total stress, pore water pressure, and horizontal effective stress, are reported at the lateral springline of the pipeline cross-section in Figures 5-25 through 5-27, respectively.

At the base and crown of the pipeline, the evolution of vertical total stress with time (Figures 5-19 and 5-22) shows clearly the effect of sloping ground. This effect can be recognized by a faster increase of stress with time and lower long-term stress level. In the case of sloping ground, the long-term stress level is reached faster due to the higher gradient for deformation. This deformation gradient is created by the weight of soil above the depression's trough level (level of the excavation top). On the other hand, due to the free boundary at the slope surface, the soil overlying the trough level in the vicinity of the trench is not under the same lateral K_o stress conditions as the deeper soil and therefore, it is not directly subjected to the same unloading forces. The lateral forces in the slope's soil mass are a direct result of external forces induced by the deformation of the lower soil mass which is unloading towards the trench. The energy dissipated in deforming the soil in the slopes above the trough level results in reducing the amount of lateral soil movement near the top of the trench and therefore reduces the downward "squeezing" effect on the backfill soil. This is clearly demonstrated in Figure 5-14 which shows that smaller lateral soil movement into the trench is associated with larger slopes of the adjacent ground. This explains the higher vertical stresses computed in the analysis of Case 1 where the surface at the level of the excavation top is a free boundary.

For the same reasons discussed above, a significant difference in the dissipation of excess pore water pressure at the base and crown of the pipeline is observed between Case 1 (level ground) and the three other cases. In addition, as shown in Figures 5-20 and 5-23, the steeper the slopes around the pipeline, the faster the pore water pressure dissipates. By observing the pore water pressure dissipation in Figures 5-20 and 5-23, The effect of delayed soil unloading after excavation is clearly visible in Case 1. When the clay fill is placed, an immediate buildup of pore water pressure is observed at the base and crown of the pipeline section. This built up pore water pressure dissipates at a fast rate under an initial high gradient. As the pressure diminishes to about 5 kPa, an equilibrium is reached between the new pore water pressure generated by the slow lateral thrust caused by delayed unloading, and the pore water pressure dissipating under the existing gradient. This effect is more visible at the crown (Figure 5-23) where the pore water pressure reaches the equilibrium state and then increases again under the effect of lateral soil thrust. During the first 300 days, excess pore water pressures generated by the lateral thrust exceeds any dissipated ones

Although the total stress at the base and crown are higher in the level ground case, effective stresses within the analysis time frame of four years are lower due to the slower pore water pressure dissipation and the more pronounced effect of lateral unloading (Figures 5-21 and 5-24). Eventually, effective stresses in the case of level ground would surpass those in the sloping ground cases when sufficient pore water pressure is dissipated.

The discussion presented above explaining the long term effect of lateral unloading, is confirmed by the evolution of horizontal stresses and pore water pressure at the lateral pipeline springline. The computed total horizontal stress with time, shown in Figure 5-25, demonstrates a clear distinction between sloping ground and level ground cases. When backfill material is placed between the pipeline and the trench wall, an immediate lateral stress is induced at the springline under the confining load of the fill. Subsequently, as the trench walls start yielding, this lateral stress is gradually released until an equilibrium is reached between the pressure applied on either side of the trench wall. This behavior is confirmed since the equilibrium is reached at higher stress level with higher ground slopes as shown in Figure 5-25. In the case of level ground, however, a completely different behavior is observed whereby the total horizontal stress at the springline continues to increase for about 100 days after backfilling before it starts to decrease at a much slower rate than in the sloping ground cases. This can be explained as well by the prolonged lateral thrust due to unloading of K_o stresses. The same reasoning explains the higher pore pressure reached at the springline in the level ground case. In addition, Figure 5-26 shows a

continuing increase in pore water pressure for about 100 days after backfilling before dissipation starts. This behavior cannot be explained without the presence of delayed lateral thrust. Negative effective stress in the horizontal direction at the springline indicate the absence of any contact force between the soil and the pipeline at this point.

5.5. CONCLUSIONS

By simulating the pipeline installation, and the construction effect on stressing the pipeline, up to four years after installation and backfilling, the following observations are made as discussed above:

In overconsolidated clay soils, a trench excavation would trigger a release (unloading) of locked-in K_o lateral stresses. The unloading process in the vicinity of the trench walls is almost immediate; however, a delayed reaction from the unloading of the soil mass further away from the trench could continue for years, even if the trench is immediately backfilled. The prolonged unloading of the soil mass creates a lateral thrust on the backfill material. This thrust peaks in the upper half of the trench which causes a squeezing force in the backfill, acting downward on the pipeline. The long-term squeezing effect generates excess pore water pressure which counteracts the pore water pressure dissipation with time.

In a v-shaped depression, the lateral unloading due to the excavation of the trench does not directly affect the soil mass above the trough level. This soil mass in the side slopes acts as a damper by absorbing the deformation energy of the underlying soil subjected to lateral unloading. This is manifested by smaller lateral displacement of soil into the trench and faster pore water pressure dissipation in the backfill, associated with higher ground slopes. As a result, a higher total stress acts at the base and crown of the pipeline with level ground and smaller ground slopes causing more deformation than with steep ground slopes. A higher effective stress at the base and crown of the pipeline is computed with sloping ground due to slower pore water pressure dissipation.

FIGURES

CHAPTER 5

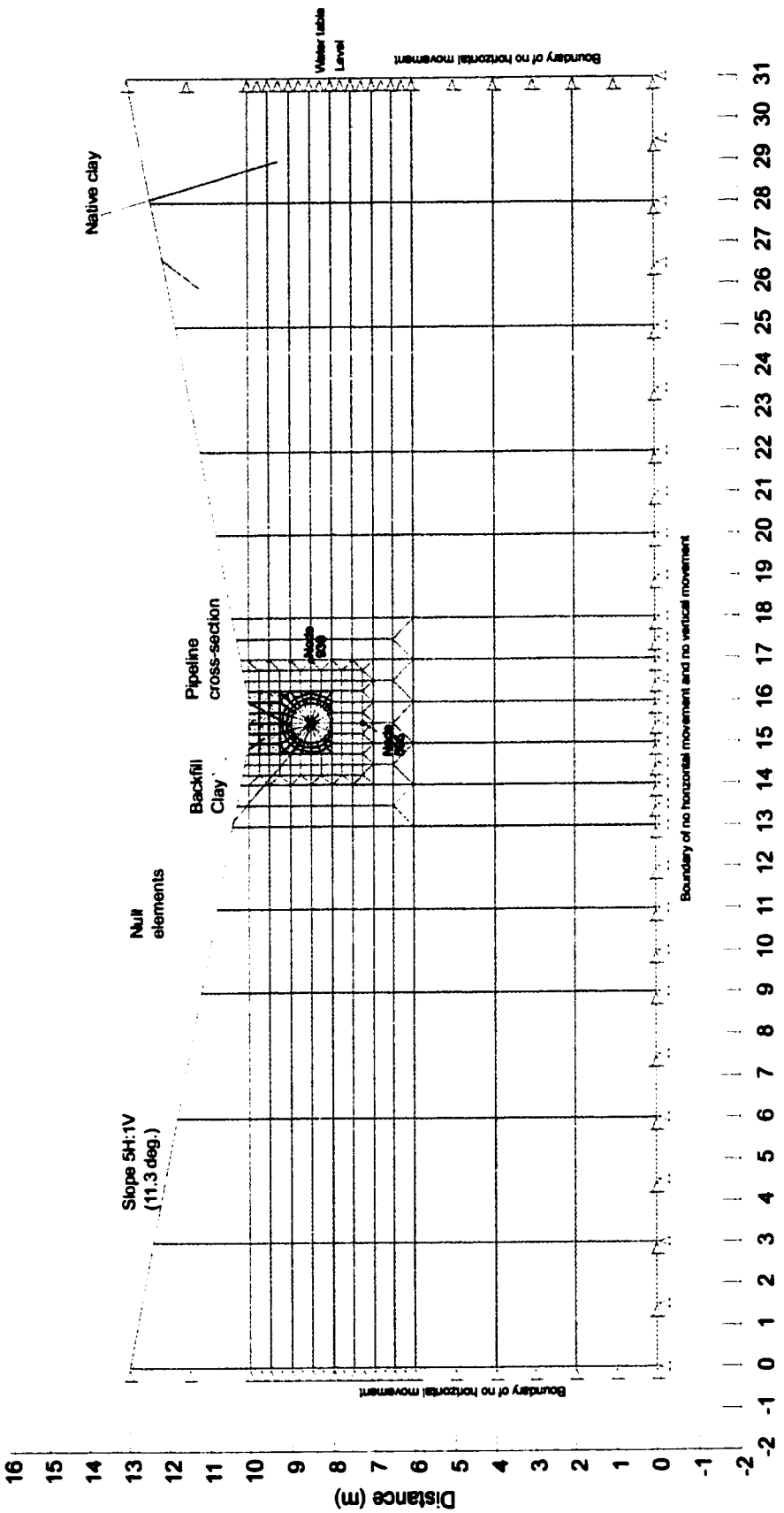

Figure 5-1: Finite element mesh for excavation and pipe installation in v-shaped depression

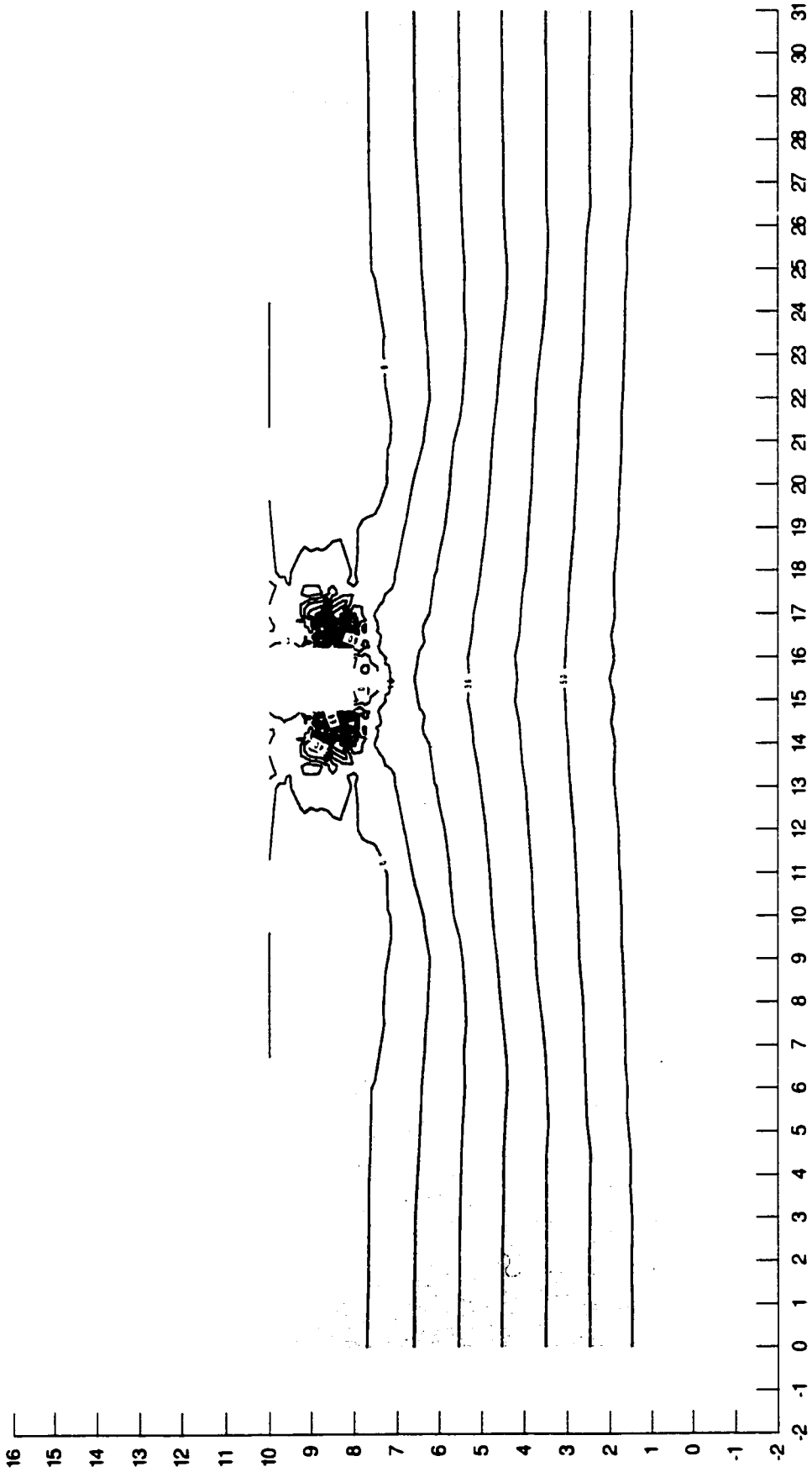

Figure 5-2: Pore water pressure contours (kPa), 0.0° slopes, one hour after excavation start

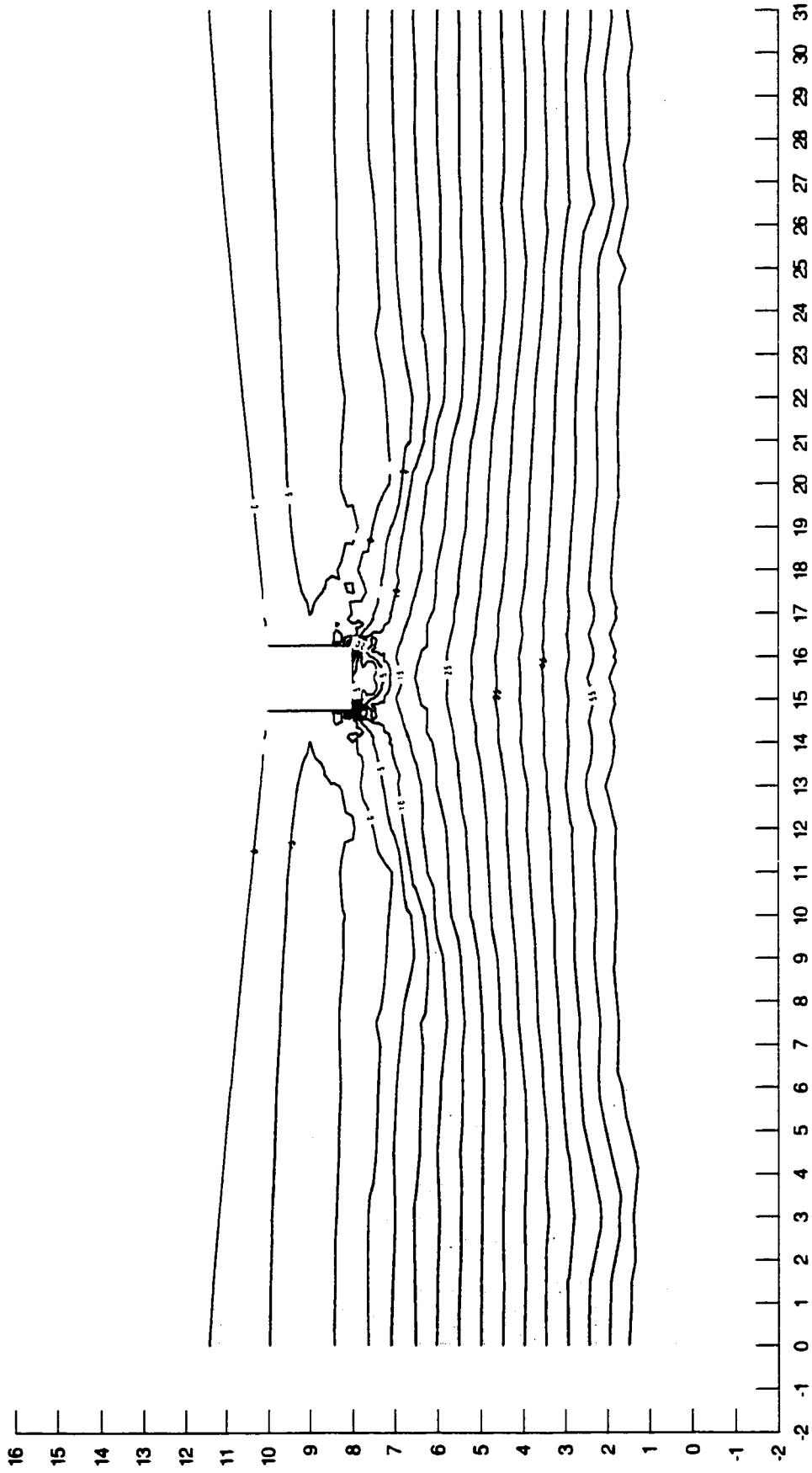

Figure 5-3: Pore water pressure contours (kPa), 5.7° slopes, one hour after excavation start

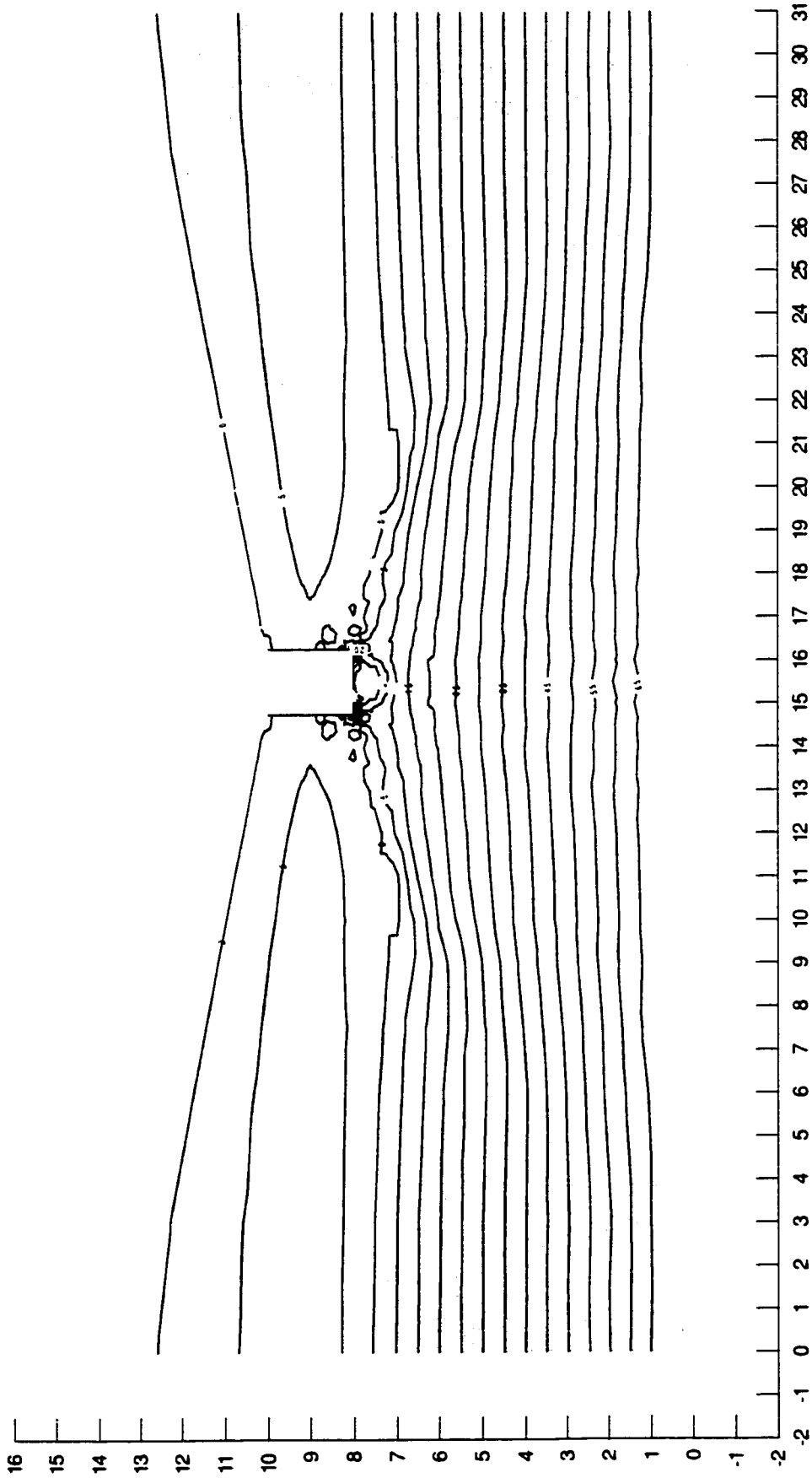

Figure 5-4: Pore water pressure contours (kPa), 11.3° slopes, one hour after excavation start

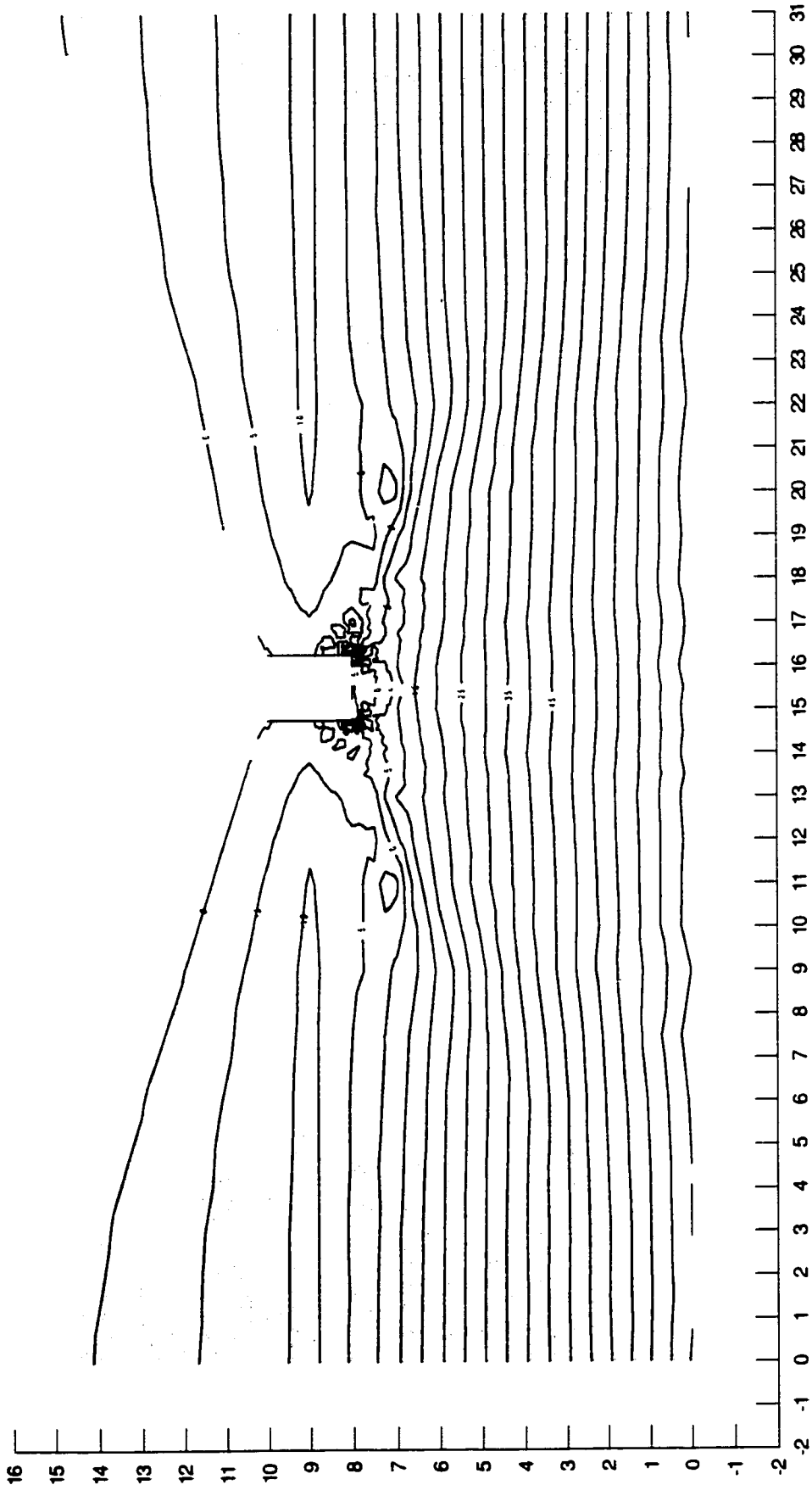

Figure 5-5: Pore water pressure contours (kPa), 20° slopes, one hour after excavation start

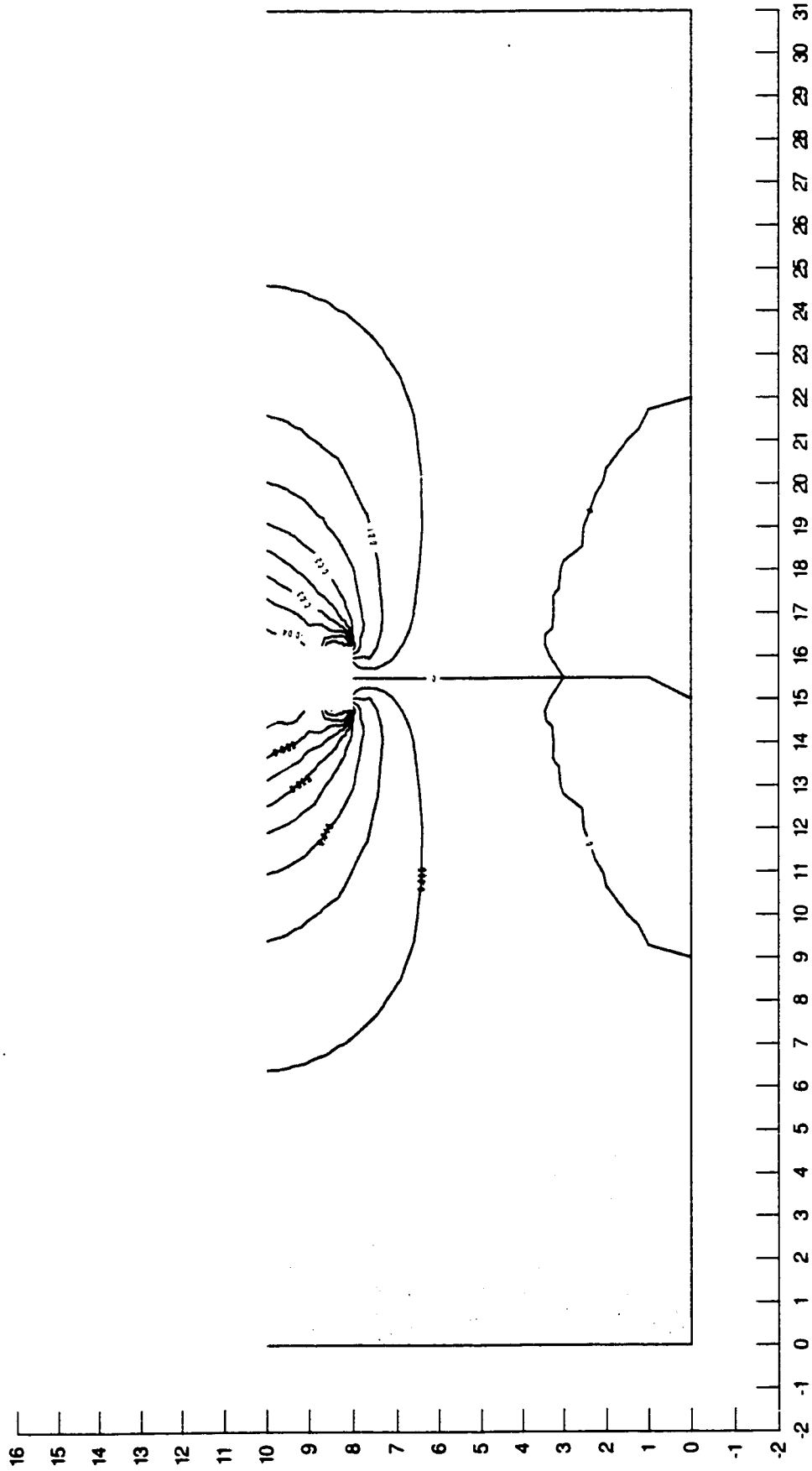

Figure 5-6: Horizontal displacement contours (m), 0.0° slopes, one hour after excavation start

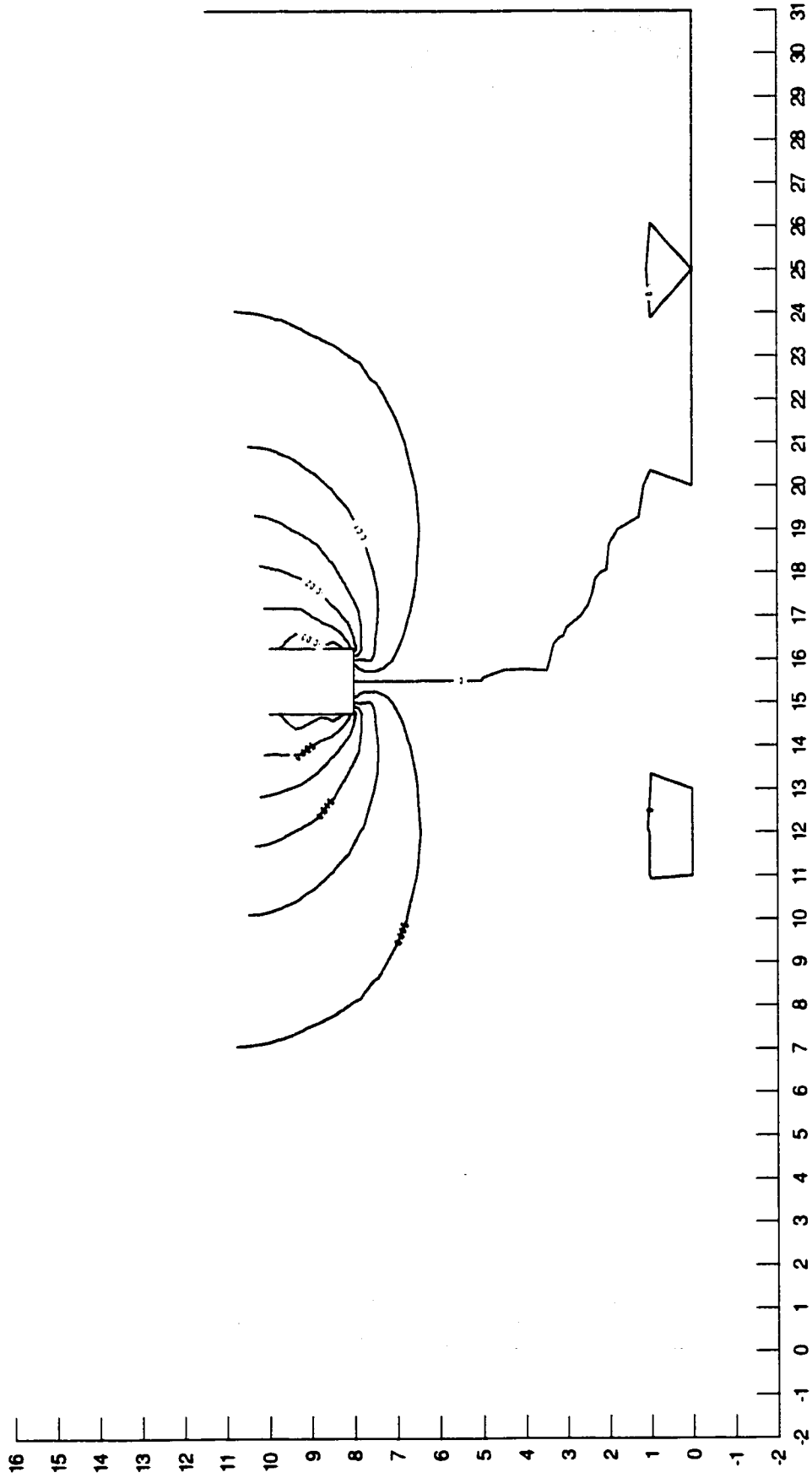

Figure 5-7: Horizontal displacement contours (m), 5.7° slopes, one hour after excavation start

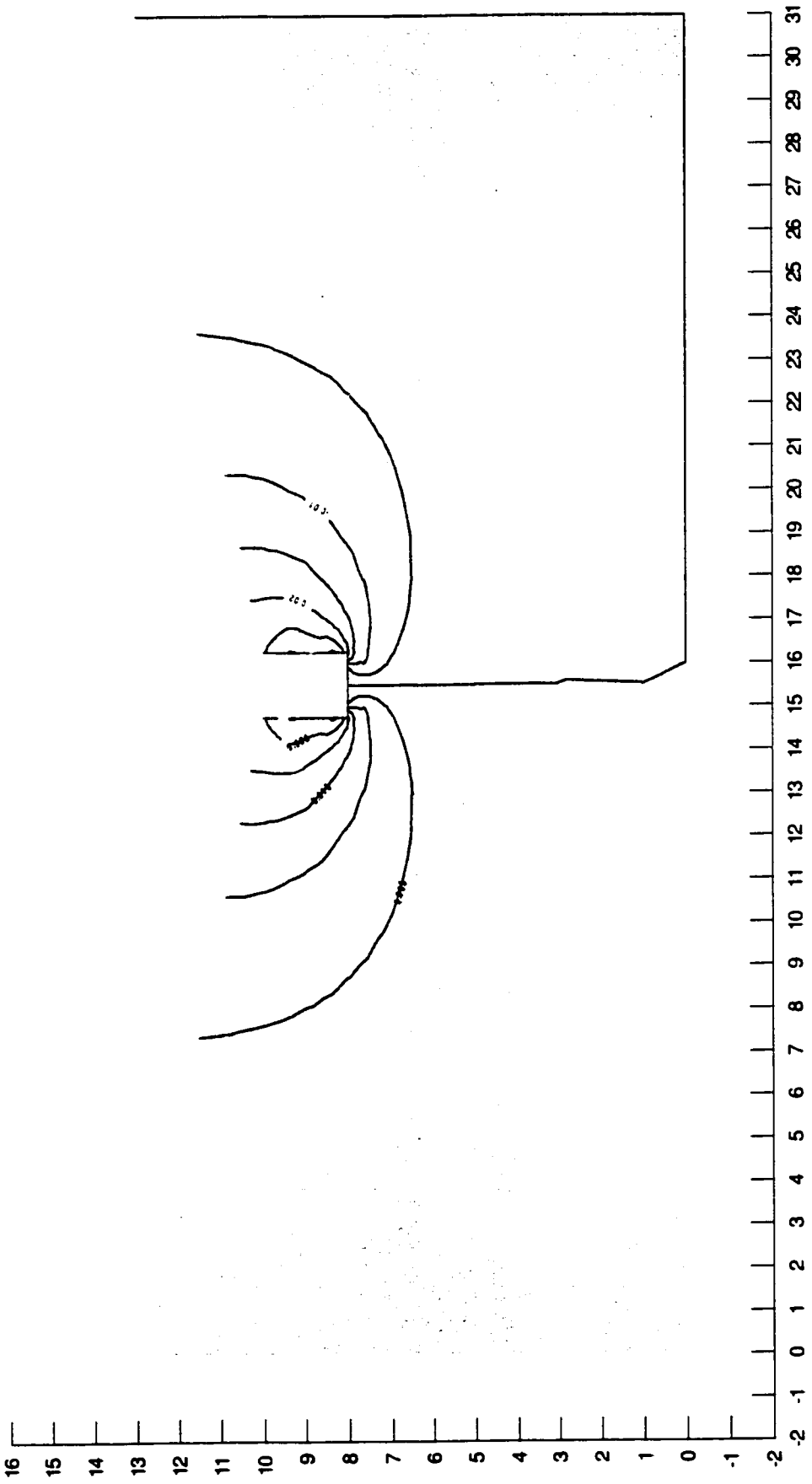

Figure 5-8: Horizontal displacement contours (m), 11.3° slopes, one hour after excavation start

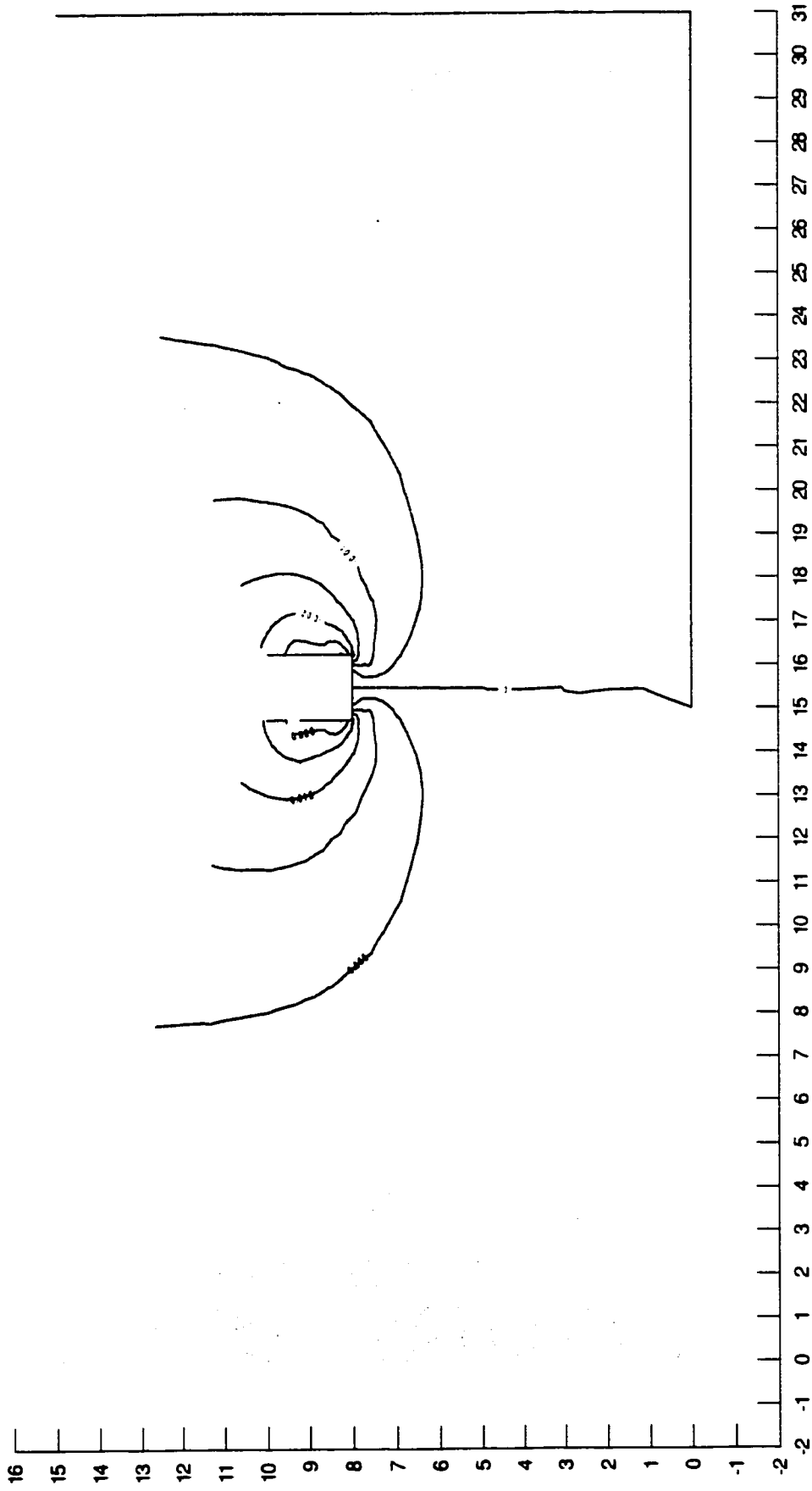

Figure 5-9: Horizontal displacement contours (m), 20° slopes, one hour after excavation start

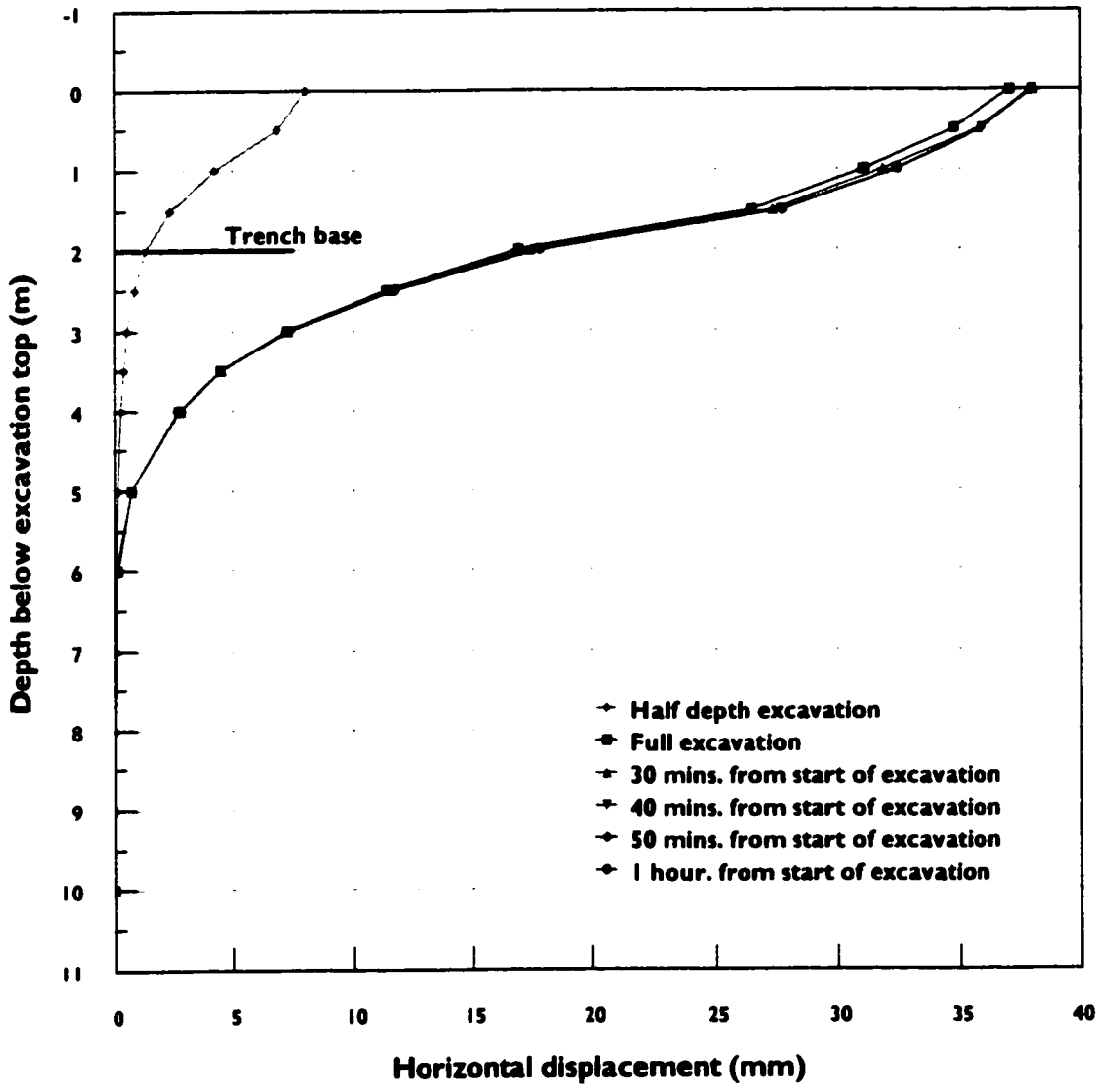

Figure 5-10: Horizontal displacement profile (0.0° slopes, 0.75 m from trench wall)

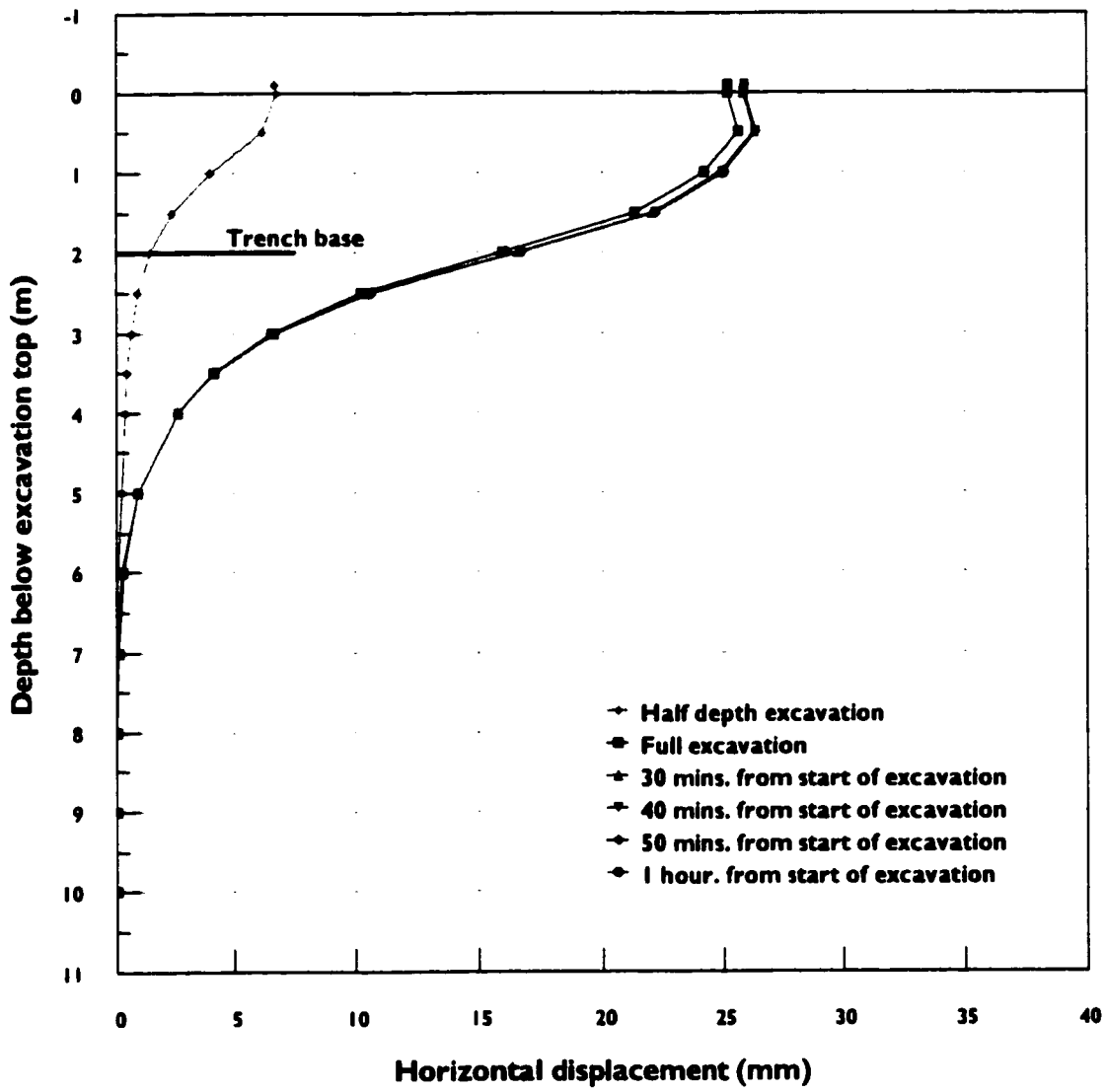

Figure 5-11: Horizontal displacement profile (5.7° slopes, 0.75 m from trench wall)

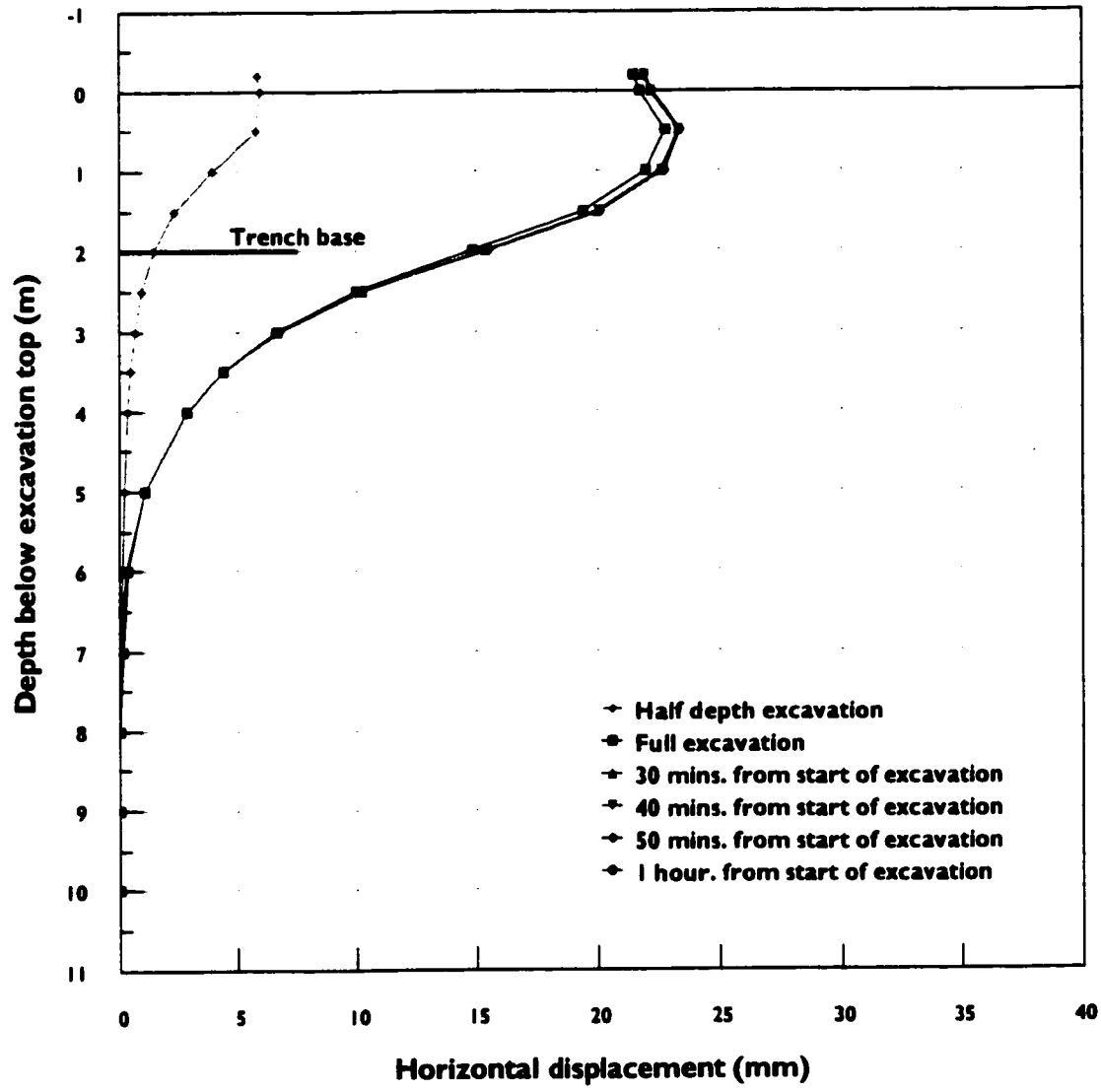

Figure 5-12: Horizontal displacement profile (11.3° slopes, 0.75 m from trench wall)

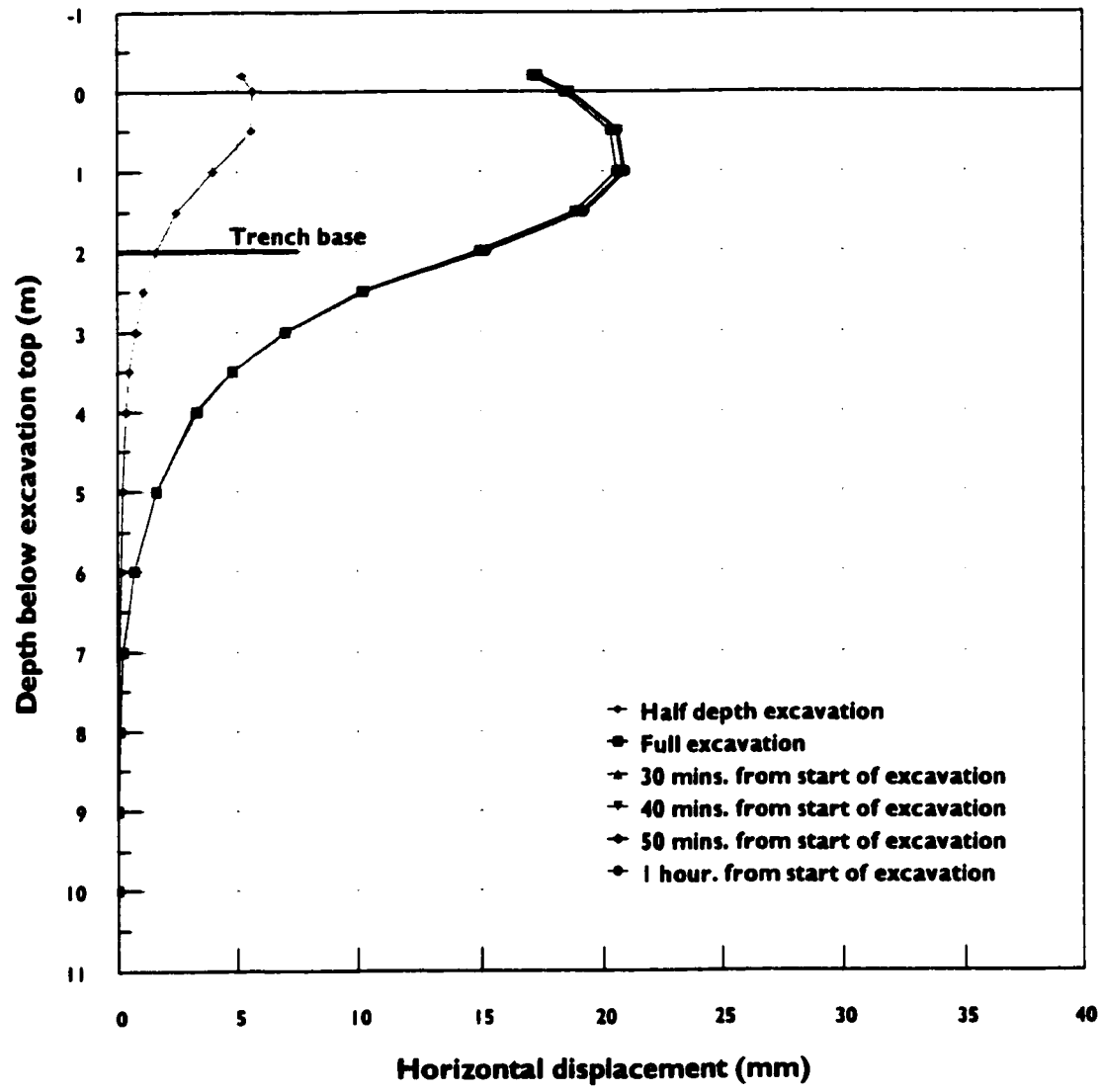

Figure 5-13: Horizontal displacement profile (20.0° slopes, 0.75 m from trench wall)

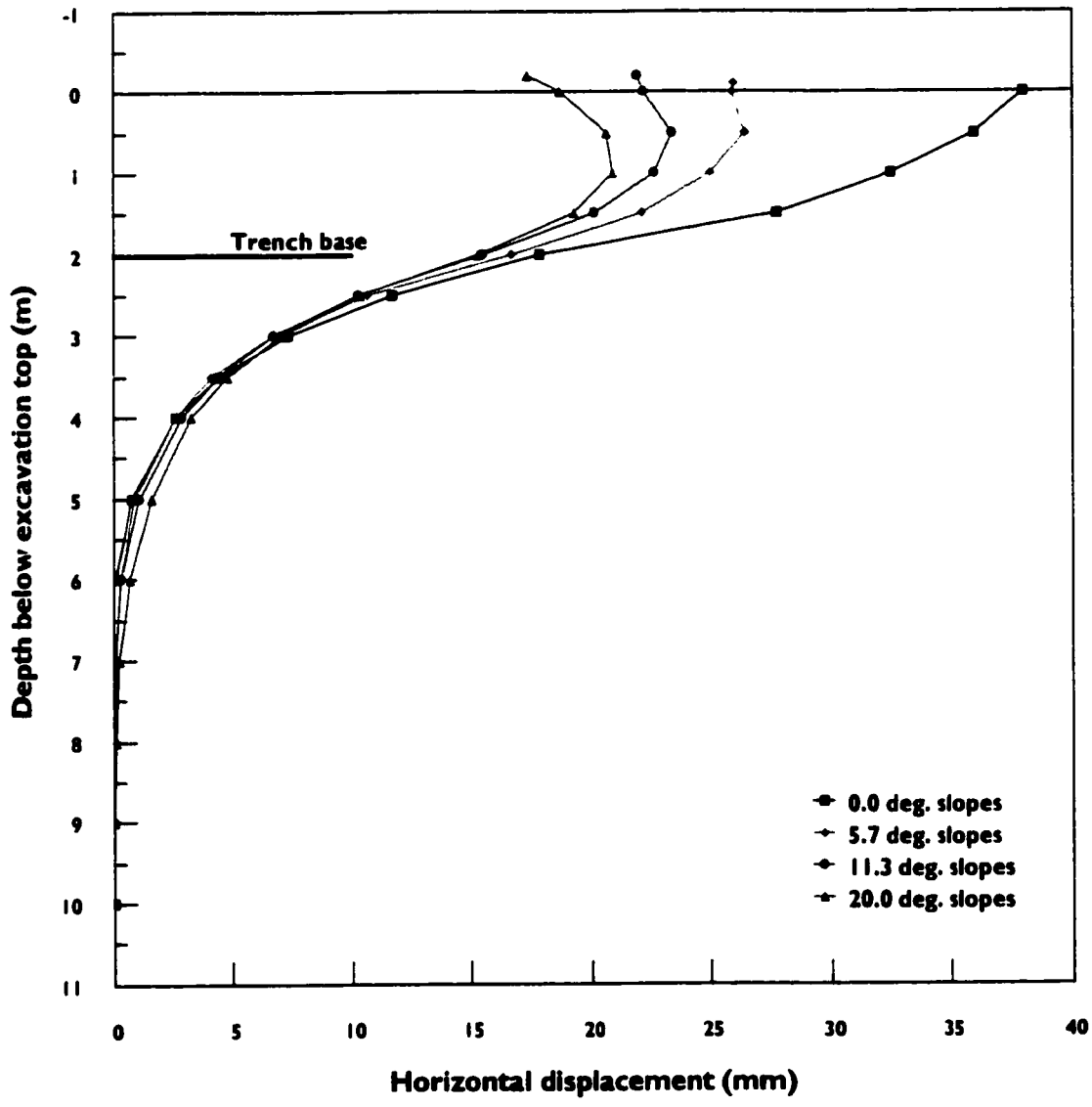

Figure 5-14: Horizontal displacement profiles (0.75 m from trench wall, one hour after the start of excavation)

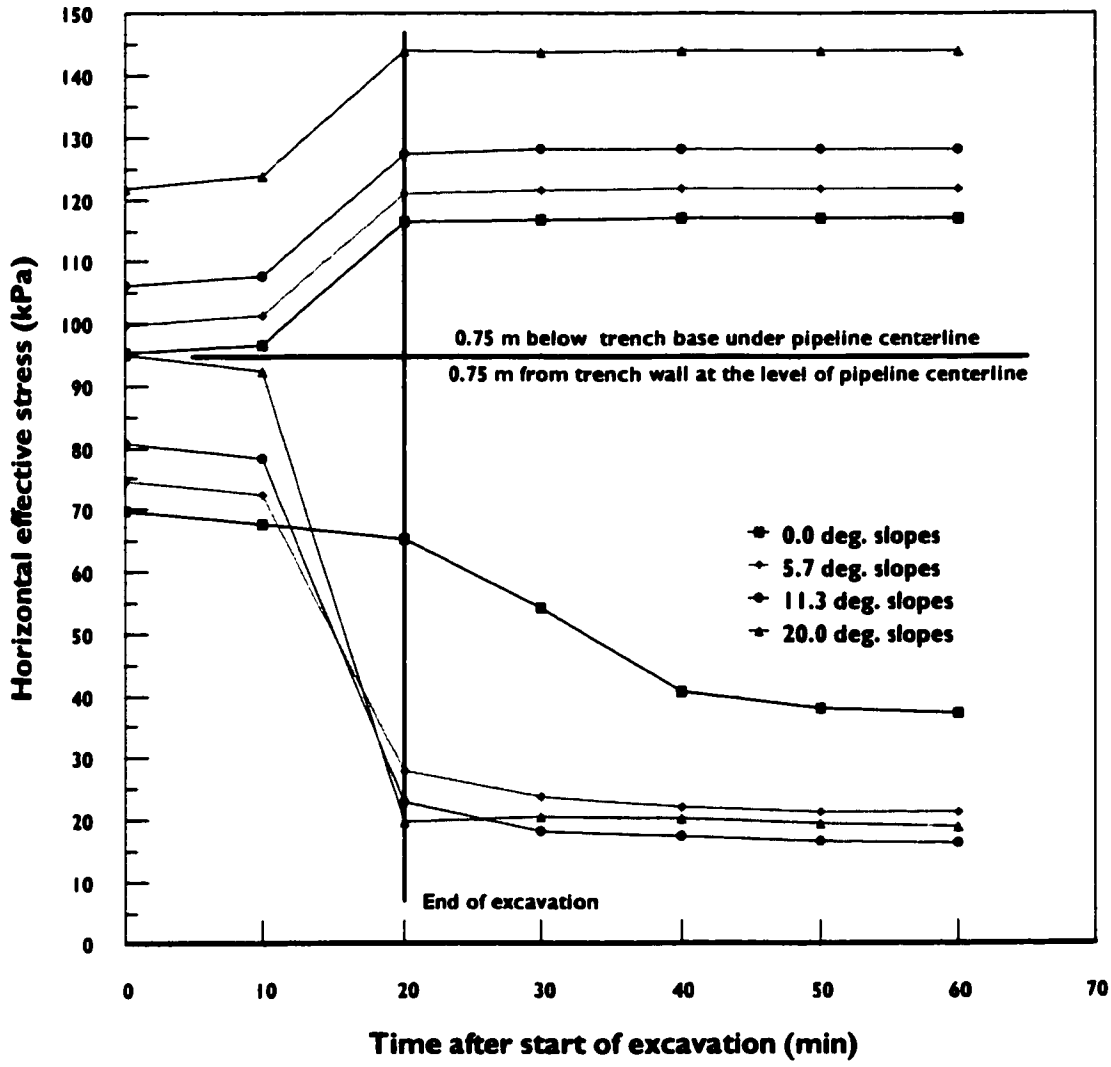

Figure 5-15: Horizontal effective stress during and after excavation (0.75 m from trench wall and 0.75 m below trench base)

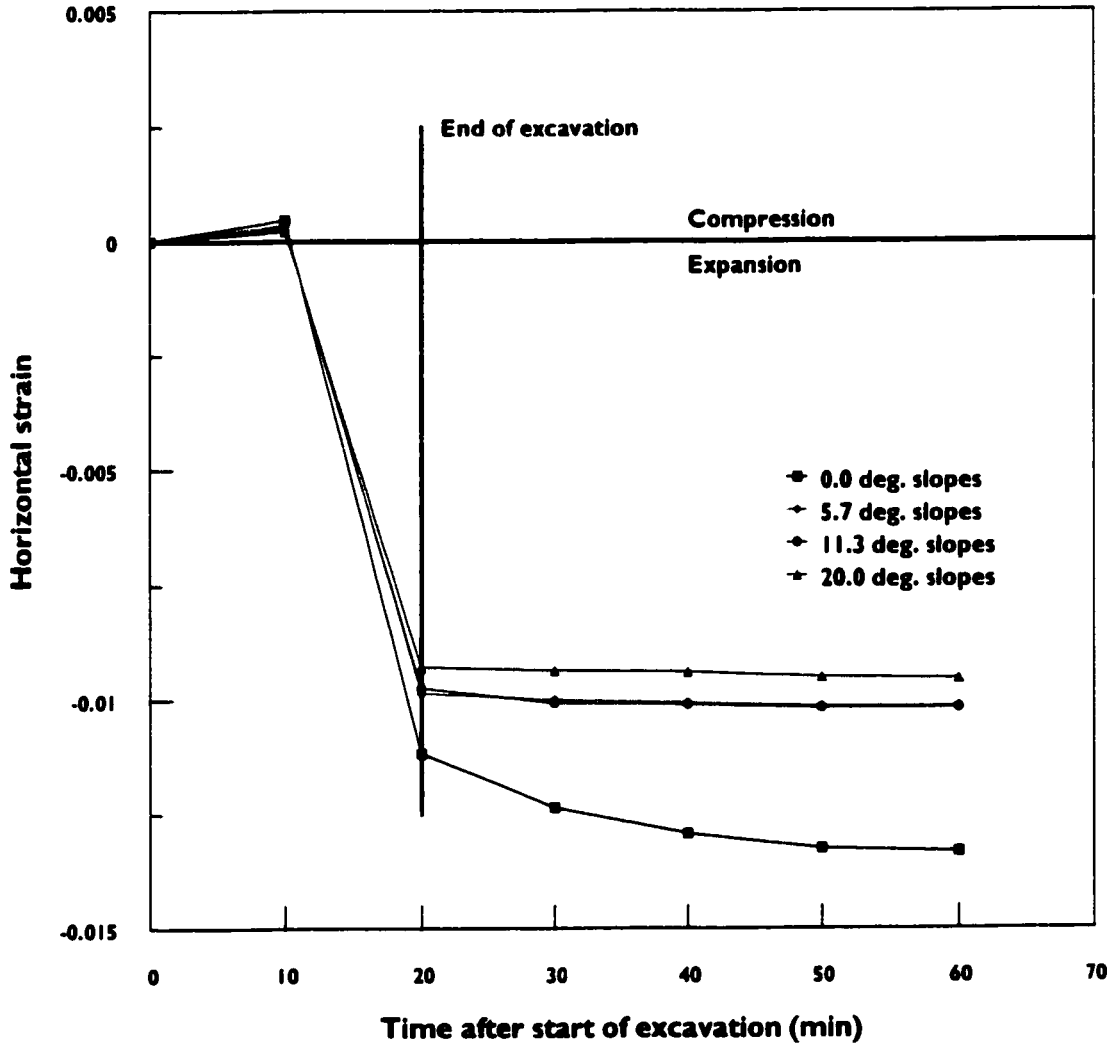

Figure 5-16: Horizontal strain during and after excavation (0.75 m from trench wall at the level of pipeline centerline)

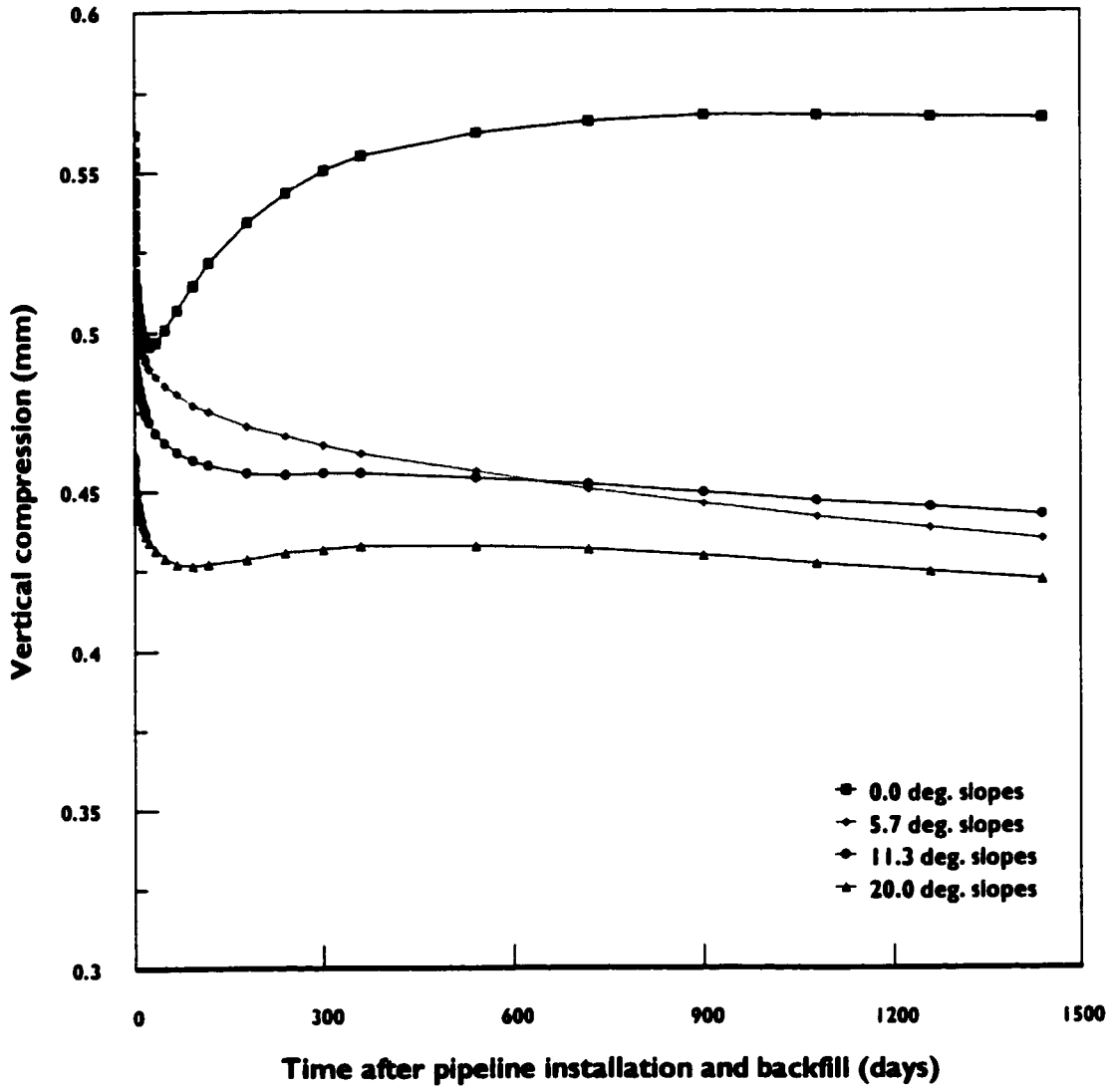

Figure 5-17: Vertical compression of pipeline

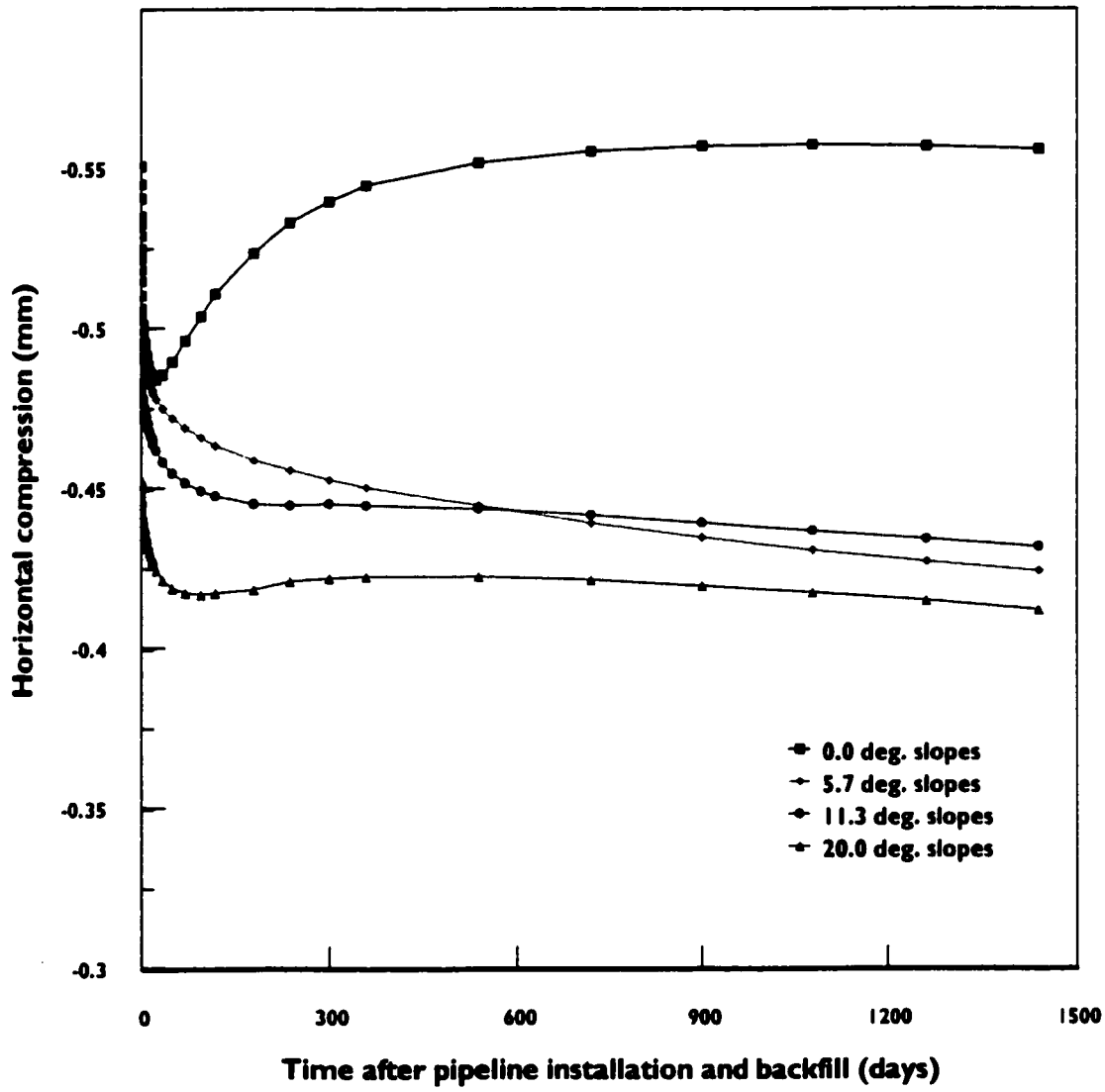

Figure 5-18: Horizontal compression of pipeline (negative <=> expansion)

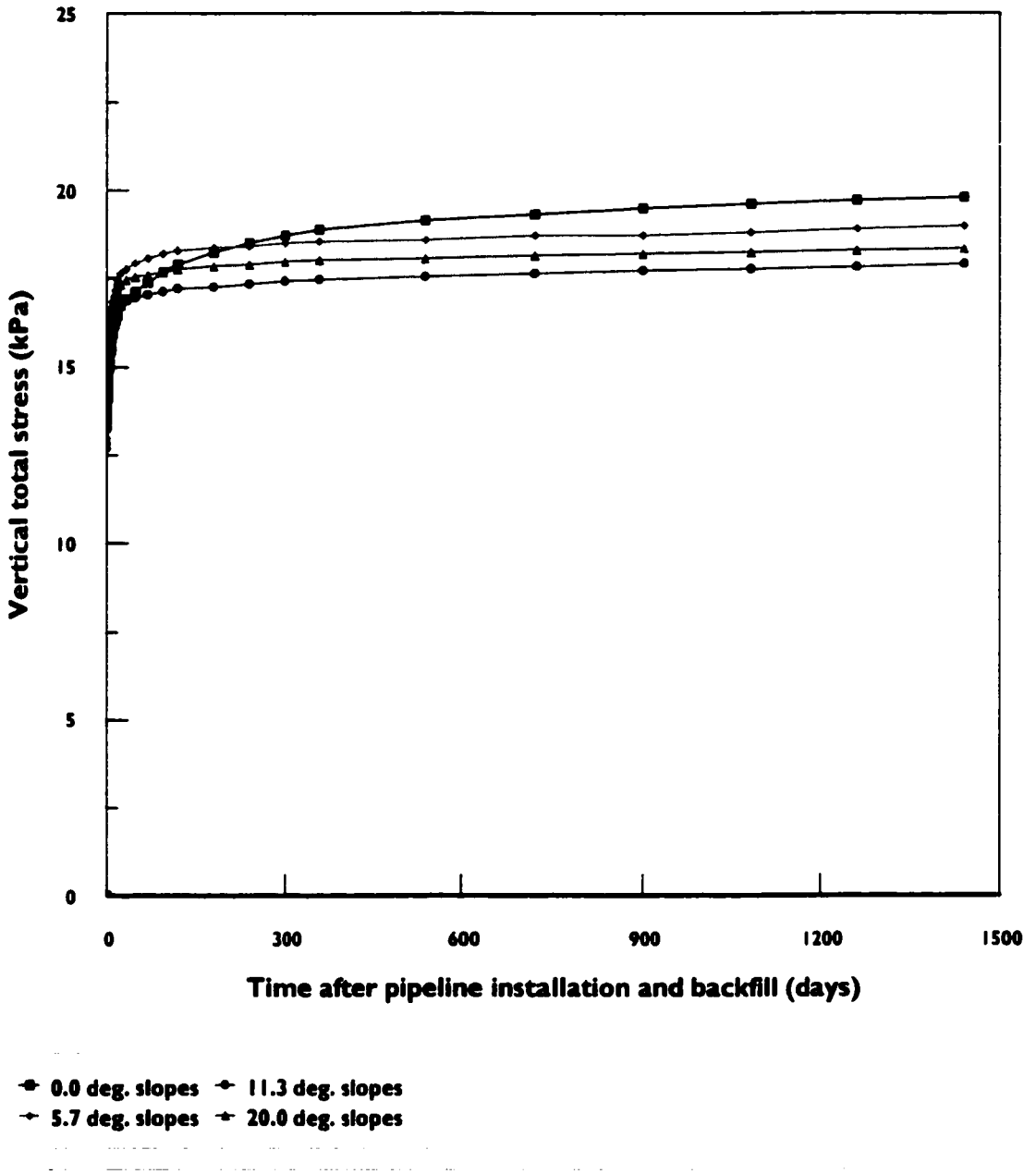

Figure 5-19: Vertical total stress at the pipeline base

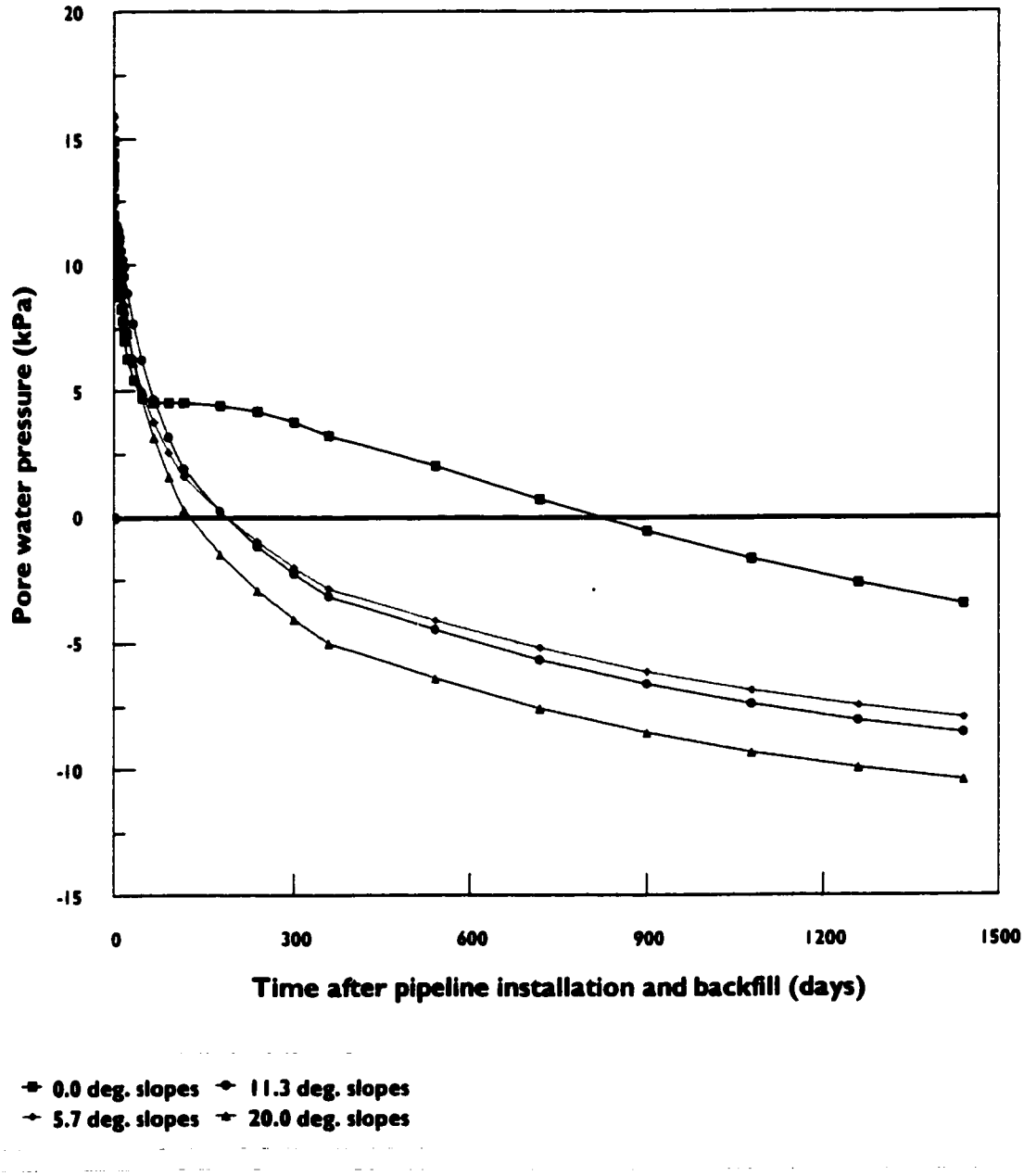

Figure 5-20: Pore water pressure at the pipeline base

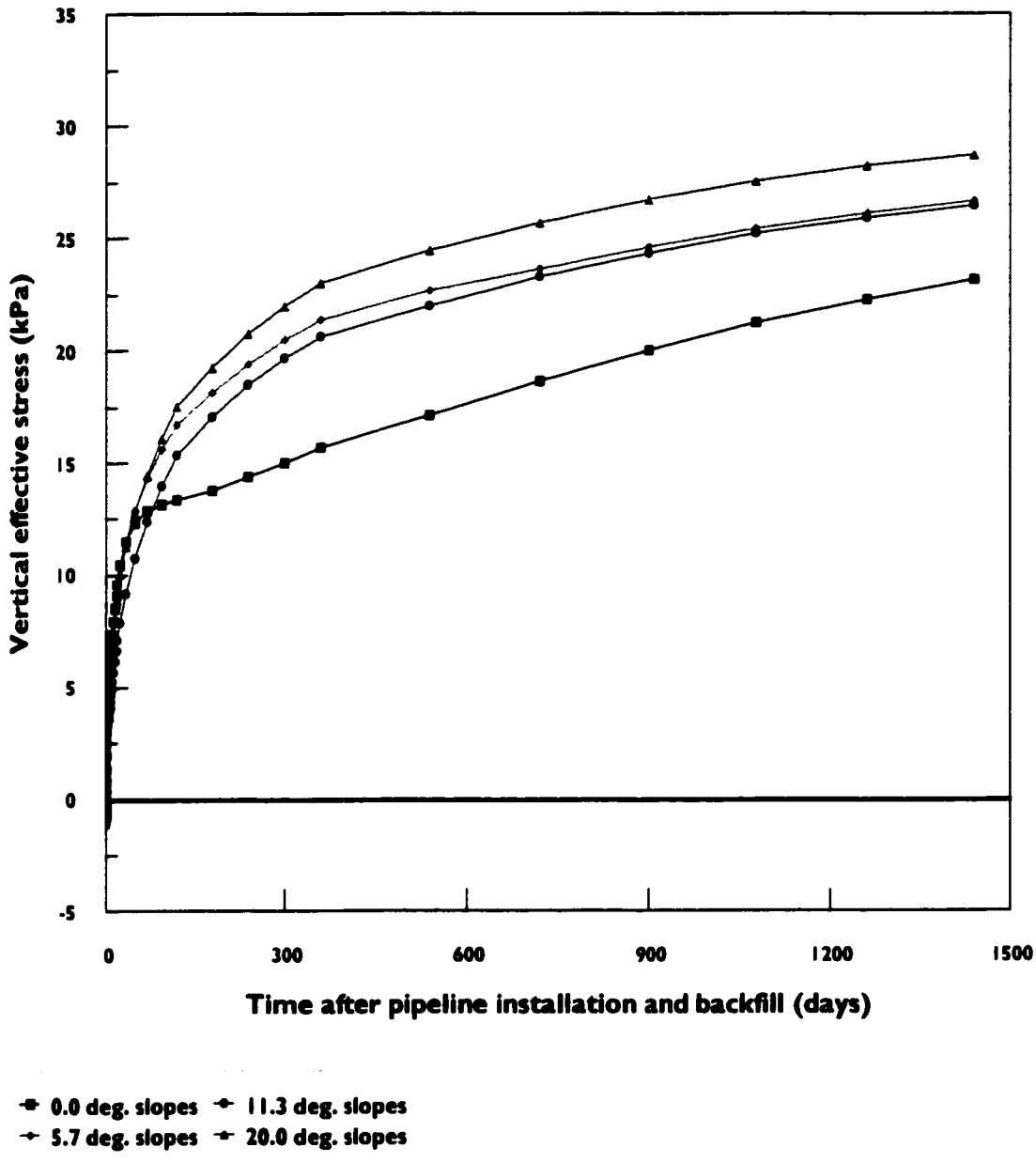

Figure 5-21: Vertical effective stress at the pipeline base

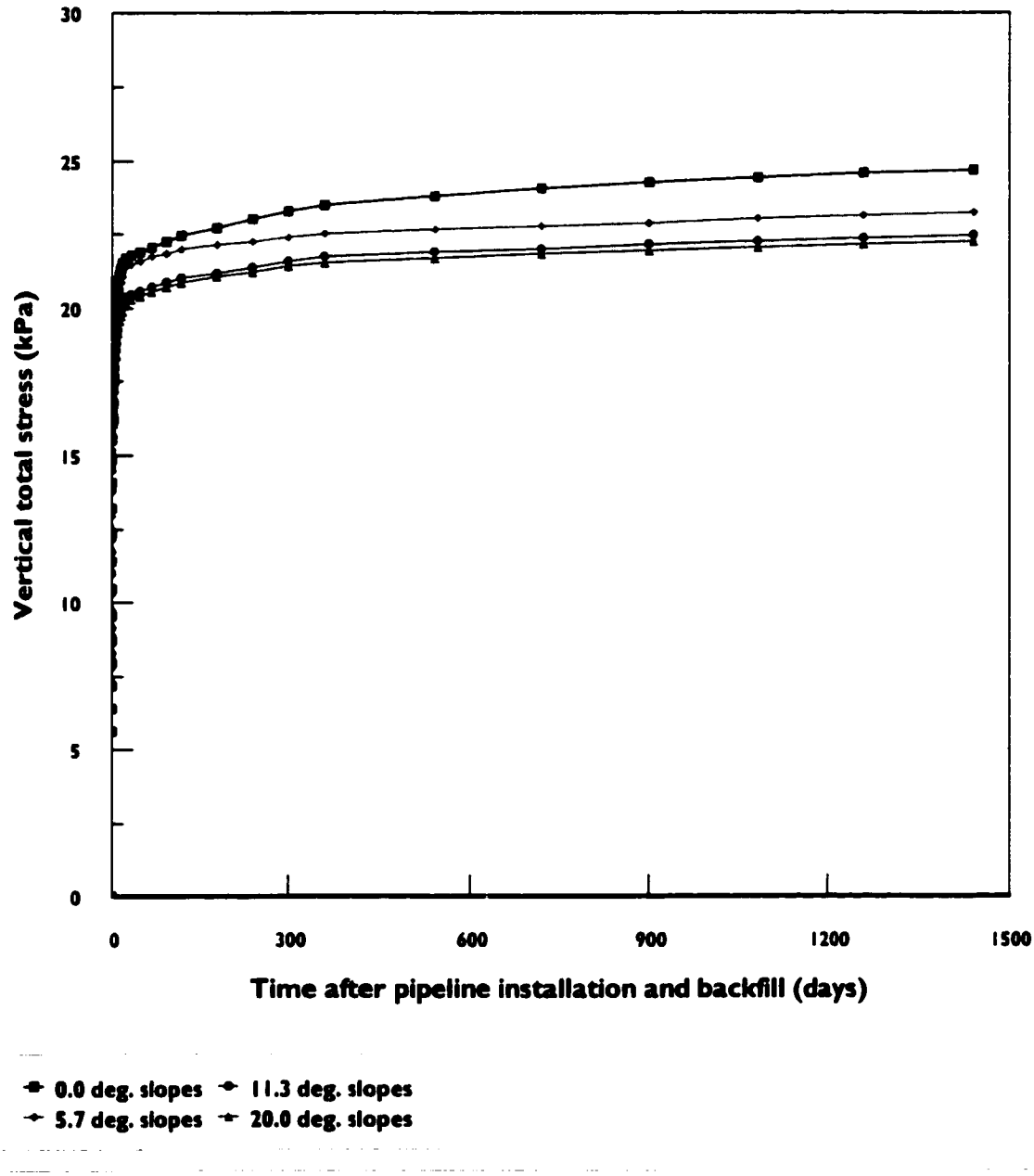

Figure 5-22: Vertical total stress at the pipeline crown

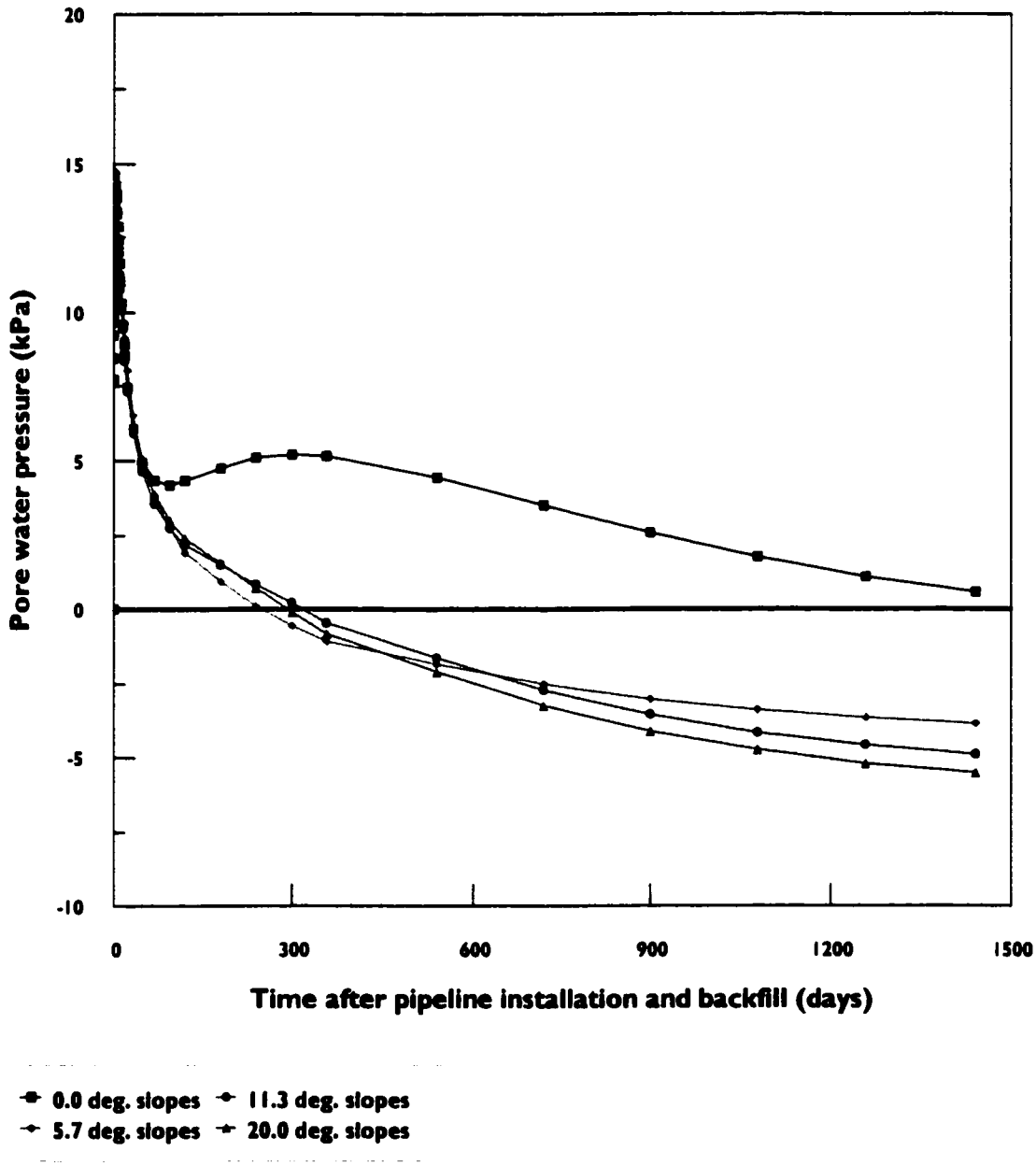

Figure 5-23: Pore water pressure at the pipeline crown

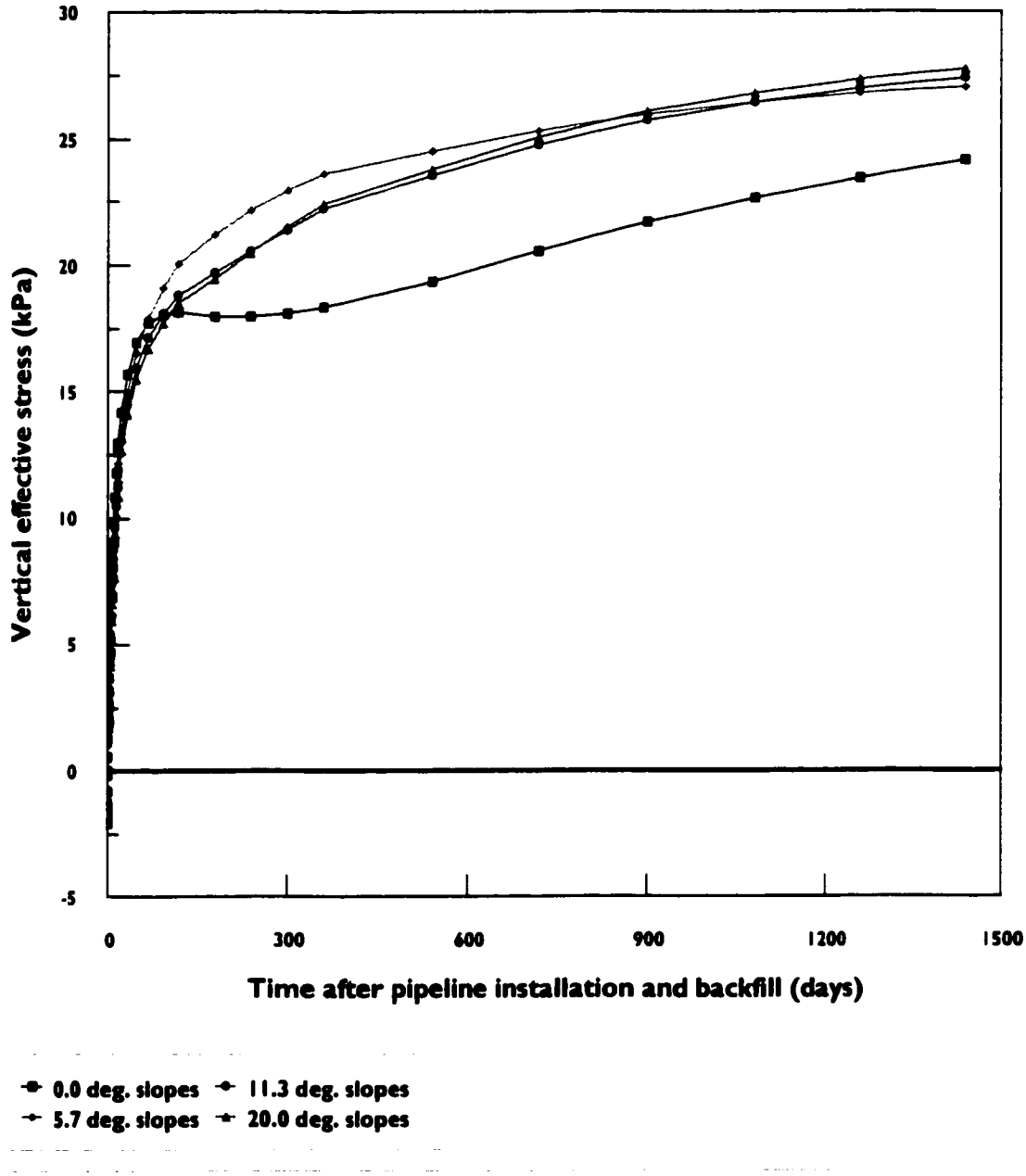

Figure 5-24: Vertical effective stress at the pipeline crown

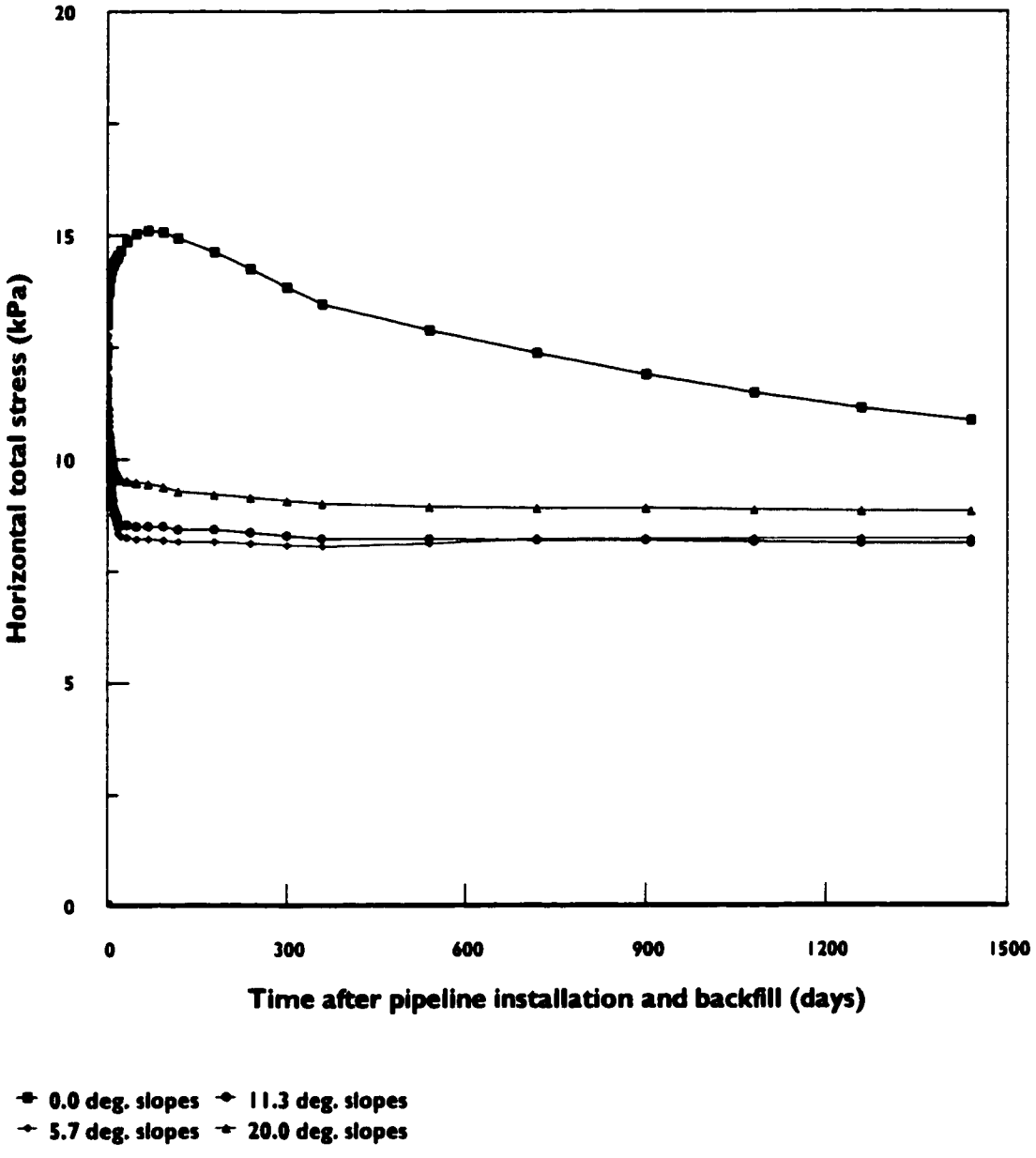

Figure 5-25: Horizontal total stress at the lateral pipe springline

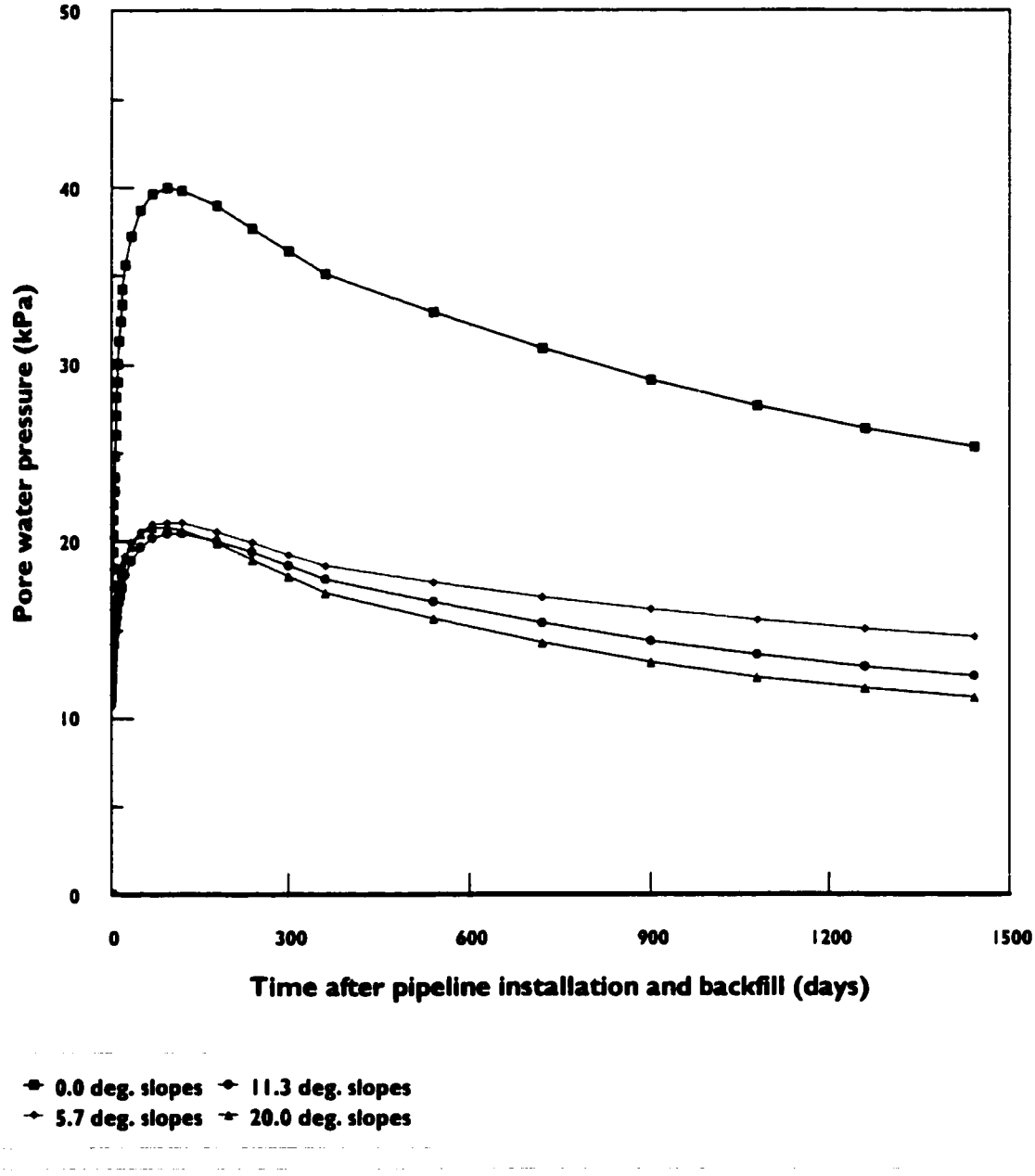

Figure 5-26: Pore water pressure at the lateral pipe springline

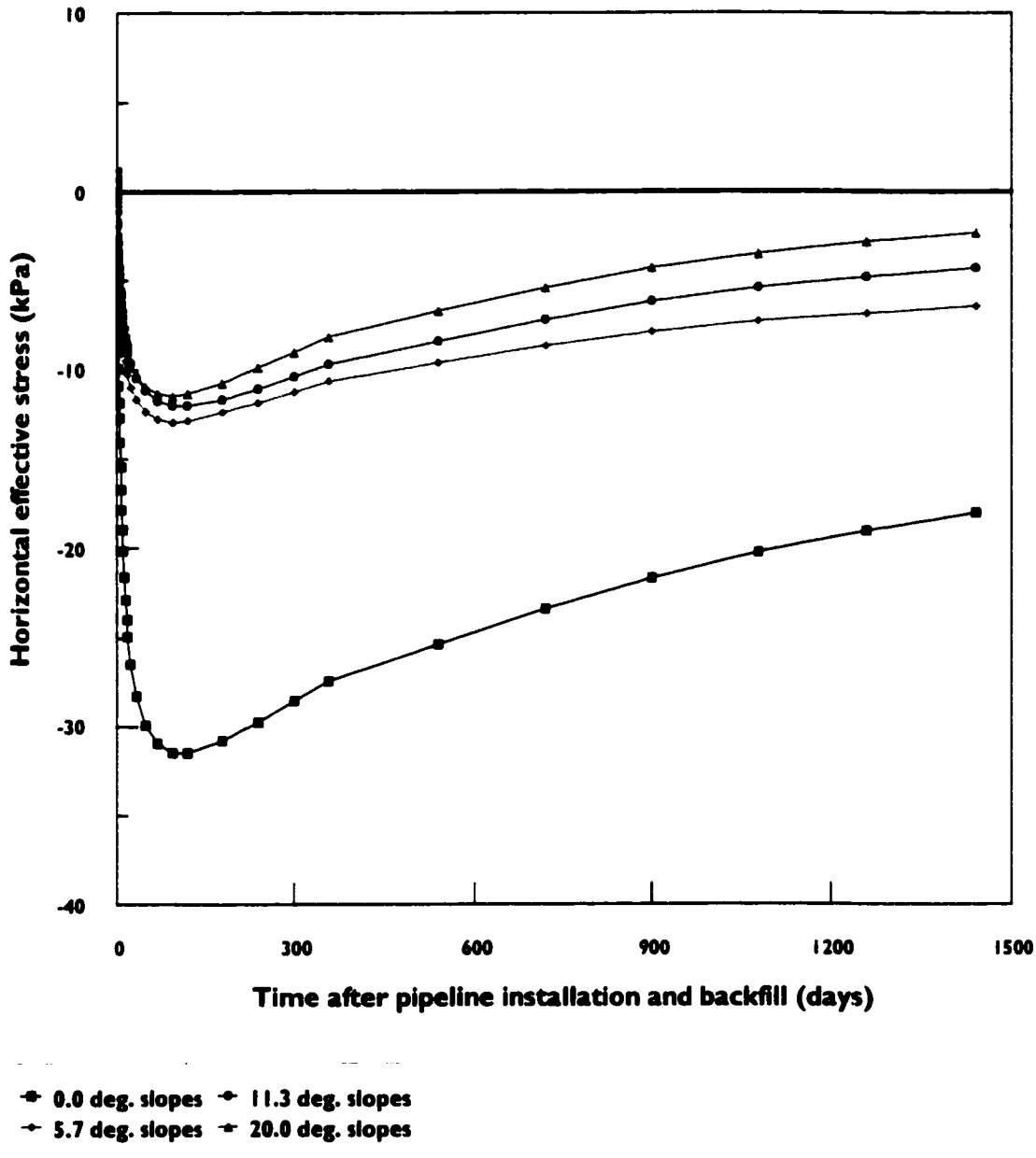

Figure 5-27: Horizontal effective stress at the lateral pipe springline

CHAPTER 6

COMPACTION EFFECT ON SOIL/PIPELINE INTERACTION

CHAPTER 6

EFFECT OF COMPACTION ON SOIL/PIPELINE INTERACTION

6.1. INTRODUCTION

In Chapter 5, a finite element model was used to simulate the sequence of trench excavation (2 m deep by 1.5 m wide), installing a pipeline segment, and backfilling, at the bottom of a V-shaped depression. The simulation was performed with three different magnitudes of the ground surface slopes toward the trench to investigate their effect on the pipeline/soil interaction. The native soil simulated in the model is overconsolidated London clay with a coefficient of earth pressure at rest, $K_o = 2$. The same soil was used as backfill, but the overconsolidation factor was omitted.

In these studies, the same simulation as in Case 4 (20° slopes) is performed, however, three study cases are analyzed with different methods of compaction applied to the backfill. The objective in this chapter is to investigate the effect of backfill compaction on the pipeline/soil interaction.

The simulation performed in the following analyses, as in the previous analyses, considers the long term effects of construction procedures (excavation and backfilling). The change in pore water pressure, stresses, and strains, are evaluated for a period of about four years after the construction of the pipeline.

6.2. THE FINITE ELEMENT MODEL

As mentioned earlier, the analysis performed in this chapter is similar to the one performed earlier for the pipeline installation in a v-shaped depression, with side slopes of 20° (2.7H:1V). Therefore, a two-dimensional finite element mesh, similar to the one shown in Figure 5-1 (the sloping angle being the only difference), is used in the following analyses in this chapter.

6.3. ANALYSIS PROCEDURE

The same in–situ conditions obtained with $K_o = 2$ for Case 4 in the previous chapter followed by the same two-stage excavation and 40 minute wait until the placement of the pipeline segment and backfill, are used as initial conditions for each of the three study cases (the various compaction schemes). The compaction is then applied as boundary condition at the surface of the fill elements as shown in Figure 6-1 in three different methods, separating three study cases (Case 5 through Case 7). The results of these cases are presented in comparison with Case 4 (uncompacted backfill) to investigate the compaction effect. After compaction, the stress-deformation-consolidation analysis is continued in all three cases to simulate the time dependant effects of excavation, pipeline placement, backfilling, and compaction, over the following 1440 days (about four years).

In all three cases in this chapter, the compaction The compaction method simulated in each of the three cases is described in the following subsections:

6.3.1. CASE 5 COMPACTION

As mentioned earlier, the compaction load is applied at the surface of the backfill as a boundary function. This loading function applies a pressure of 25 kPa over the backfill for a one minute duration. The pressure is then removed for a duration of one minute and then applied again. This process is repeated to simulate three cycles of loading and unloading. Figure 6-2 illustrates the three loading-unloading cycles.

6.3.2. CASE 6 COMPACTION

In this case, the boundary function simulates a surcharge of 10 kPa applied at the surface of the backfill for a duration of ten days after backfilling. After the ten days the surcharge is removed and the analysis is continued for the four year duration.

6.3.3. CASE 7 COMPACTION

This case is similar to Case 6, however, the boundary function simulates a surcharge of 20 kPa applied at the surface of the backfill for a duration of ten days after backfilling. After the ten days the surcharge is removed and the analysis is continued for the four year duration.

6.4. ANALYSIS RESULTS

As mentioned earlier, the initial conditions for the three analysis cases are the computed conditions of the section with excavated trench, one hour after the start of excavation (i.e. 40 minutes after the end of excavation) where the pipeline segment and the London Clay backfill were placed. Compaction simulation is applied at this time as well. In Case 5 (cyclic loading compaction), the duration of the compaction activity is very short compared to the time frame of the analysis, and therefore, the immediate effect of the compaction can be considered as part of the initial conditions in this particular case. The following is a presentation of some analysis results from the three cases (Case 5 through Case 7) along with similar results from Case 4 where no compaction is applied to the backfill

6.4.1. PIPELINE DEFORMATION

The first effect to examine is the pipeline deformation with time. Pipeline compression is defined as the relative displacement between two edges of the same diameter line. The computed vertical compression with time for all analysis cases are presented in Figure 6-3. The computed horizontal compression with time for all analysis cases are presented in Figure 6-4. The same results for vertical and horizontal compression, but only during the first 95 days after backfilling, are shown in Figures 6-5 and 6-6, respectively. As in the analysis cases reported previously, the magnitude of the compression is very small (less than 1 mm) due to the rigidity of the pipeline, however, the effect of the different compaction methods is obvious.

In the uncompacted backfill case (Case 4), which was also reported previously, a vertical compression of about 0.4 mm was induced as the backfill was placed, and was more or less maintained throughout the analysis period. A corresponding expansion in the horizontal direction of about 0.4 mm was also maintained.

In Case 5, where the fill was subjected to three quick loading cycles, showed a similar behavior as the uncompacted fill case, however, the magnitude of the vertical compression and horizontal expansion were about 0.3 mm, say about 25 % smaller.

In Case 6, where a 10 kPa surcharge was maintained for ten days over the fill surface, an initial compression of about 0.2 mm in the vertical direction was maintained while the surcharge is applied then dropped to almost zero within 10 to 20 days after the surcharge was removed. In the horizontal direction, however, almost zero compression or expansion was computed during and after surcharge. In this case, it seems that the spring forces in the horizontal direction, resulting from the vertical compression during the surcharge, is in equilibrium with the lateral soil pressure on the pipeline section. Once the surcharge is removed, the spring forces locked in the pipeline section were released, bringing the pipeline to a state of zero deformation, especially at long term.

The effect of the heavier surcharge in Case 7 caused a reversed behavior in the pipeline section, such that an expansion is computed in the vertical direction while the pipeline section is compressed in the horizontal direction. This behavior, however, is limited to the duration of the surcharge. A state of zero deformation is gradually reached after the surcharge removal, same as in Case 6.

It is obvious from the pipeline compression results that a compacted backfill would result in smaller pipeline deformation, especially when long duration surcharges are used for compaction.

6.4.2.2. STRESSES AND PORE WATER PRESSURE AROUND THE PIPELINE

The results of the three analysis cases in terms of stresses and pore water pressure with time after pipeline installation and backfilling are reported at three points around the pipeline section as in the previous chapter. Vertical total stress, pore water pressure, and vertical effective stress, are reported at the base (lowest point of the pipeline cross-section) in Figures 6-7 through 6-12, and at the crown (highest point of the pipeline cross-section) in Figures 6-13 through 6-18. In the same manner, horizontal total stress, pore water pressure, and horizontal effective stress, are reported at the lateral springline of the pipeline cross-section in Figures 6-19 through 6-24. Stress and pore water pressure with time are presented over the duration of the analysis (about 4 years after backfilling), followed in the next figure by a presentation of the same data, but on a shorter time scale of 100 days to show a clearer picture of the short-term behavior.

At the base of the pipeline, the change in vertical total stress with time (Figures 6-7 and 6-8) shows clearly the effect of backfill compaction methods. In the case of uncompacted fill, a vertical total stress of about 17 kPa is reached about 20 days after backfilling and remains unchanged after that. In Case 5, after the last load cycle, a fast drop in vertical total stress which reaches about –58 kPa within 20 days after backfilling. A small and very slow rebound to about –53 kPa is observed over the rest of the four years. In Cases 6 and 7, however, a vertical total stress at the pipeline base reached during the ten day surcharge, drops quickly to about zero kPa once the surcharge is removed, and remains at the zero level for the rest of the simulated four years.

In Cases 6, and 7, the surcharge load is applied for a fairly long duration which allows lateral deformation of the trench wall and compaction of the fill material on both sides of the pipeline section. This compaction, which is more pronounced in the deeper fill, causes an uplift force on the pipeline section below the springline (wedging of the fill material between the pipeline section and the trench base). This uplift pressure is counteracted by the downward pressure applied on the pipeline section above the springline as a vertical resultant of the lateral compaction forces and the weight of the fill and surcharge. When the surcharge is removed after 10 days, the pipeline rebounds upward to reestablish the equilibrium, thus the zero vertical total stress at the pipeline base. The immediate development of pore water pressure at the pipeline base upon removal of the surcharge, shown in Figures 6-9 and 6-10, confirms this interpretation.

In Case 5, the short duration of each loading cycle (1 min.) prevents lateral deformations and soil compaction between the pipeline and the trench walls. Any lateral force on the pipeline is therefore temporary, and limited to the duration of the loading. The pipeline, being the most rigid element under the short duration surcharge, supports most of the vertical thrust. This causes the pipeline to be displaced downward, wedging into the fill towards the trench base. Once the last loading cycle is completed, the pipeline rebounds upward, generating significant suction at its base. This is confirmed by the significant negative pore water pressure generated at the pipeline base as shown in Figures 6-9 and 6-10.

By examining the change in pore water pressure at the pipeline base presented in Figures 6-9 and 6-10, in Case 4 where the fill is placed without compaction, a fast rise in pore water pressure can be seen immediately after backfilling, to about 15 kPa. This fast rise is due to the vertical load acting on the pipeline section due to the weight of fill material. The excess pore water pressure starts to dissipate at a fast rate. The fast dissipation is mostly due the compaction of the fill under

its own weight, around and under the pipeline, creating an increasing uplift force with time which relieves the pressure at the base. This behavior can be verified by observing the pore water pressure evolution in Cases 6 and 7, where the fill compaction around the pipeline is accelerated due to the surcharge. The accelerated compaction is visible in the smaller pore water pressure rise upon backfilling and a faster rate of dissipation during the surcharge. Negative pore water pressure is developed at the pipeline base immediately after the surcharge removal in both cases, where the locked in compaction uplift forces are maintained while the downward pressure from the surcharge is omitted. In Case 5, as discussed earlier, the quick loading wedges the pipeline into the fill material with a large thrust causing elastic deformations in the clay. The rebound of the pipeline upon the load removal creates a significant suction at the base (about -84 kPa). A recovery to about –44 kPa pore water pressure is observed after about 10 days. The uplift forces due to fill compaction become noticeable after 10 days and a reduction in pore water pressure, at almost the same rate as in Case 4, is observed throughout the simulated duration.

The change in effective stress with time at the pipeline base (Figures 6-11 and 6-12) reflects the vertical total stress and pore water pressure behavior discussed above. In Case 4, effective stress at the base continuously increases (for about 4 years) in a hyperbolic fashion where the rate of increase reduces with time. A similar increase at almost the same rate is observed in Case 5, however, this increase starts about 100 days from the end of loading cycles where the starting point is a negative effective stress of about -10 kPa. The negative effective stress is a result of the recovery from pipeline rebound discussed earlier. In Cases 6 and 7, where a surcharge is applied at the fill surface, the final effective stress level of about 10 and 17 kPa, respectively, is reached shortly after the surcharge removal (within 10 days). It is obvious from Figures 6-11 and 6-12 that a smaller effective stress at the pipeline base can be achieved by compacting the backfill, however, a long duration surcharge can achieve a lower long-term effective stress in a much shorter time after backfilling than cyclic loading compaction.

When examining the conditions at the pipeline crown, a simpler behavior than that at the base can be seen. The effect of compaction methods is seen clearly by comparing the change in vertical total stress after backfilling, presented in Figures 6-13 and 6-14. In Case 4, a sharp rise in vertical total stress at the pipeline crown is observed within about 20 days after backfilling. A significant portion of this total stress is due to pore water pressure (see Figure 6-16), which builds up under the weight of the fill and the delayed K_o unloading discussed earlier in this study. The same behavior is seen in Case 5, with even higher vertical total stress due to residual stresses generated by the quick loading cycles. A somewhat different behavior is observed in Cases 6 and 7. The

surcharge placed at the backfill surface causes compaction of the fill around the pipeline and lateral deformations in the trench walls. As a result, a lateral flow of soil is created at the pipeline crown to either side of the pipeline cross-section. This flow results in lower vertical effective stresses as shown in Figures 6-17 and 6-18 with fairly high pore water pressure still generated at the crown. The resulting vertical total stress at the crown, during the surcharge, is still lower than that of Cases 4 and 5. Once the surcharge is removed after 10 days, the unloading rebound results in a fast drop in pore water pressure at the crown to negative levels, maintaining low vertical effective stresses (Figures 6-17 and 6-18), even in the absence of lateral flow of soil at the crown. The effect of K_o unloading can still be seen, causing the slow increase in pore water pressure starting about 10 days after the surcharge removal (see Figure 6-16). This results in further reduction in vertical effective stress at the crown to negligible levels. It is clear from Figure 6-17 that the surcharge compaction methods are very useful in this case, for maintaining low vertical effective stresses at the pipeline crown, especially with the smaller surcharge of 10 kPa.

The last point to examine is at the pipe springline. Horizontal total stresses, pore water pressure, and horizontal effective stresses, with time, are presented in Figures 6-19 through 6-24. In terms of horizontal total stress, it is shown in Figure 6-19 that Cases 6 and 7 still maintain the lowest levels throughout, while a much higher stress is observed in Case 5. The same observation can be made with regard to pore water pressure shown in Figures 6-21 and 6-22. In all cases, a negative effective stress is maintained, especially in Case 5, which indicates low lateral resistance of the soil surrounding the pipeline at the springline level. A higher lateral resistance may be desirable in some cases to reduce pipeline flattening.

6.5. CONCLUSIONS

In the example used in this study, where a pipeline is installed in a trench, excavated in overconsolidated clay and backfilled with normally consolidated clay, it is shown that a surcharge-type compaction for a reasonable duration can reduce damaging stresses at the base and crown of the pipeline. Hence, a higher embankment over the pipeline may not result in more damaging stresses than a simple filling of the trench. Somewhat higher lateral stresses against the trench wall caused by a surcharge over the backfill would help counteract the effect of delayed K_o unloading into the trench.

FIGURES

CHAPTER 6

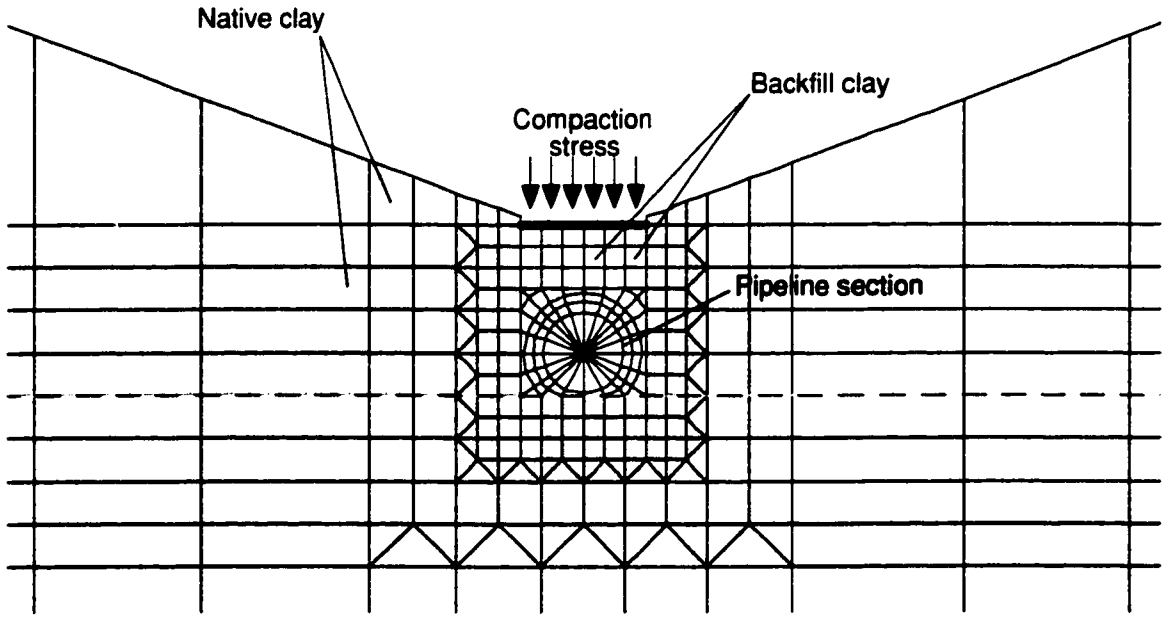

Figure 6-1: Finite element model with applied compaction stress

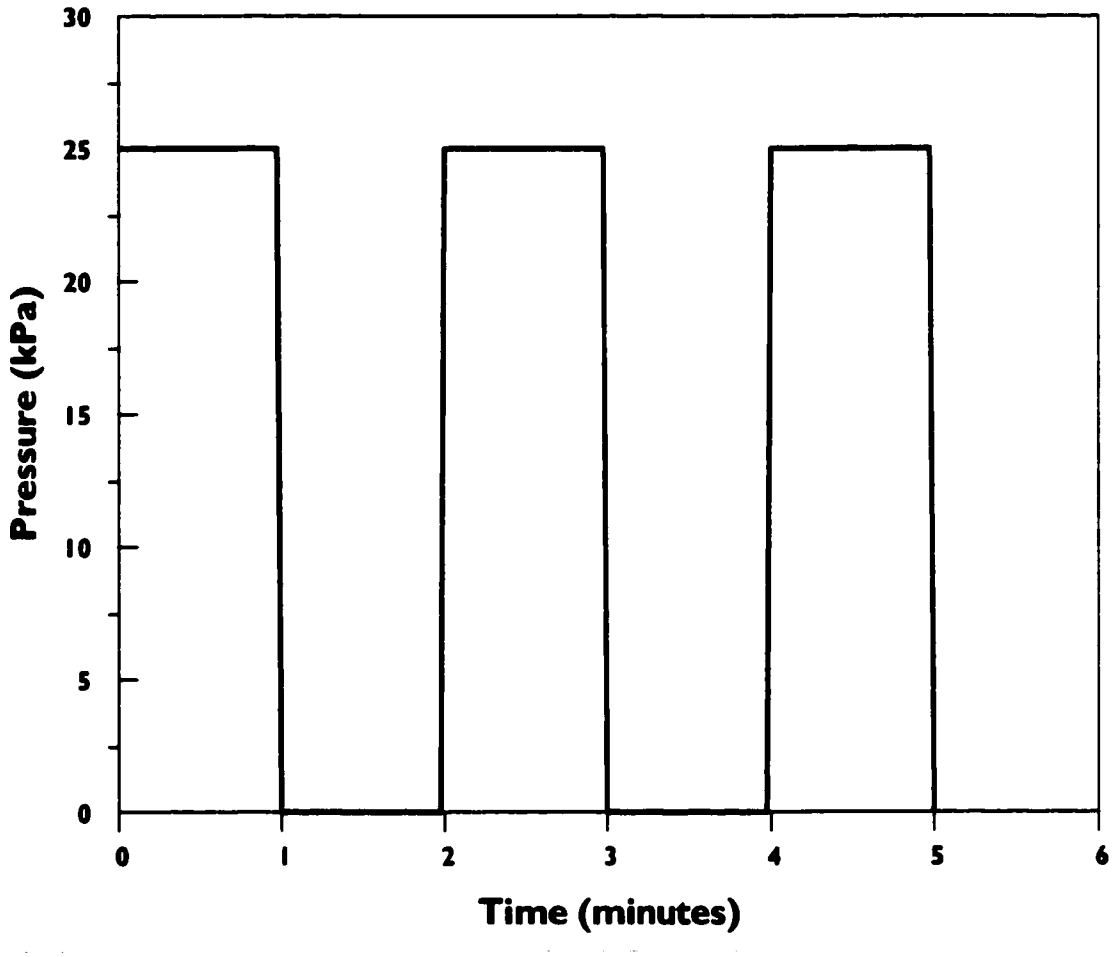

Figure 6-2: Cyclic compaction loading

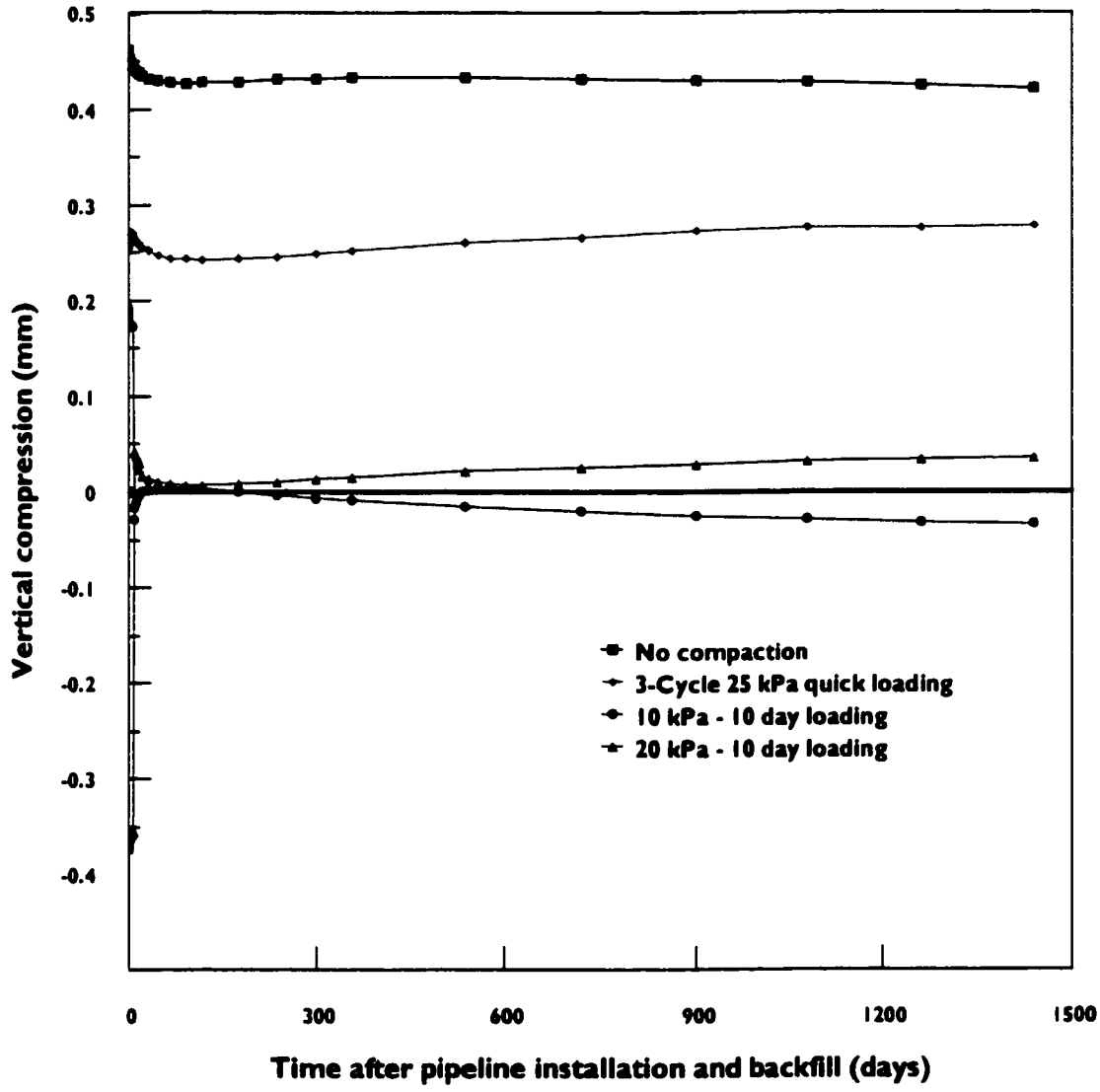

Figure 6-3: Vertical compression of pipeline, 20° slopes (With different compaction methods, 4 years)

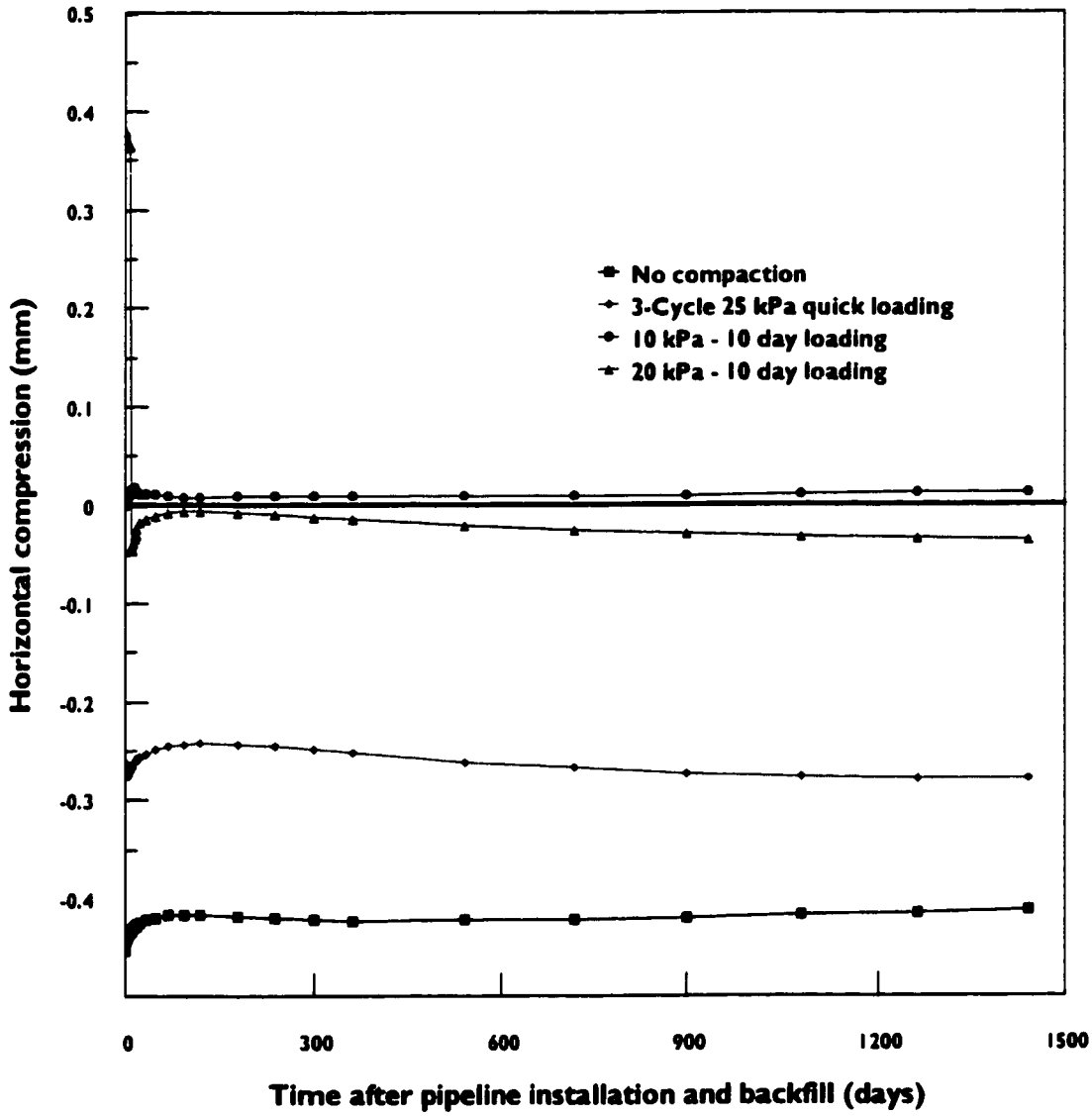

Figure 6-4: Horizontal compression of pipeline, 20° slopes (With different compaction methods, 4 years)

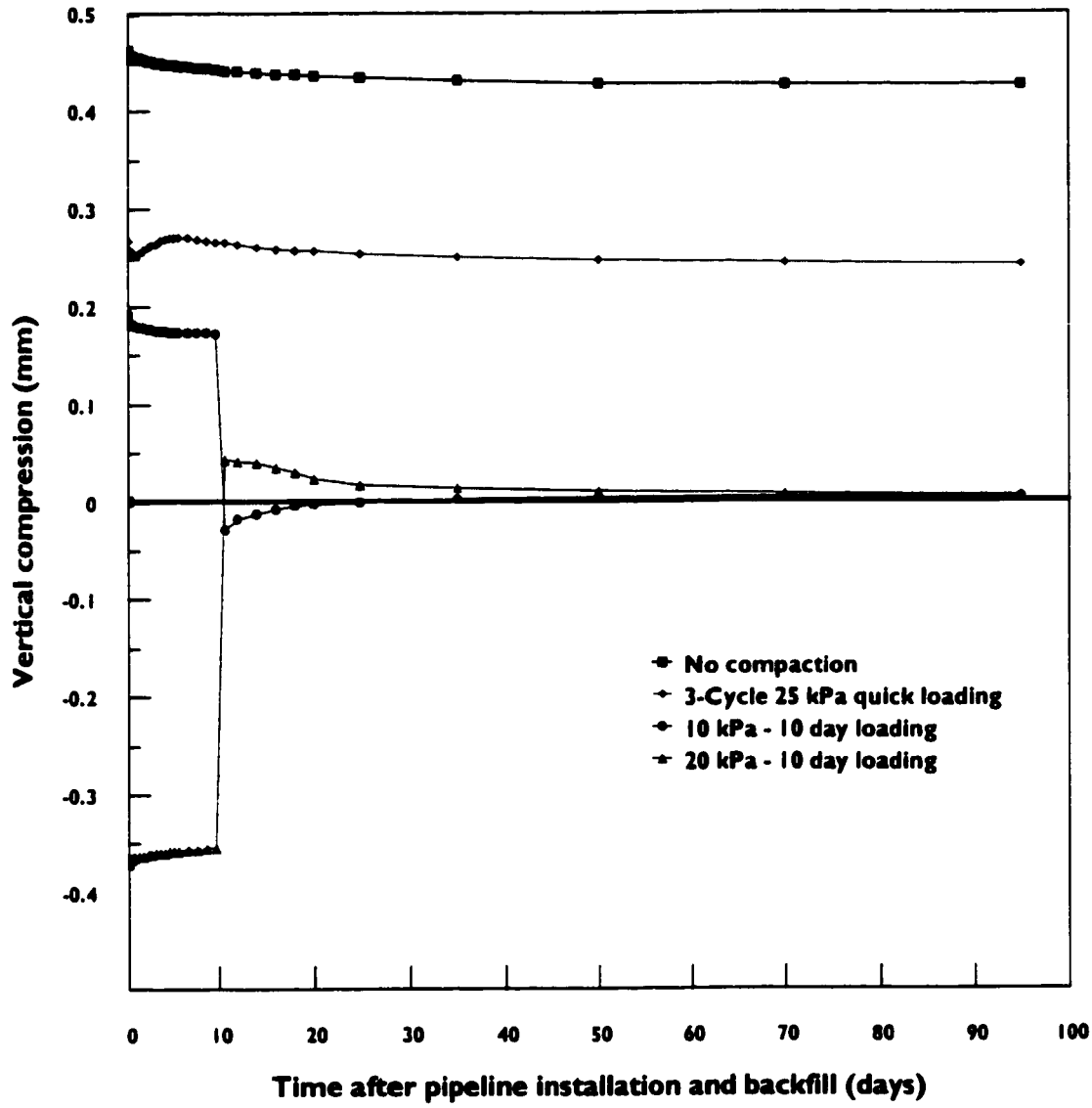

Figure 6-5: Vertical compression of pipeline, 20° slopes (With different compaction methods, 100 days)

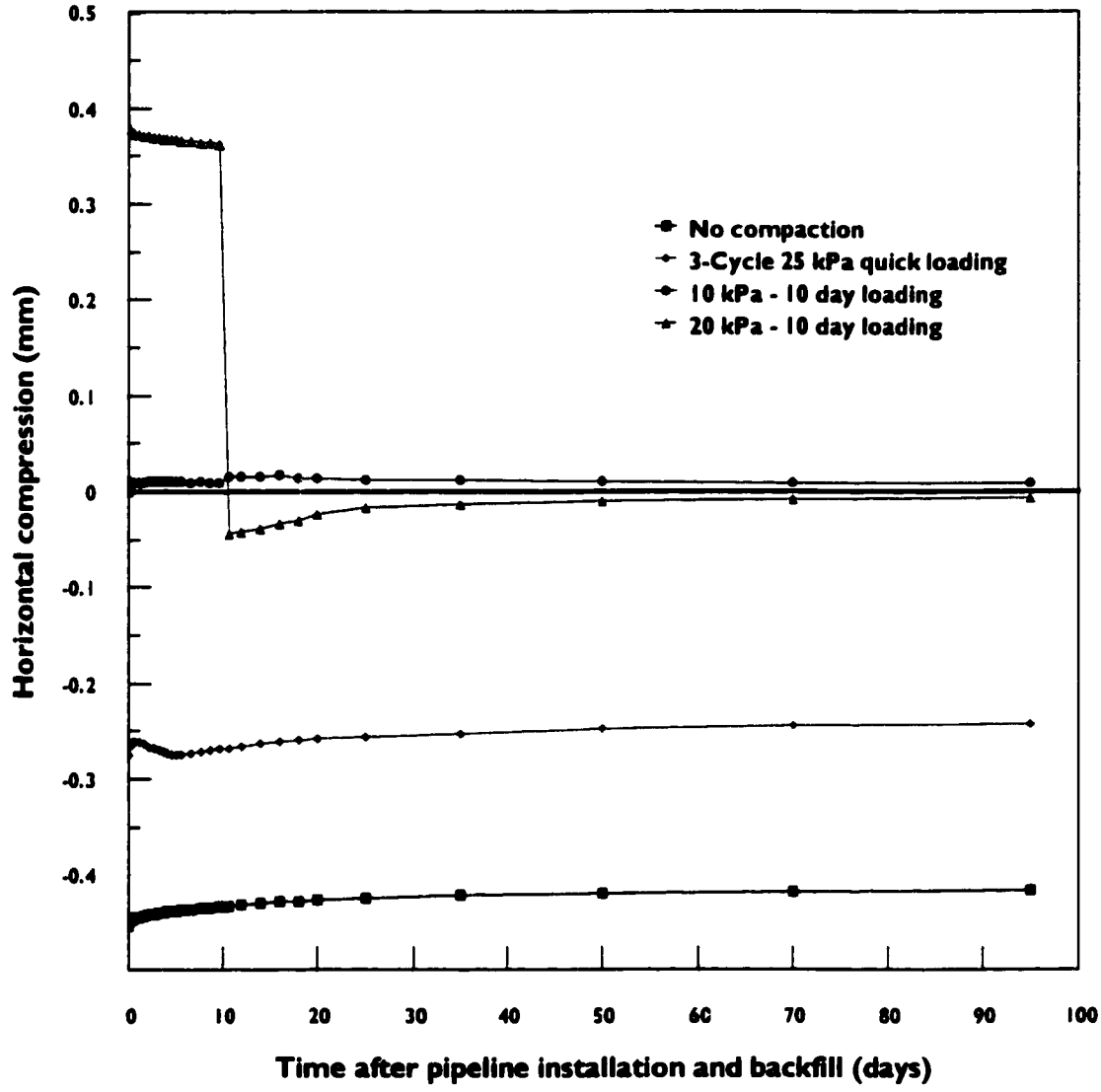

Figure 6-6: Horizontal compression of pipeline, 20° slopes (With different compaction methods, 100 days)

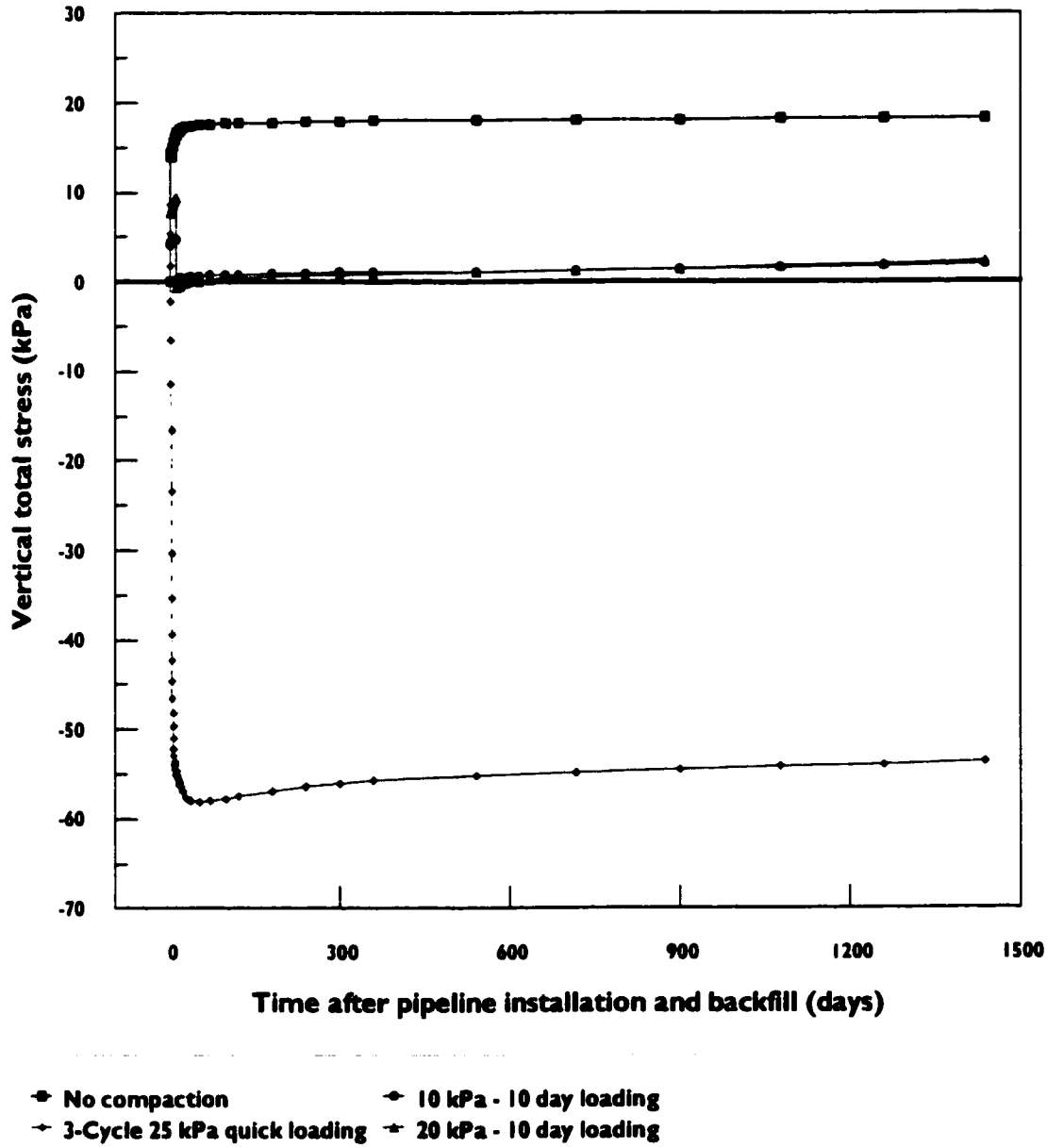

Figure 6-7: Vertical total stress at the pipeline base (With different compaction methods, 4 years)

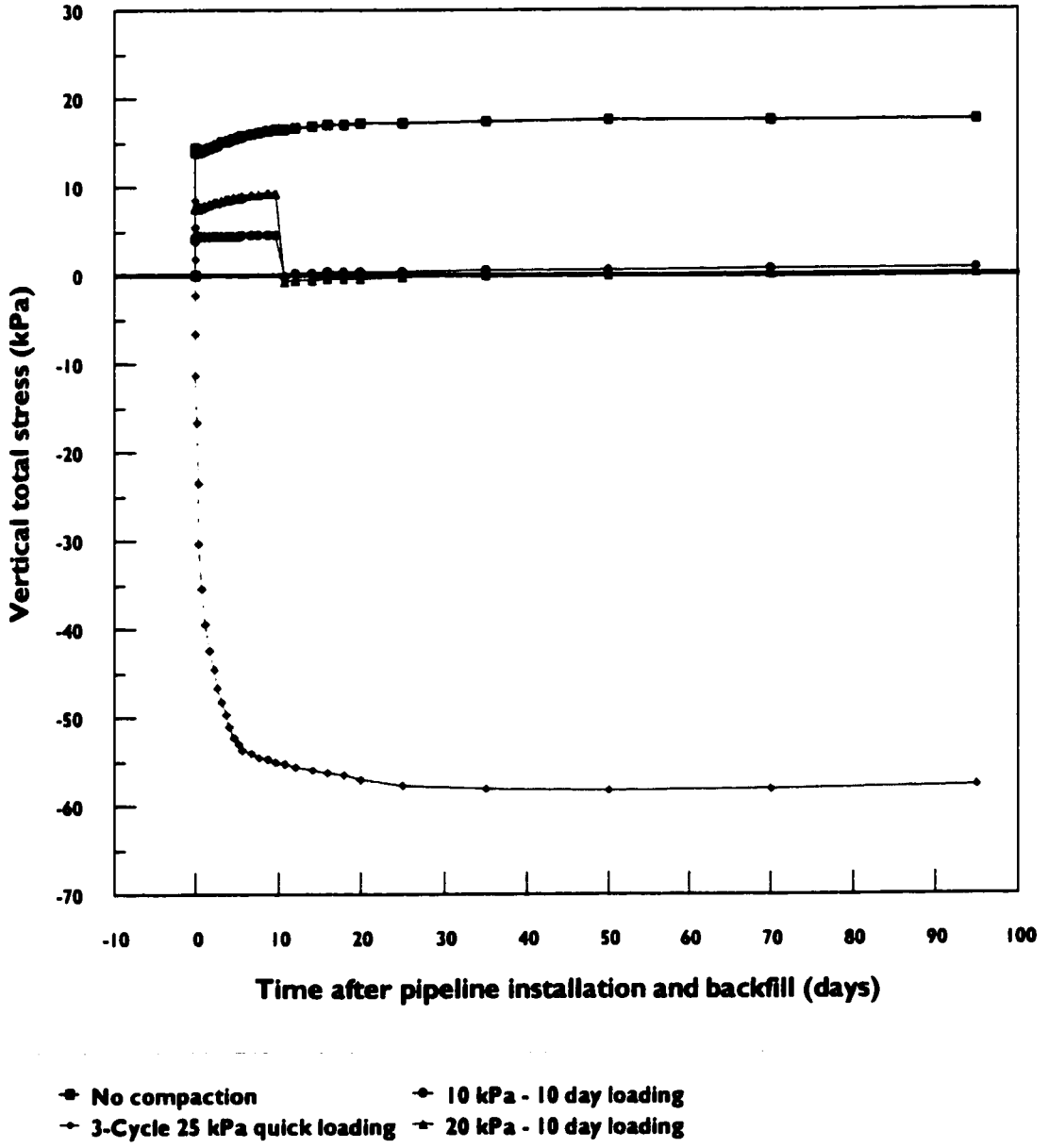

Figure 6-8: Vertical total stress at the pipeline base (With different compaction methods, 100 days)

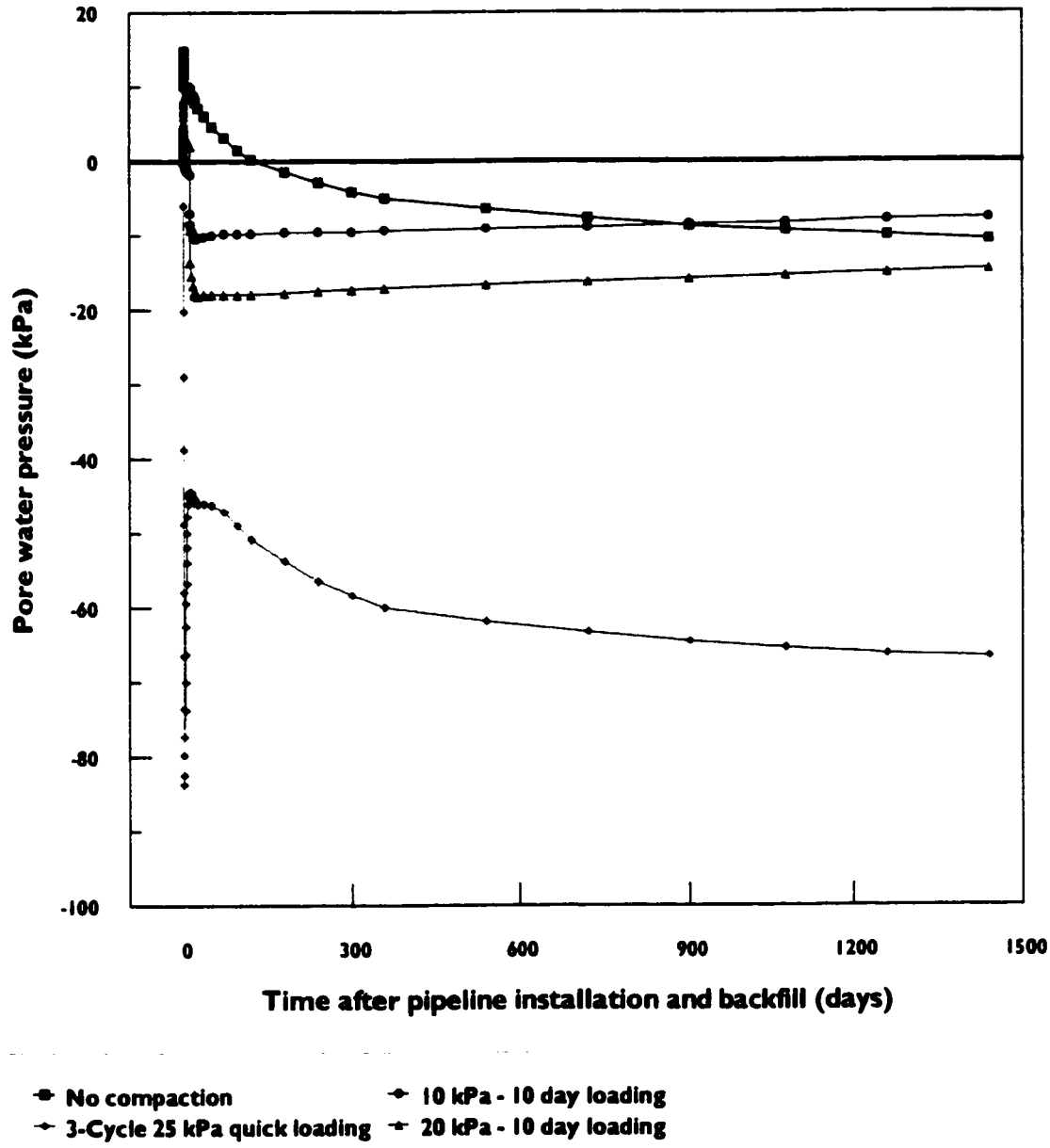

Figure 6-9: Pore water pressure at the pipeline base (With different compaction methods, 4 years)

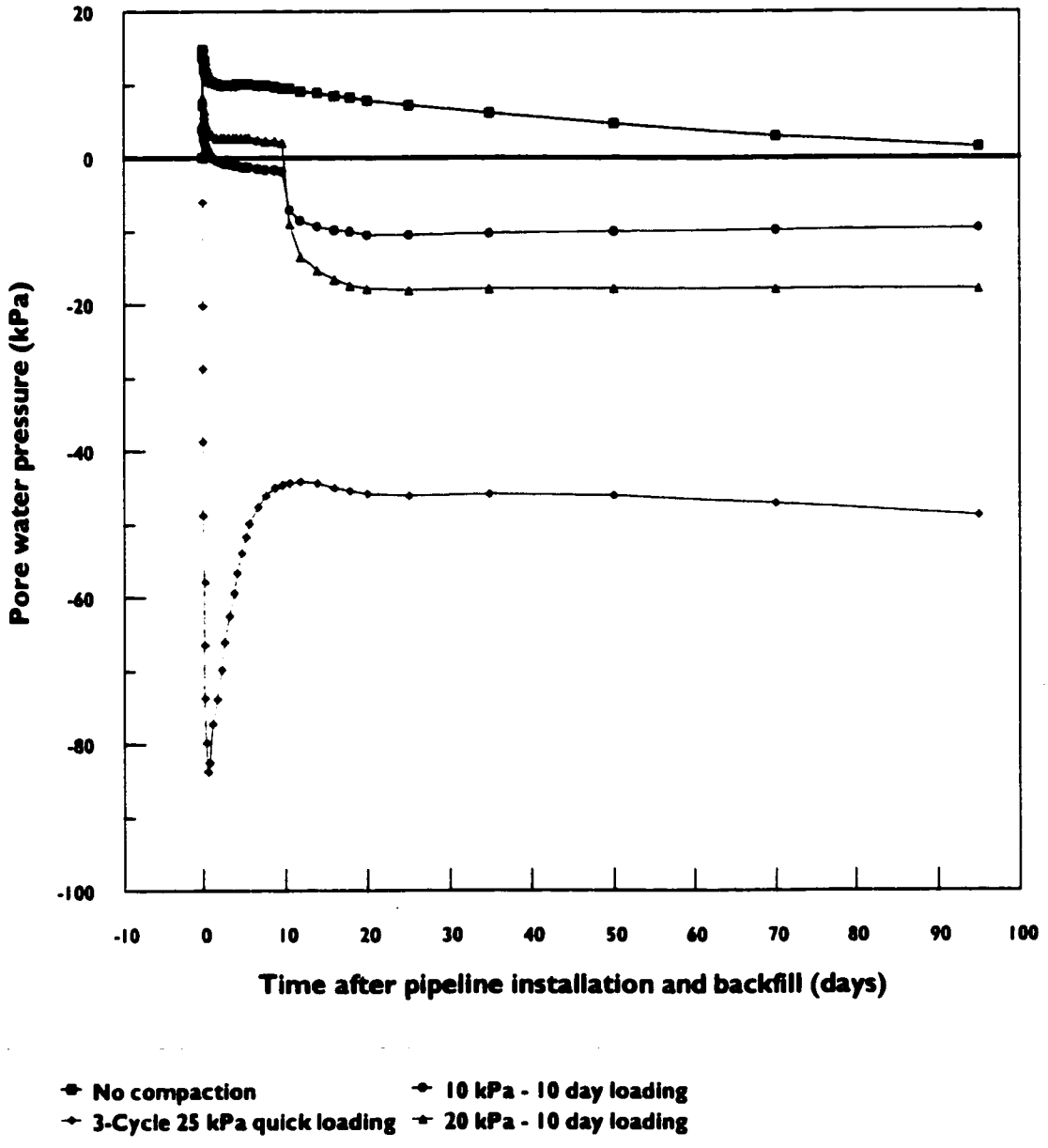

Figure 6-10: Pore water pressure at the pipeline base (With different compaction methods, 100 days)

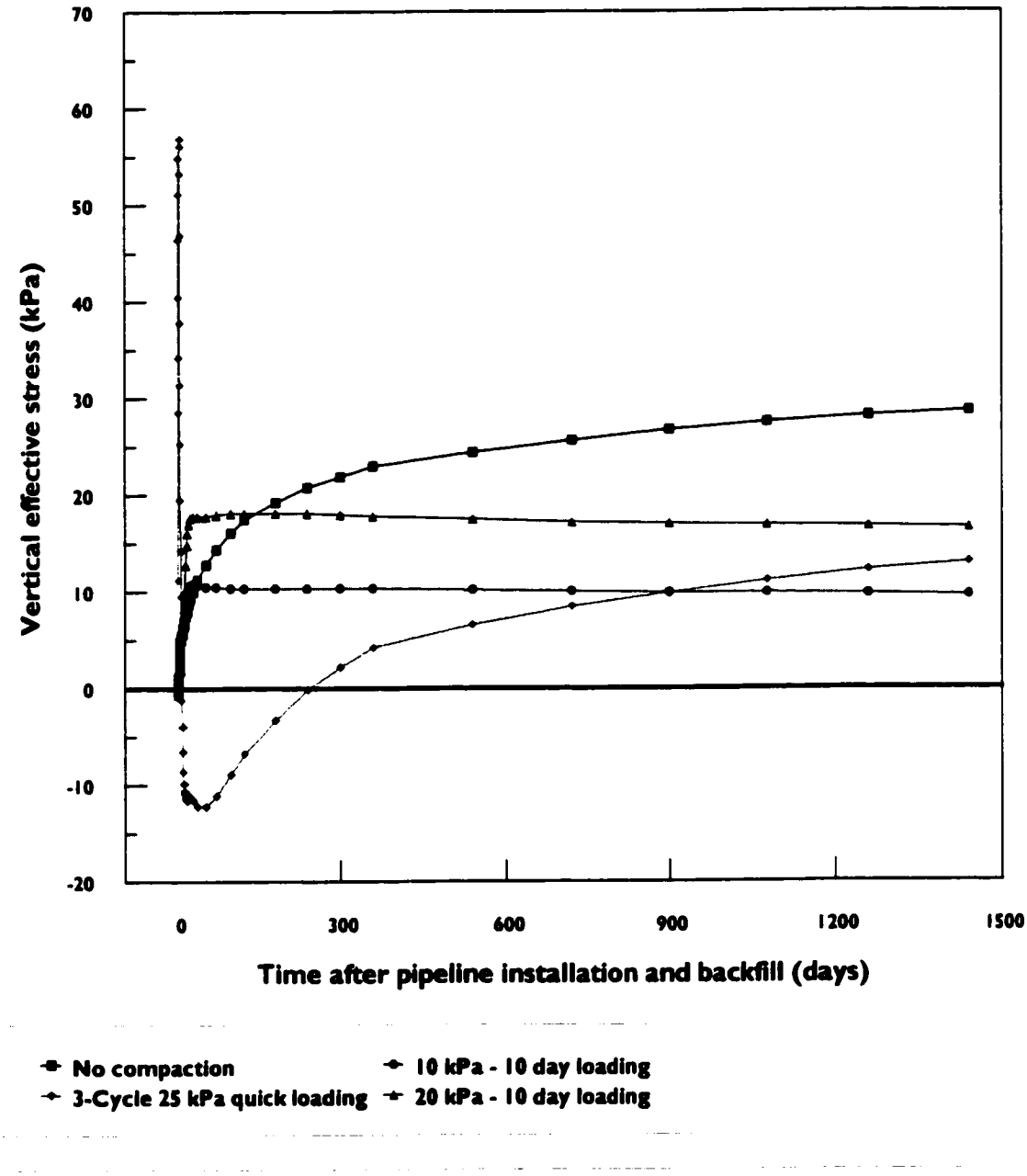

Figure 6-11: Vertical effective stress at the pipeline base (With different compaction methods, 4 years)

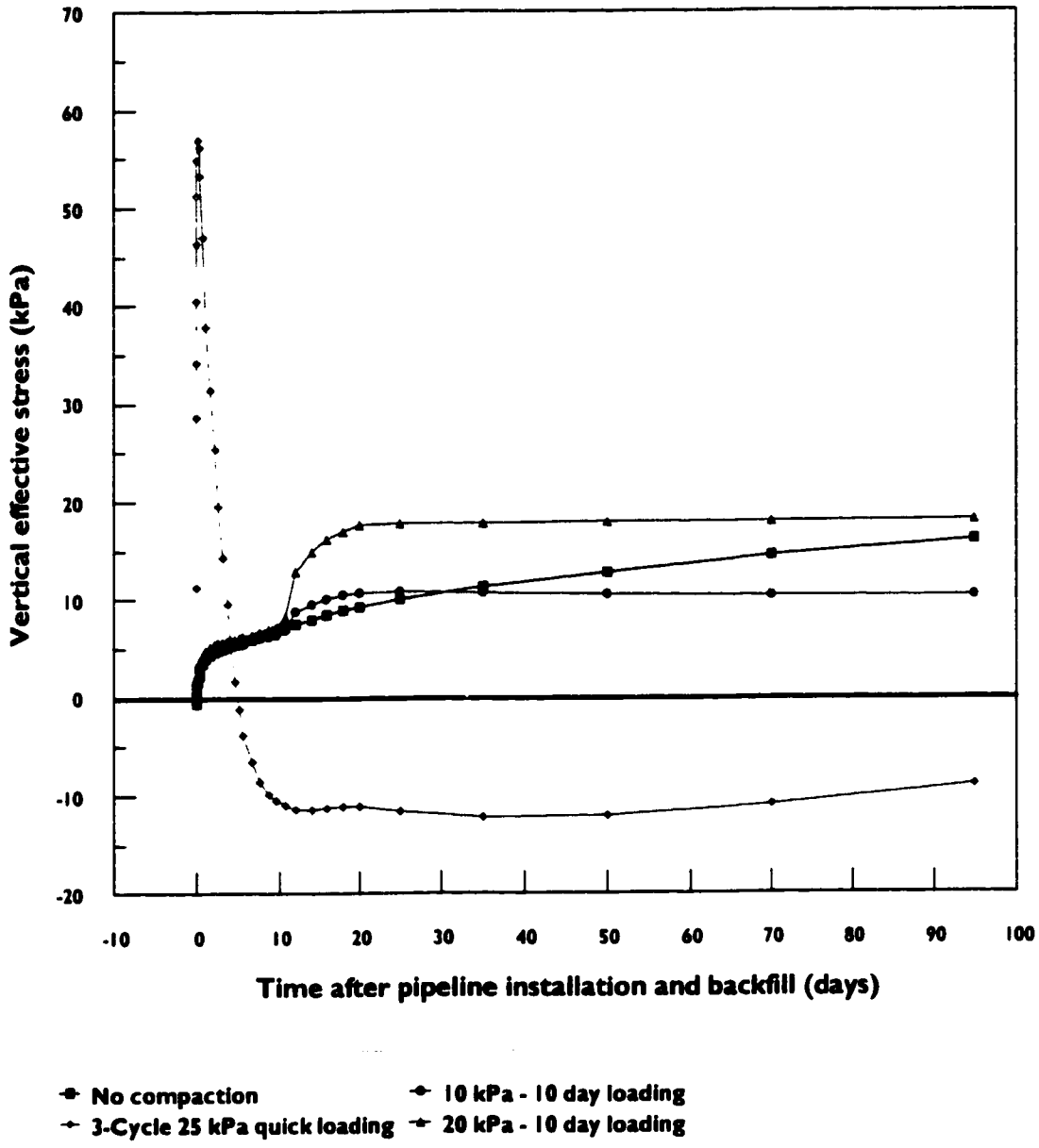

Figure 6-12: Vertical effective stress at the pipeline base (With different compaction methods, 100 days)

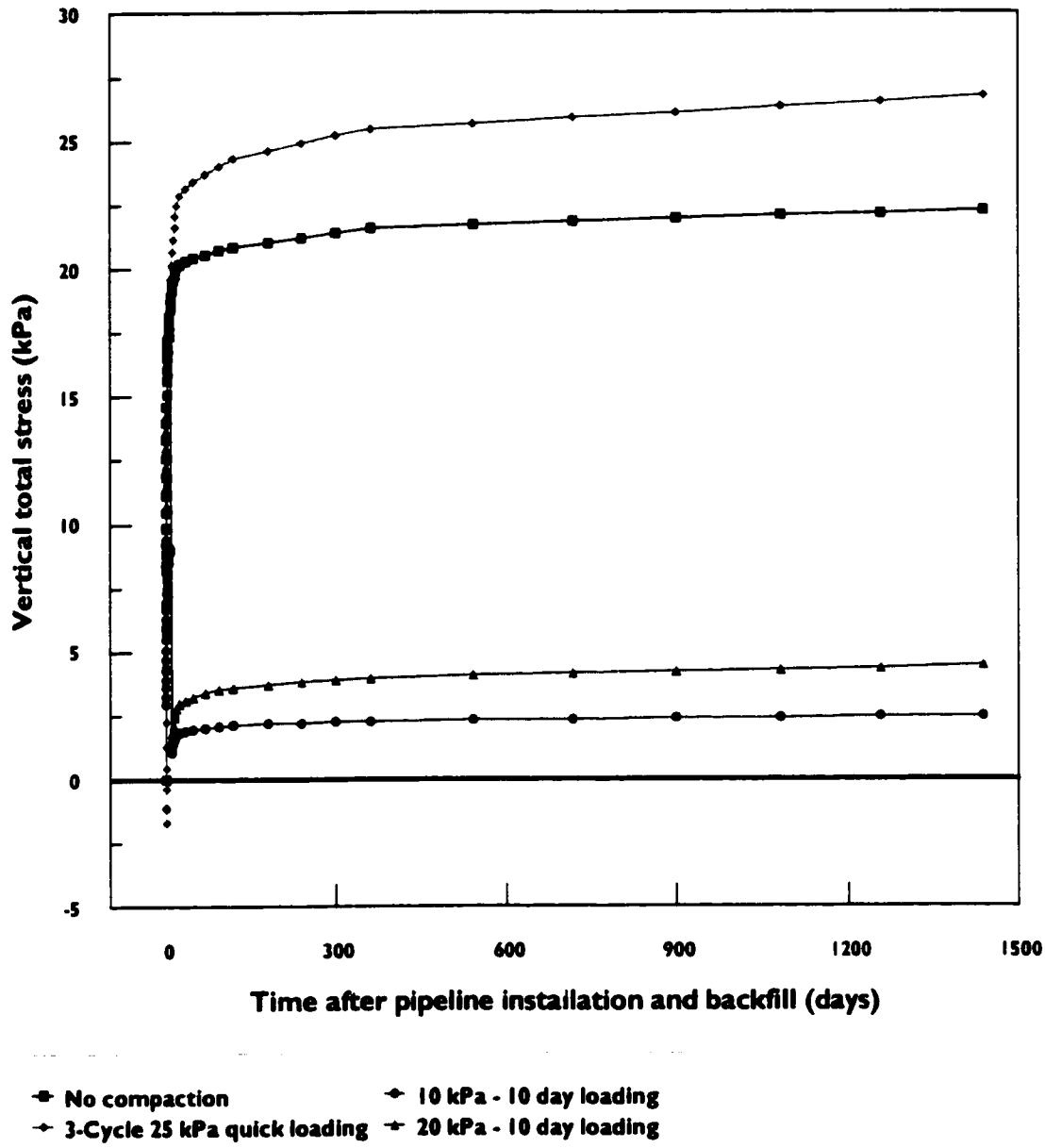

Figure 6-13: Vertical total stress at the pipeline crown (With different compaction methods, 4 years)

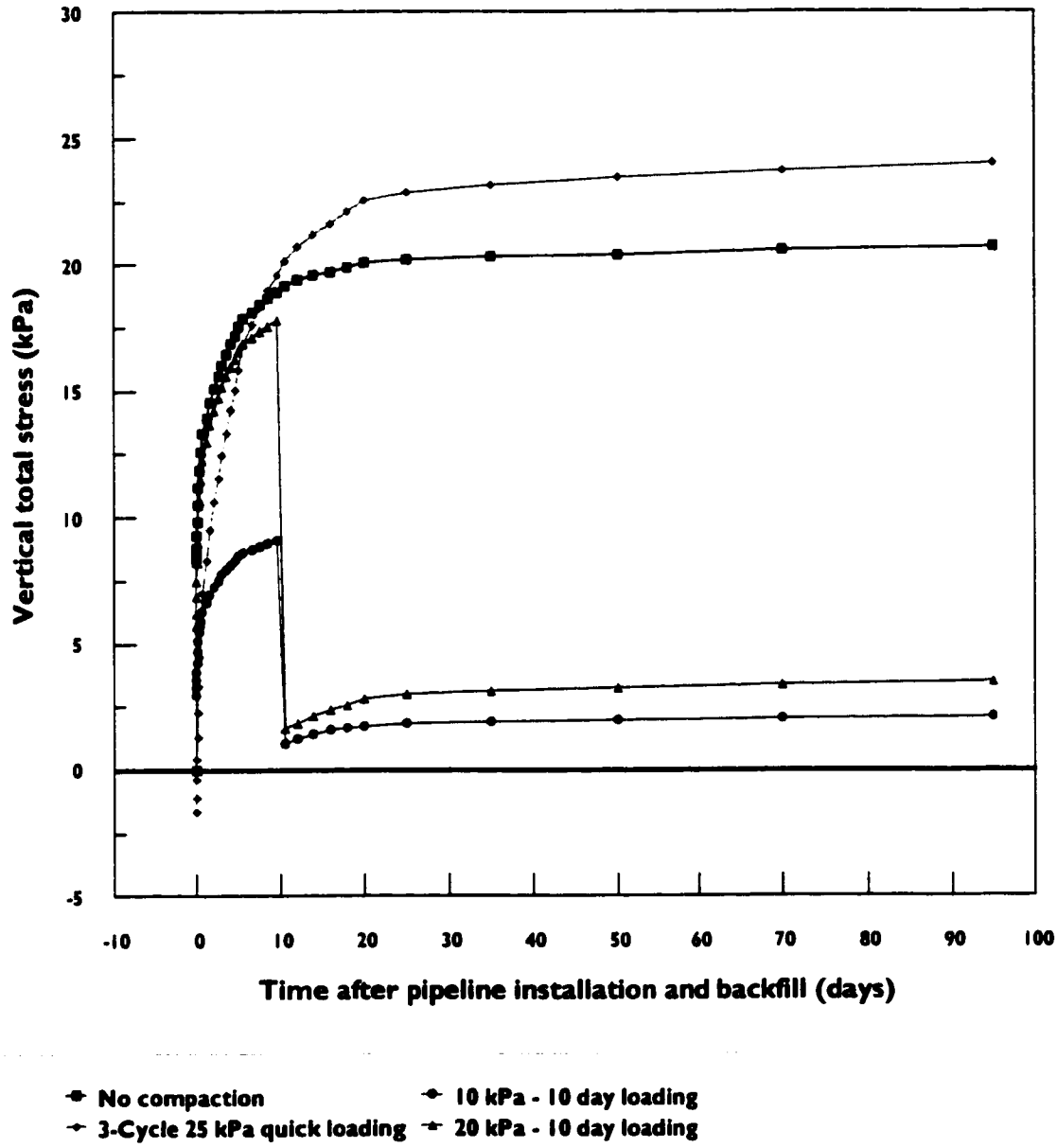

Figure 6-14: Vertical total stress at the pipeline crown (With different compaction methods, 100 days)

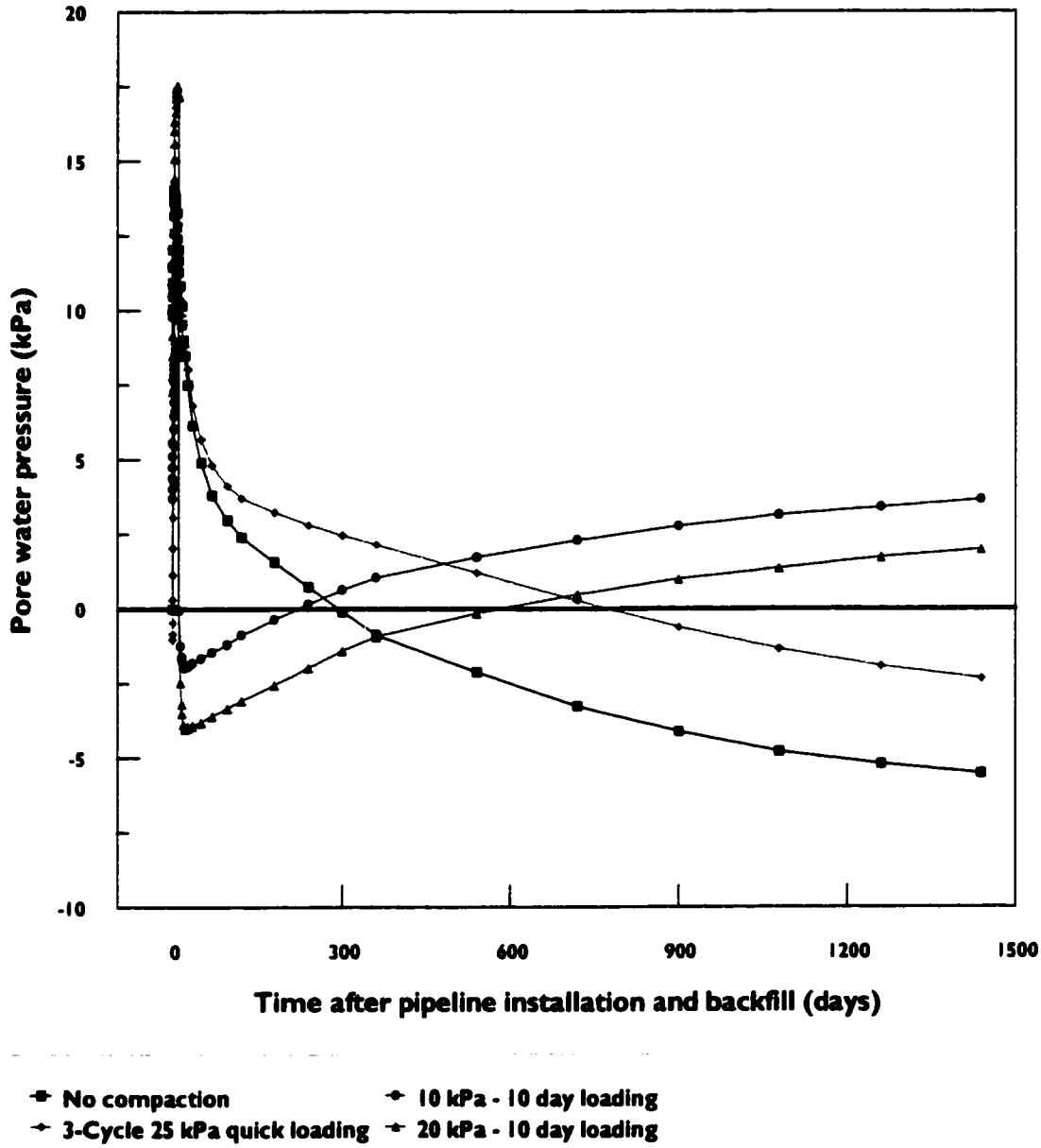

Figure 6-15: Pore water pressure at the pipeline crown (With different compaction methods, 4 years)

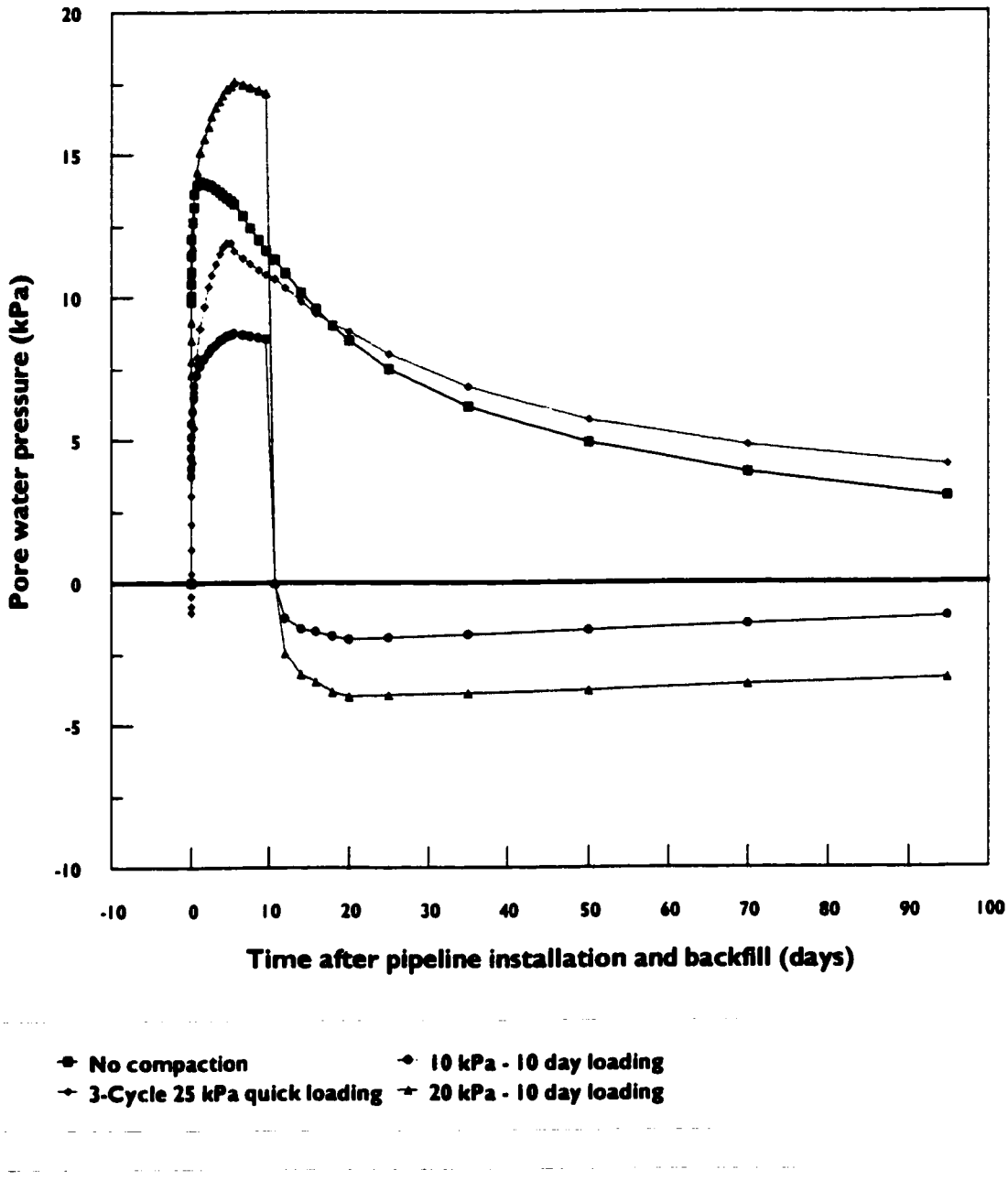

Figure 6-16: Pore water pressure at the pipeline crown (With different compaction methods, 100 days)

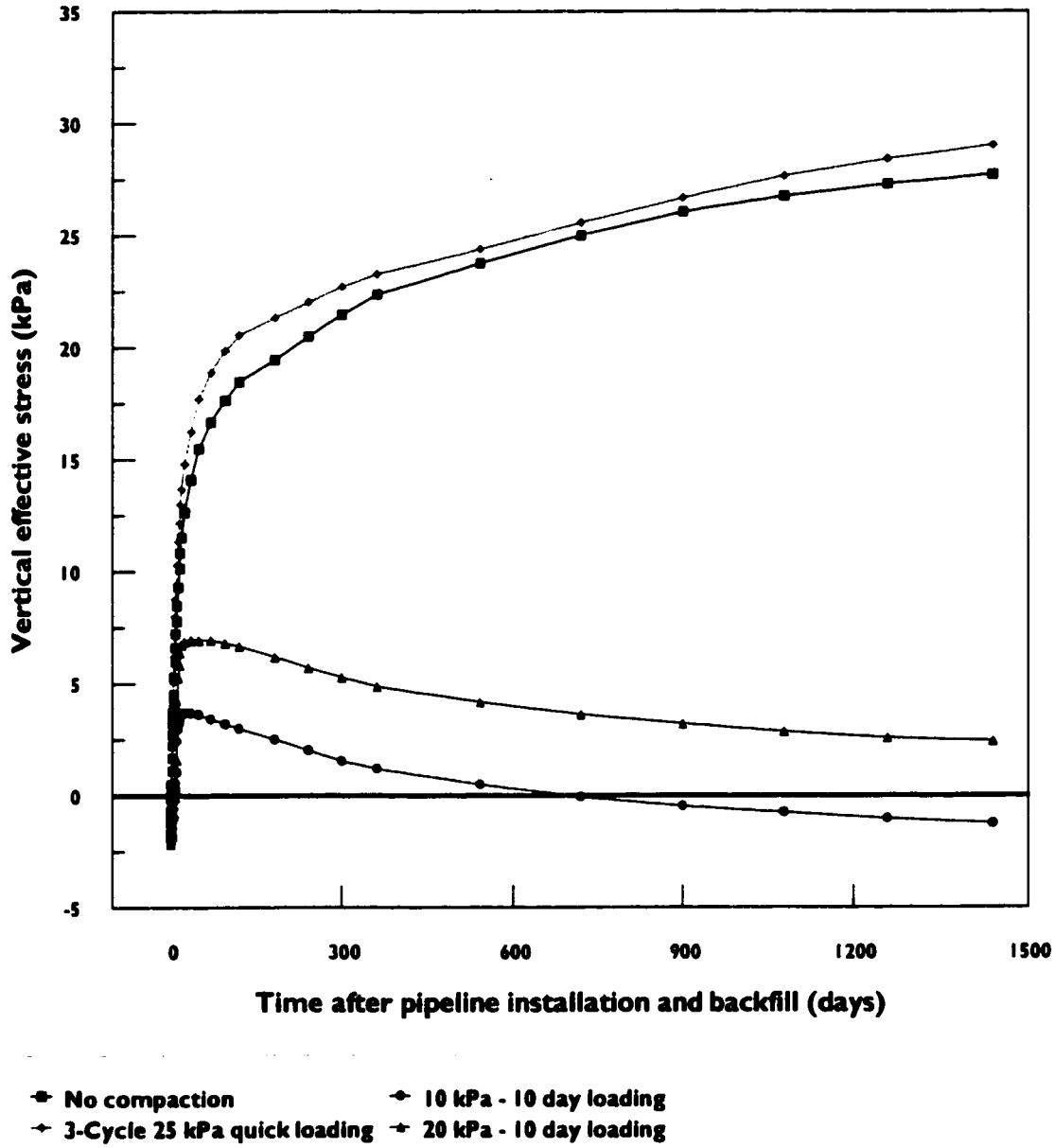

Figure 6-17: Vertical effective stress at the pipeline crown (With different compaction methods, 4 years)

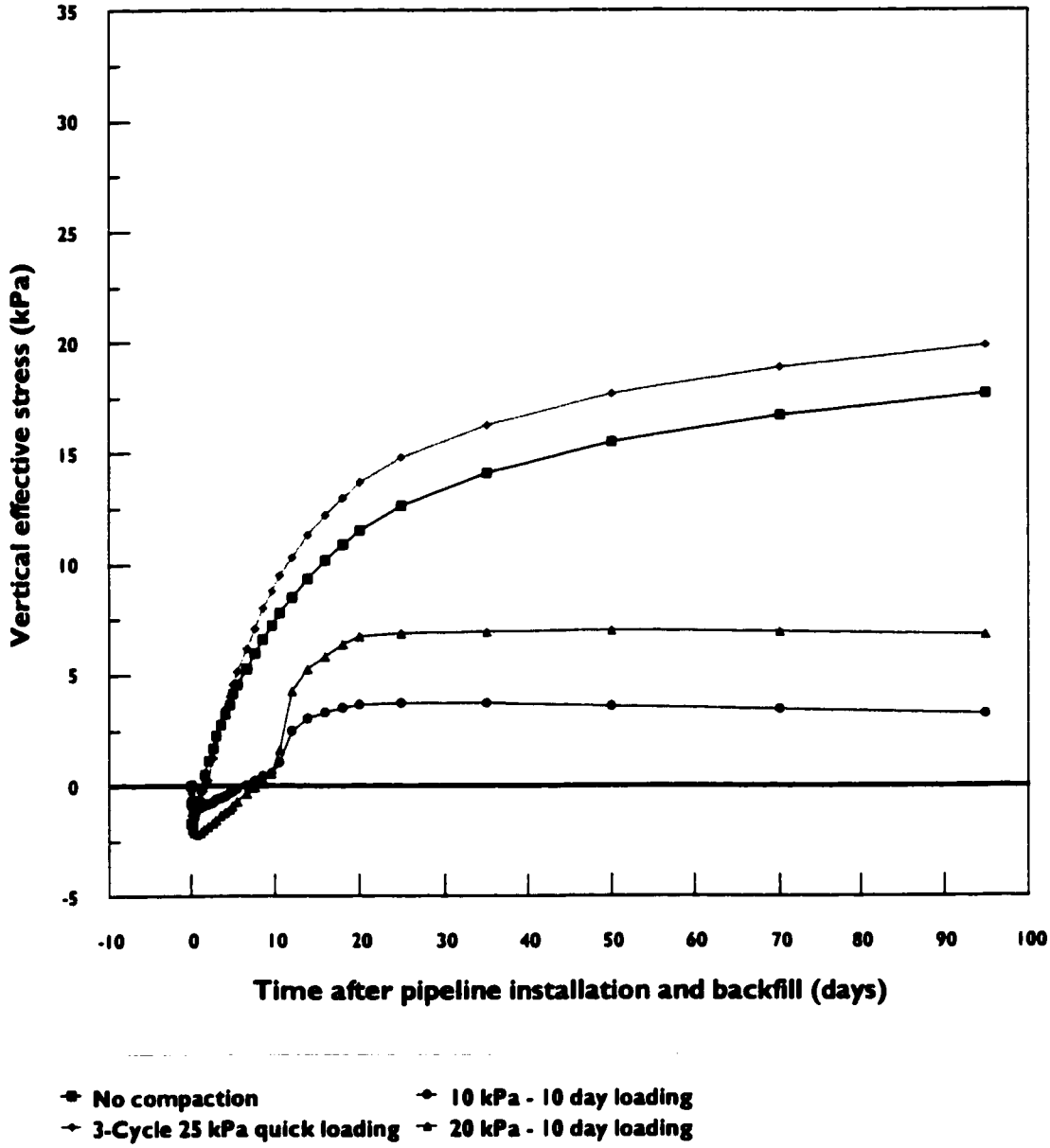

Figure 6-18: Vertical effective stress at the pipeline crown (With different compaction methods, 100 days)

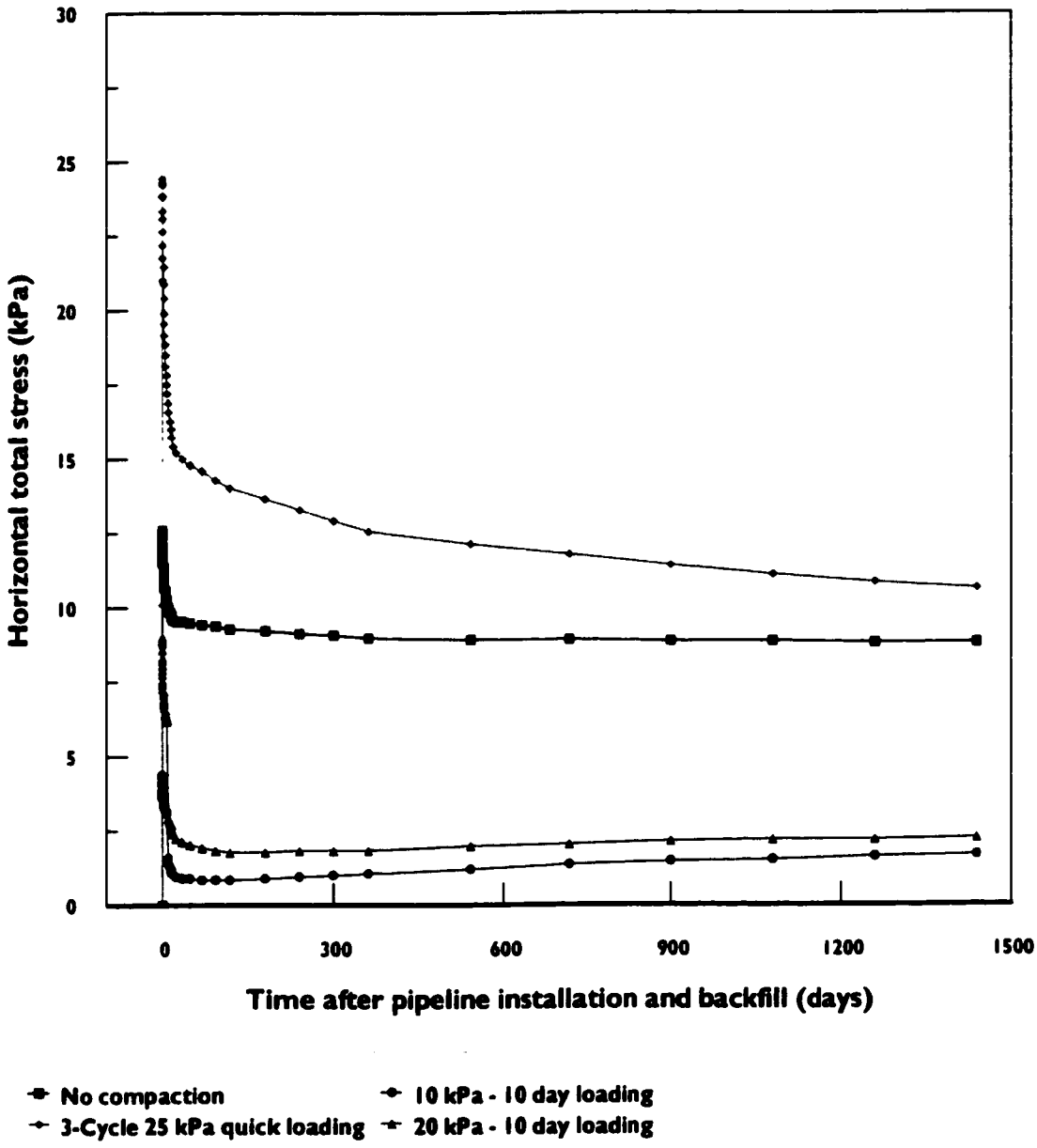

Figure 6-19: Horizontal total stress at the lateral pipe springline (With different compaction methods, 4 years)

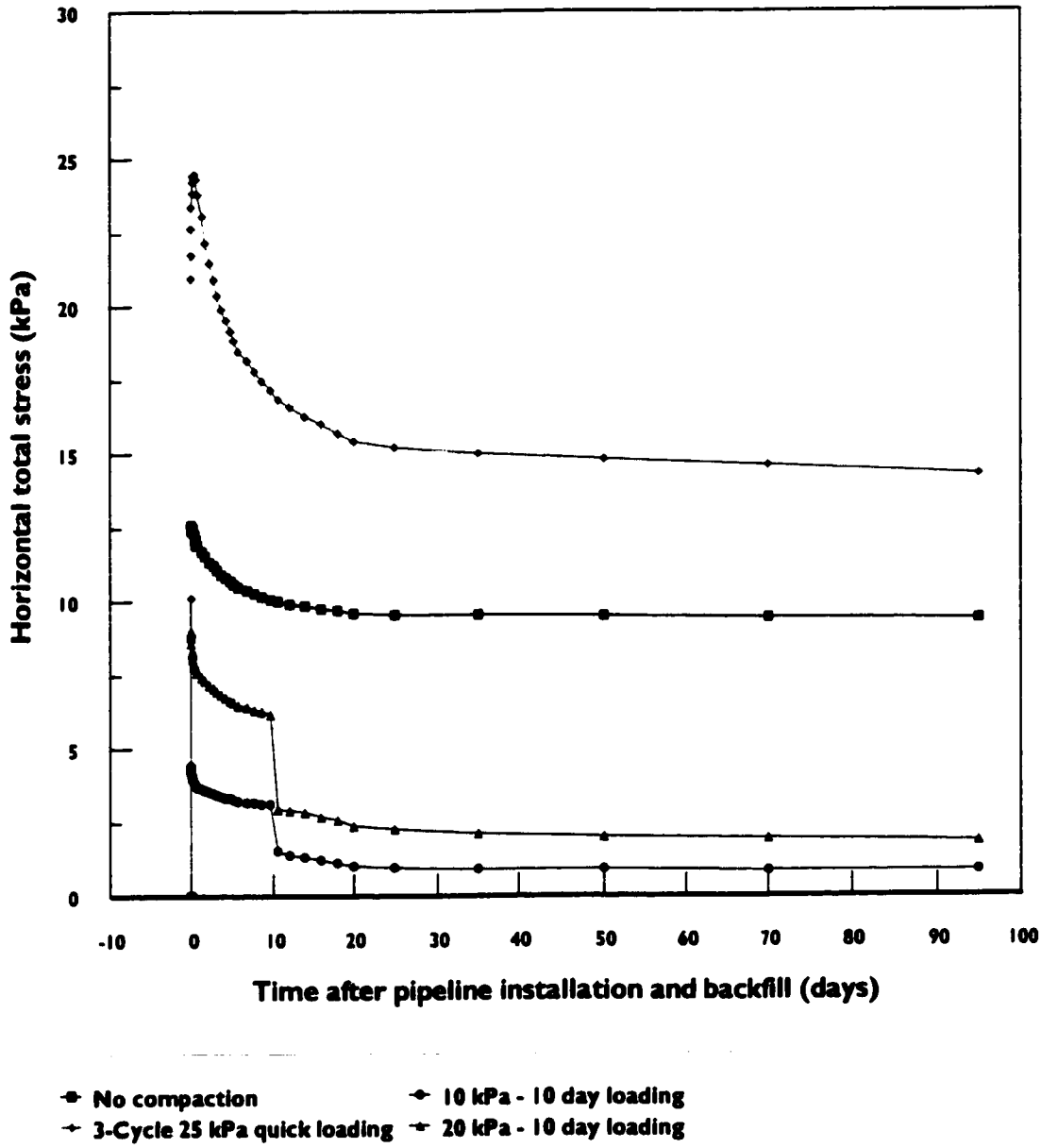

Figure 6-20: Horizontal total stress at the lateral pipe springline (With different compaction methods, 100 days)

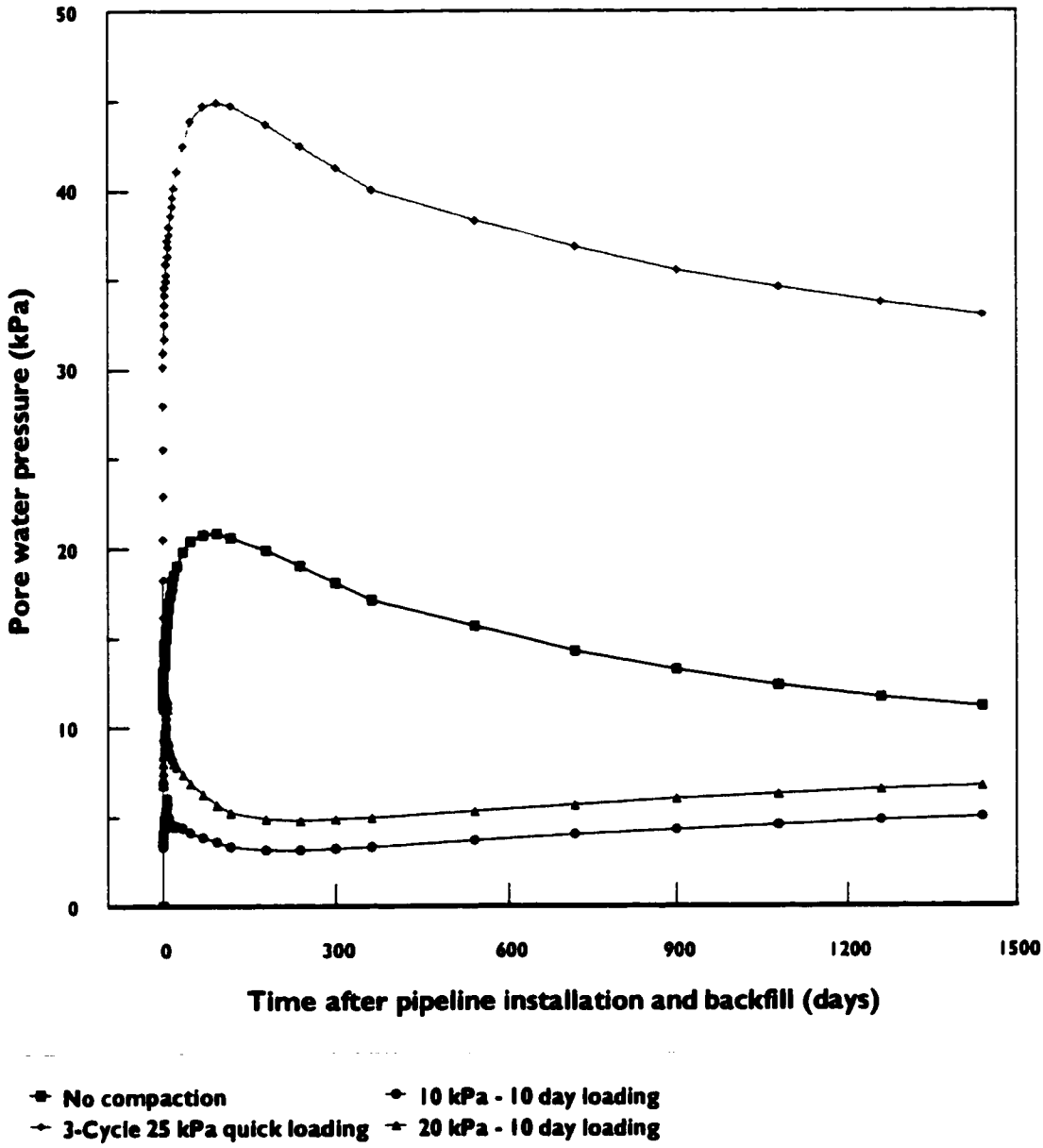

Figure 6-21: Pore water pressure at the lateral pipe springline (With different compaction methods, 4 years)

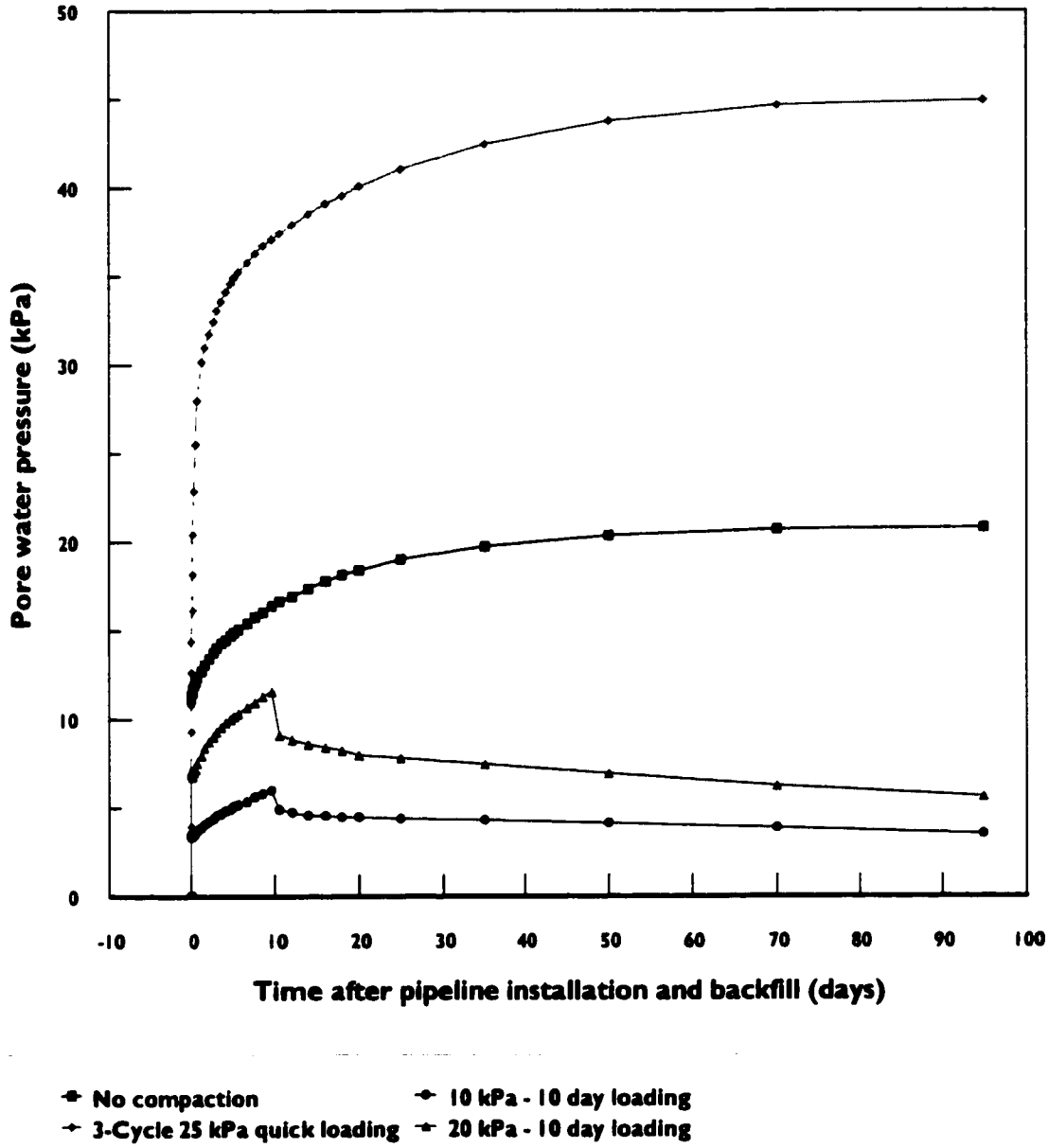

Figure 6-22: Pore water pressure at the lateral pipe springline (With different compaction methods, 100 days)

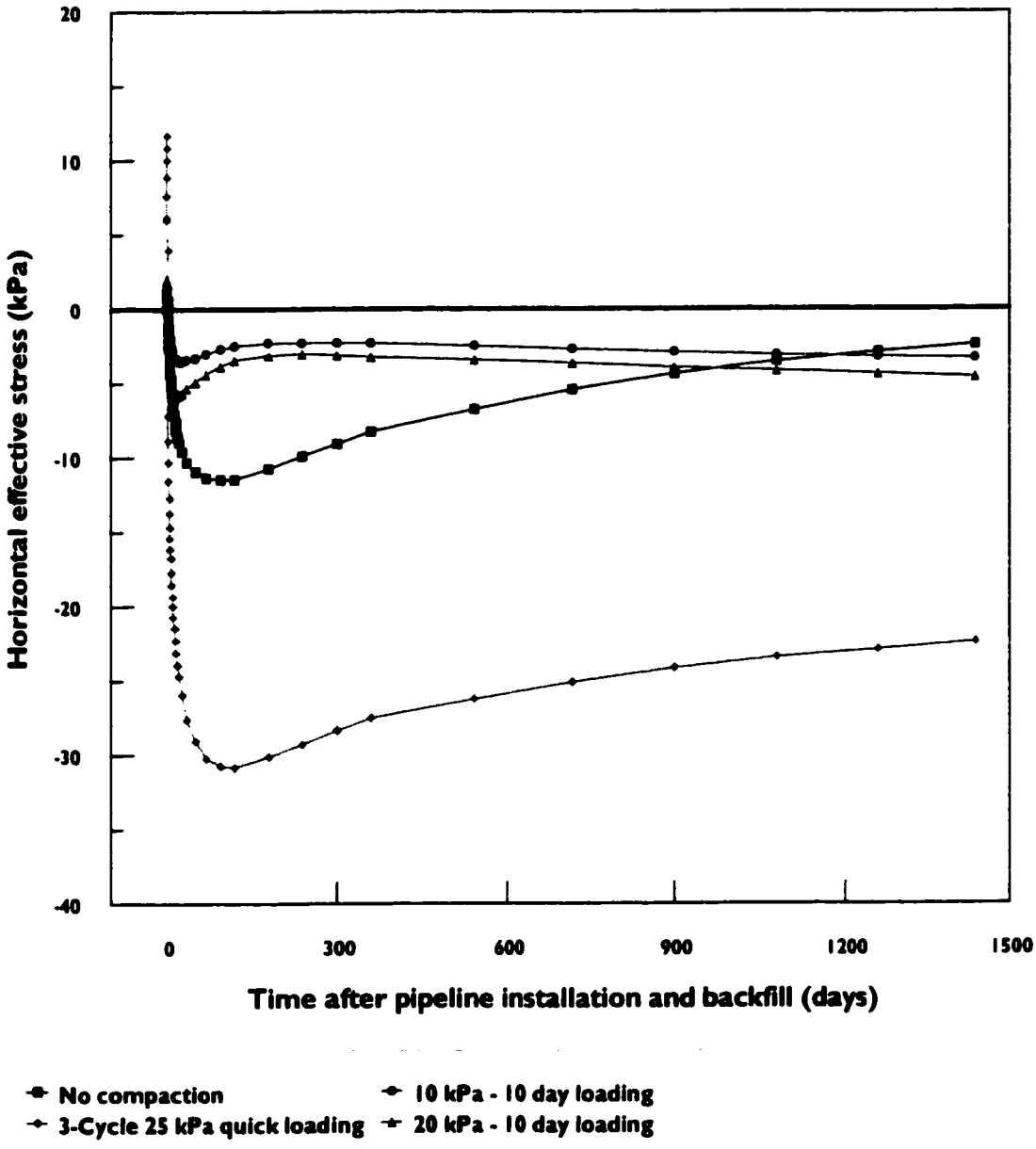

Figure 6-23: Horizontal effective stress at the lateral pipe springline (With different compaction methods, 4 years)

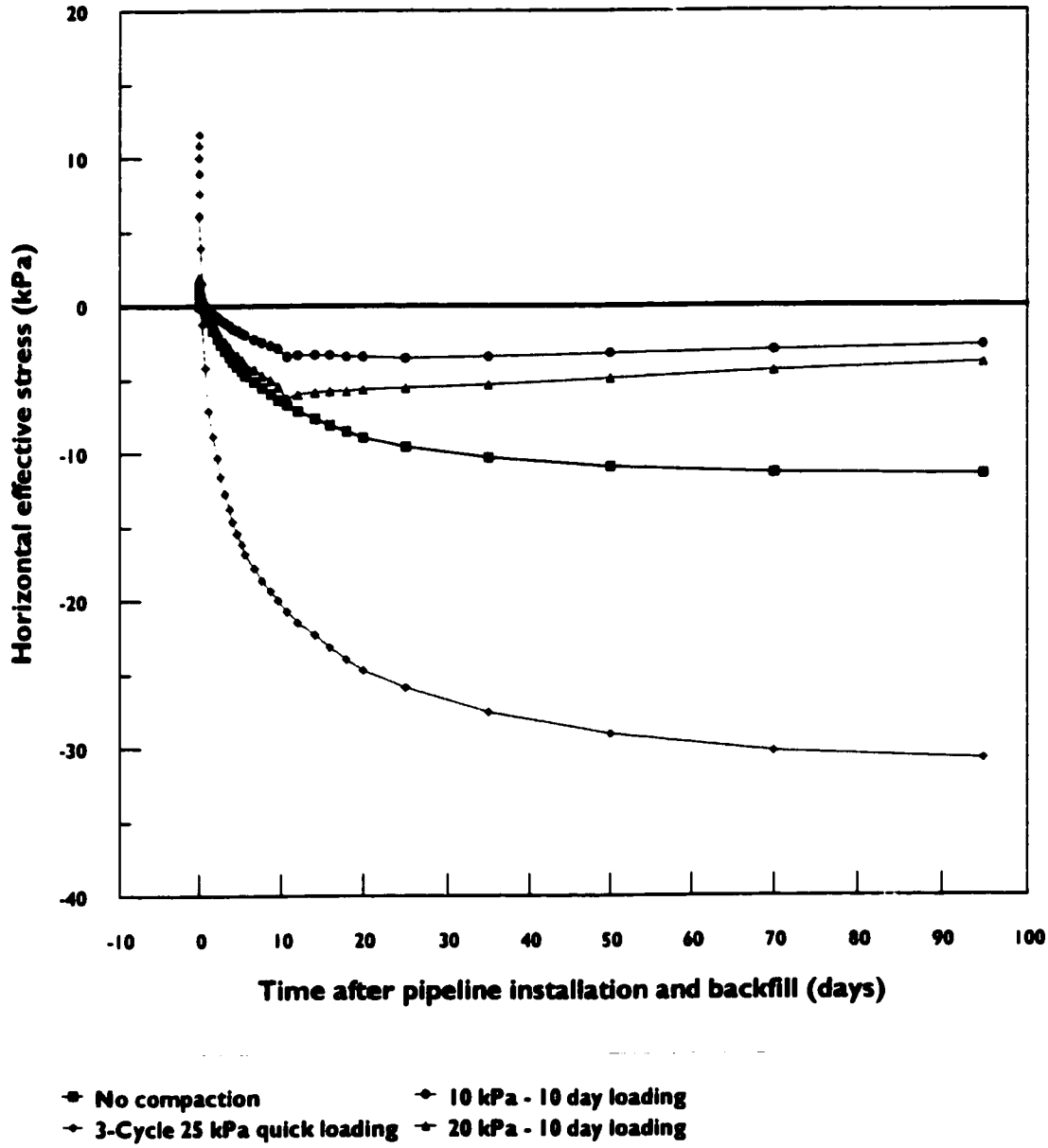

Figure 6-24: Horizontal effective stress at the lateral pipe springline (With different compaction methods, 4 years)

CHAPTER 7

PIPELINE STIFFNESS EFFECT ON SOIL/PIPELINE INTERACTION

CHAPTER 7

EFFECT OF PIPELINE STIFFNESS ON SOIL/PIPELINE INTERACTION

7.1. INTRODUCTION

In the previous chapter, three study cases are analyzed with different methods of compaction applied to the backfill. These cases were studied using the finite element model with 20° slopes and 25 mm pipeline wall thickness. The same parameters were used for the soil model as in the initial analysis investigating the effect of different slope angles.

In this chapter, the same finite element model described above is used to investigate the effect of pipeline wall thickness on the interaction. All other parameters and variables fixed, the only variable modified to conduct this study is the thickness of the structural elements simulating the pipeline section, and obviously the corresponding moment of inertia and cross-section area of each element. Five cases with different values of the pipeline wall thickness, in addition to the initial 25 mm wall, a total of six cases, are investigated.

The simulation performed in the following analyses, as in the previous analyses, considers the effects of construction procedures (excavation and backfilling), however, the simulation is limited to about 95 days (about three months) after backfilling.

7.2. THE FINITE ELEMENT MODEL

As mentioned earlier, the analysis performed in this chapter is similar to the one performed earlier for the pipeline installation in a v-shaped depression, with side slopes of 20° (2.7H:1V). Therefore, a two-dimensional finite element mesh, similar to the one shown in Figure 5-1 (the sloping angle being the only difference), is used in the following analyses in this chapter.

7.3. ANALYSIS PROCEDURE

The same in–situ conditions obtained previously with $K_o = 2$ for Case 4, followed by the same two-stage excavation and 40 minute wait until the placement of the pipeline segment and backfill, are used as initial conditions for each of the six study cases (the various pipeline wall thickness values). No compaction is applied in this study, the London clay fill is placed, and its reaction to its own weight is analyzed. Pipeline wall thickness of 5 mm, 10 mm, 15 mm, 20 mm, 25 mm, and 50 mm are investigated, separating six study cases: Case 8 through Case 13, respectively. The analysis is continued in all six cases to simulate the time dependant effects of excavation, pipeline placement, and backfilling over the following 95 days (about three months).

7.4. ANALYSIS RESULTS

As mentioned earlier, the initial conditions for the three analysis cases are the computed conditions of the model section with excavated trench, one hour after the start of excavation (i.e. 40 minutes after the end of excavation) where the pipeline segment and the London Clay backfill were placed. Following is a presentation of some analysis results from the six cases: Case 8 through Case 13. It should be noted that Case 12, with 25 mm pipeline wall thickness, is the same as Case 4 investigated earlier.

7.4.1. PIPELINE DEFORMATION

The first effect to examine is the pipeline deformation with time. Pipeline compression is defined as the relative displacement between two edges of the same diameter line. The computed vertical compression with time for all analysis cases are presented in Figure 7-1. As expected, the thinner the pipeline wall the larger the compression. The Computed compression ranges from a negligible one (about 0.05 mm) for the pipeline with 50 mm wall thickness through about 5.2 mm for the pipeline with 5 mm wall thickness. Note that the deformation of pipelines with thinner walls continues to increase throughout the 95 days analyzed, while the more rigid pipelines show a negligible change past the initial deformation after fill placement.

7.4.2. STRESSES AND PORE WATER PRESSURE AROUND THE PIPELINE

Analysis results of the six cases in terms of stresses and pore water pressure with time after pipeline installation and backfilling are reported at three points around the pipeline section as in the previous discussions. Vertical effective stress and pore water pressure are reported at the base (lowest point of the pipeline cross-section) in Figures 7-2 and 7-3, and at the crown (highest point of the pipeline cross-section) in Figures 7-4 and 7-5. In the same manner, horizontal effective stress and pore water pressure are reported at the lateral springline of the pipeline cross-section in Figures 7-6 and 7-7. Stress and pore water pressure with time are presented over the duration of the analysis (about 3 months after backfilling).

The weight of the backfill is carried by both the pipeline and the fill material between the pipeline and the trench walls. The distribution of that load between the pipeline and the surrounding soil is in proportion to the stiffness of each medium. It is therefore obvious that the less rigid pipeline will carry less of the overlying fill weight and the surrounding soil will therefore carry more load. Such distribution will result in more compaction of the fill around the pipeline and hence some uplift forces applied to the pipeline below its springline. The change in vertical effective stress pore water pressure with time, at the base of the pipeline, presented in Figures 7-2 and 7-3, respectively, show clearly the effect of pipeline stiffness in accordance with the above discussion. The less rigid pipeline applies less pressure at the base, since it carries less of the fill weight and it is also subjected to higher uplift forces from the surrounding soil. For the same reasons, the less rigid pipeline generates less pore water pressure at the base initially, however, since the surrounding soil carries more load than in the case of a more rigid pipeline, and hence is subjected to higher pore water pressure, the gradient for pore water pressure dissipation at the pipeline base is smaller. This results in slower dissipation of pore water pressure at the base of the less rigid pipelines which is clearly reflected in Figure 7-3.

The principle discussed above is confirmed by observing the development of vertical effective stress and pore water pressure at the pipeline crown, presented in Figures 7-4 and 7-6, respectively. The more rigid pipelines carry more of the overlying fill weight, hence higher vertical effective stress and higher pore pressure are computed. In the case of the least rigid pipeline (5 mm wall thickness), the larger weight carried by the surrounding fill causes high pressure on the pipeline section above the springline which deforms the pipeline vertically in compression. This compression initiated by contact pressure away from the pipeline crown creates an expansion between the crown and the overlying soil which does not deform as fast.

This explains the negative effective stress computed at the crown (see Figure 7-4). Gradually, as the pipeline deformation becomes slower, the tension zone at the crown is gradually replaced by pressure from overlying soil being consolidated. Eventually, a slightly positive vertical effective stress is computed about 95 days after backfilling. Pore water pressure dissipation is also slower at the crown with less rigid pipelines for the same reasons discussed above.

In light of the above discussion, it is expected that higher horizontal effective stresses and higher pore water pressures be computed at the springline of the pipeline section of the less rigid pipelines. Figures 7-6 and 7-7 confirm these expectations, although, negative effective stresses are still computed in all cases. In addition, by carrying most of the fill weight, the more rigid pipelines cause a delay in the pore water pressure build-up along the side of the pipeline, which is also reflected in Figure 7-7.

7.4.3. CORRELATION OF RESULTS

In this section, vertical effective stresses at the pipeline base and crown, and pipeline deformation, at the end of the analysis period of 95 days, are correlated with the pipeline wall thickness. This correlation shown Figure 7-8 is a useful tool for optimizing pipeline design, however, it is limited to the specific geometry and soil conditions of this study. Further parametric studies considering a range of native and backfill soil types, as well as various site layouts, are necessary to produce a complete design tool. The correlation shows clearly a qualitative characteristic of pipeline/soil interaction, associating less rigid pipelines with lower stresses and higher deformations.

7.5. CONCLUSIONS

An important conclusion from the analyses is that a less rigid pipeline section would carry less of the weight of overlying fill material and will cause more of the load to be carried by the fill material on either side of the pipeline. This results in higher lateral pressure on the pipeline section and slower dissipation of pore water pressure around the pipeline.

FIGURES

CHAPTER 7

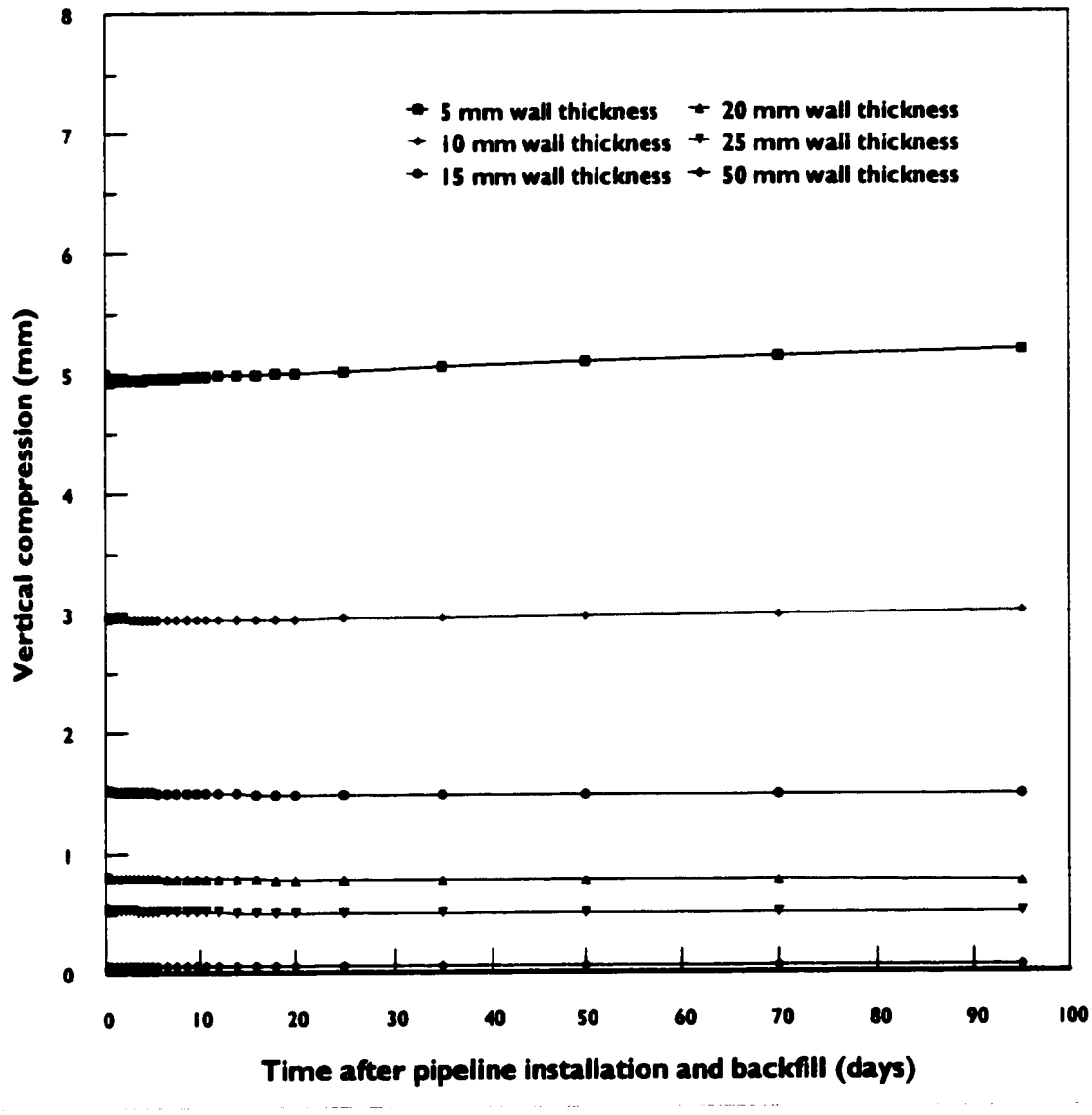

Figure 7-1: Vertical compression of pipeline

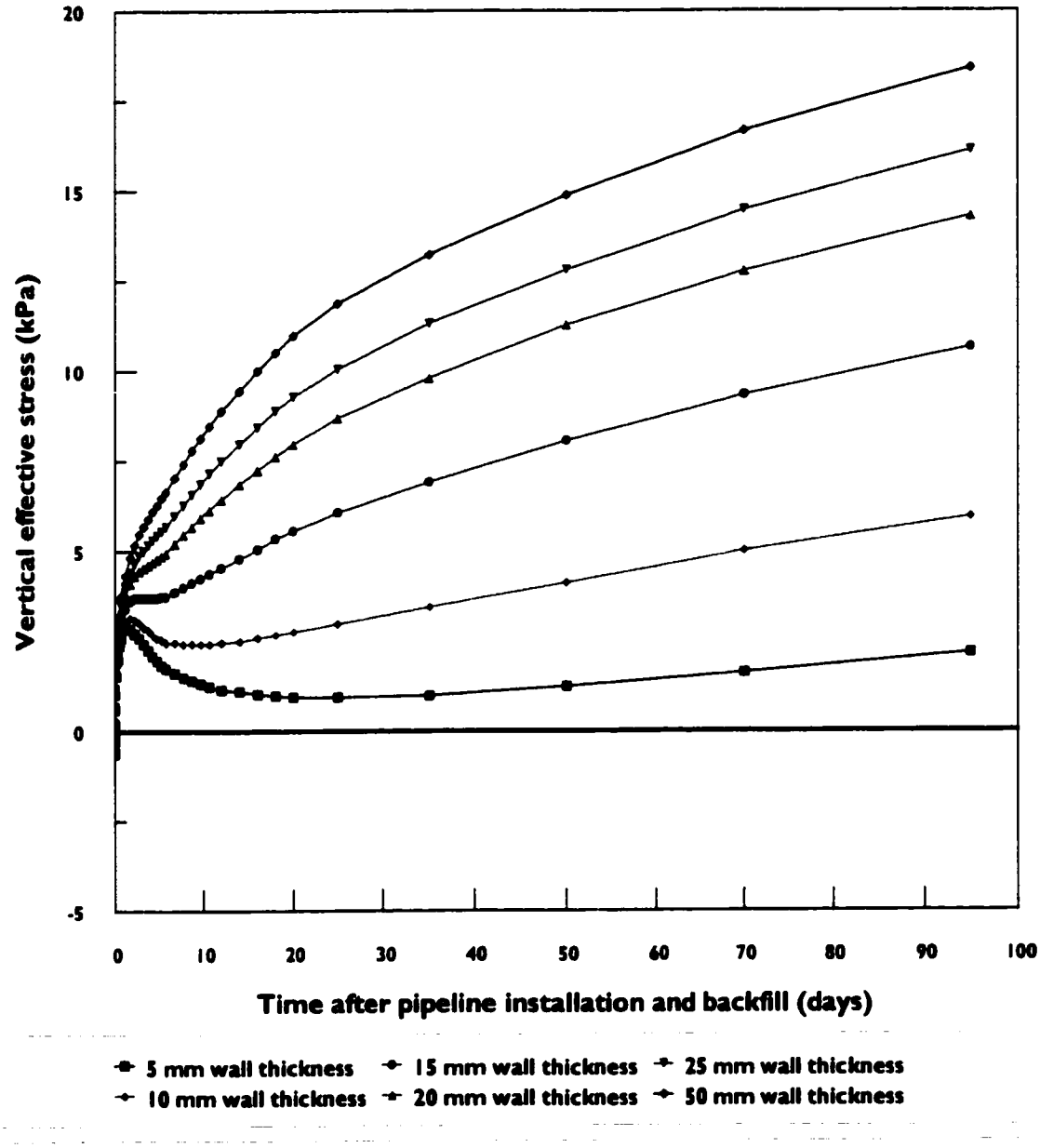

Figure 7-2: Vertical effective stress at the pipeline base

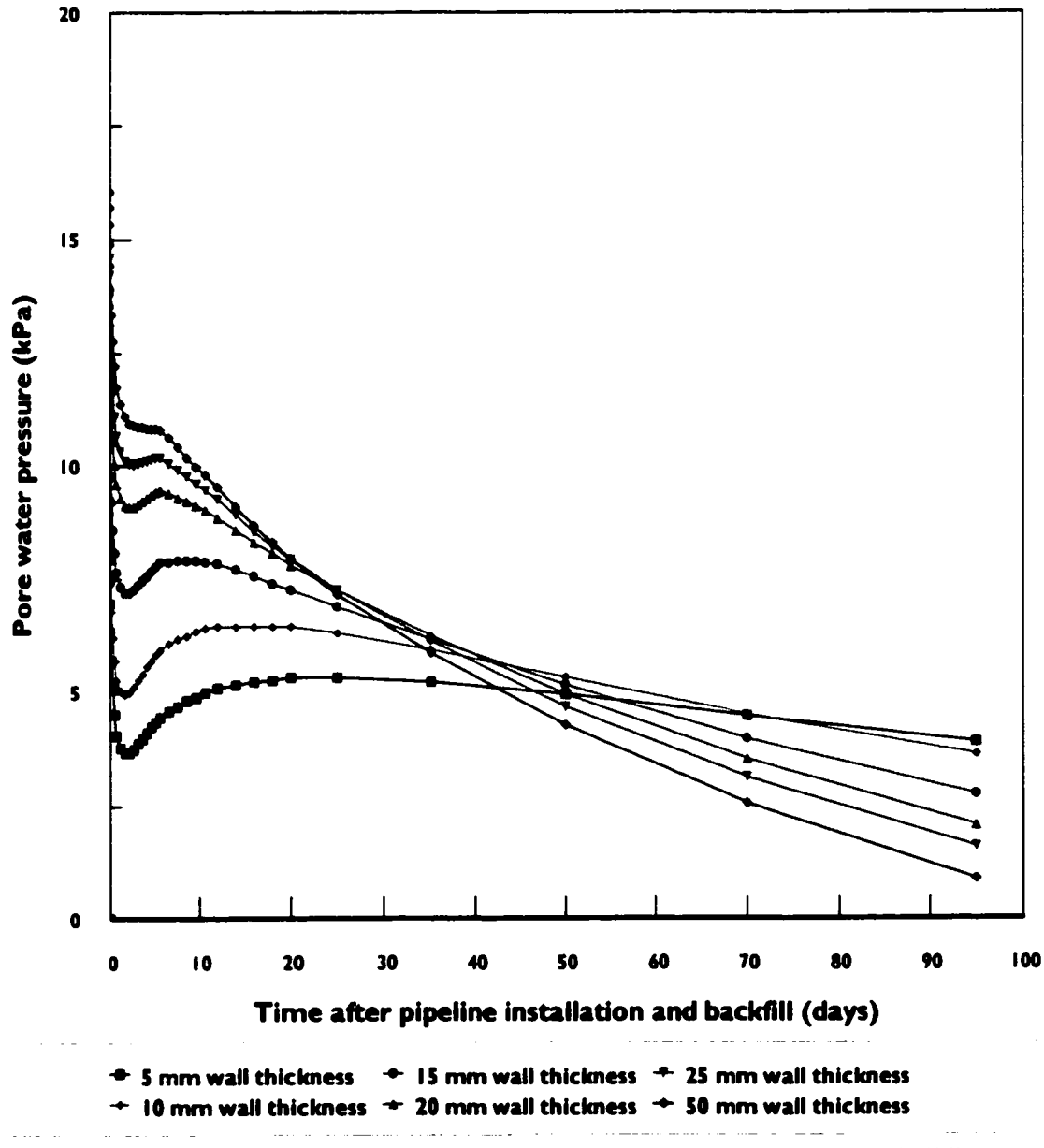

Figure 7-3: Pore water pressure at the pipeline base

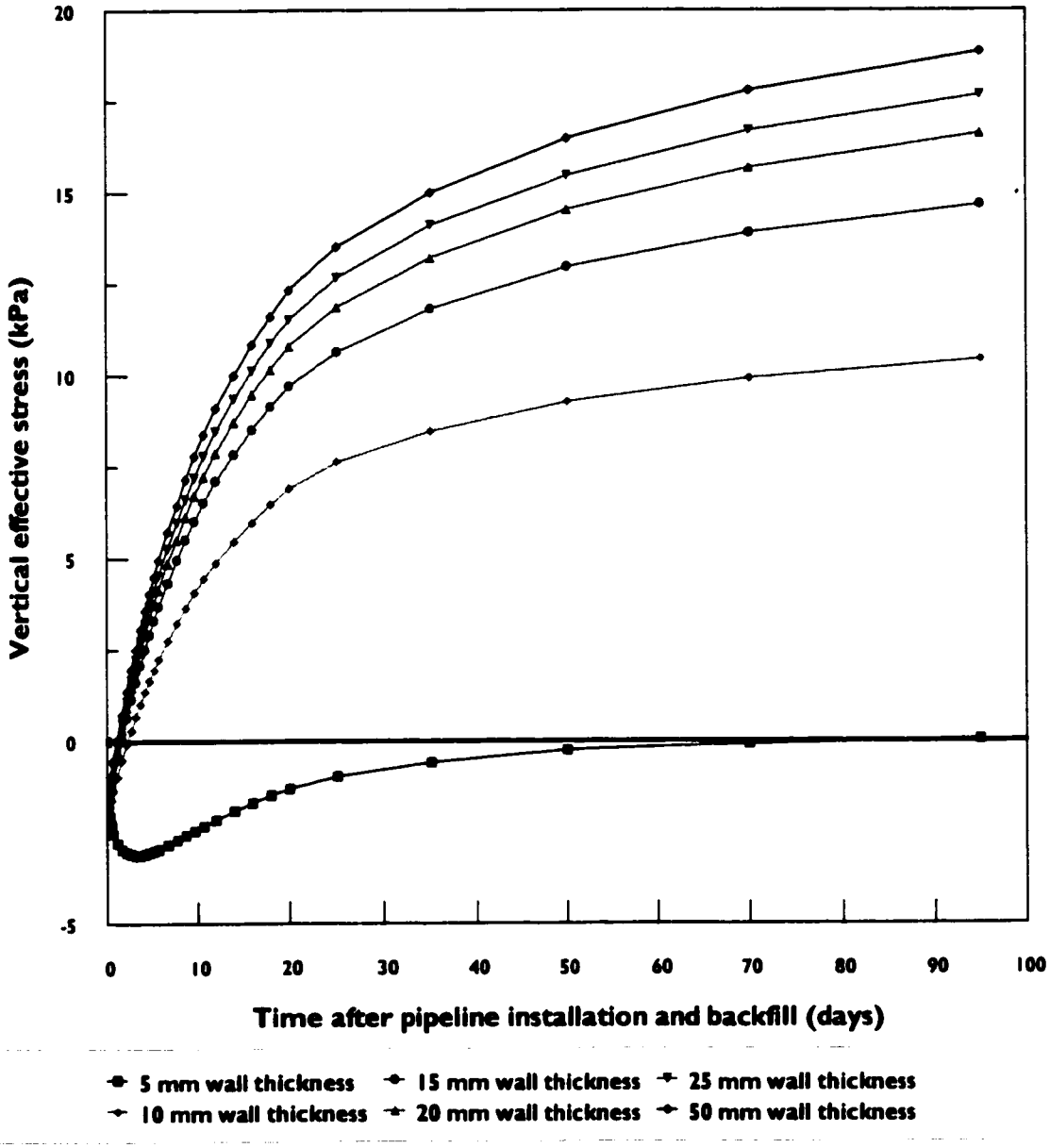

Figure 7-4: Vertical effective stress at the pipeline crown

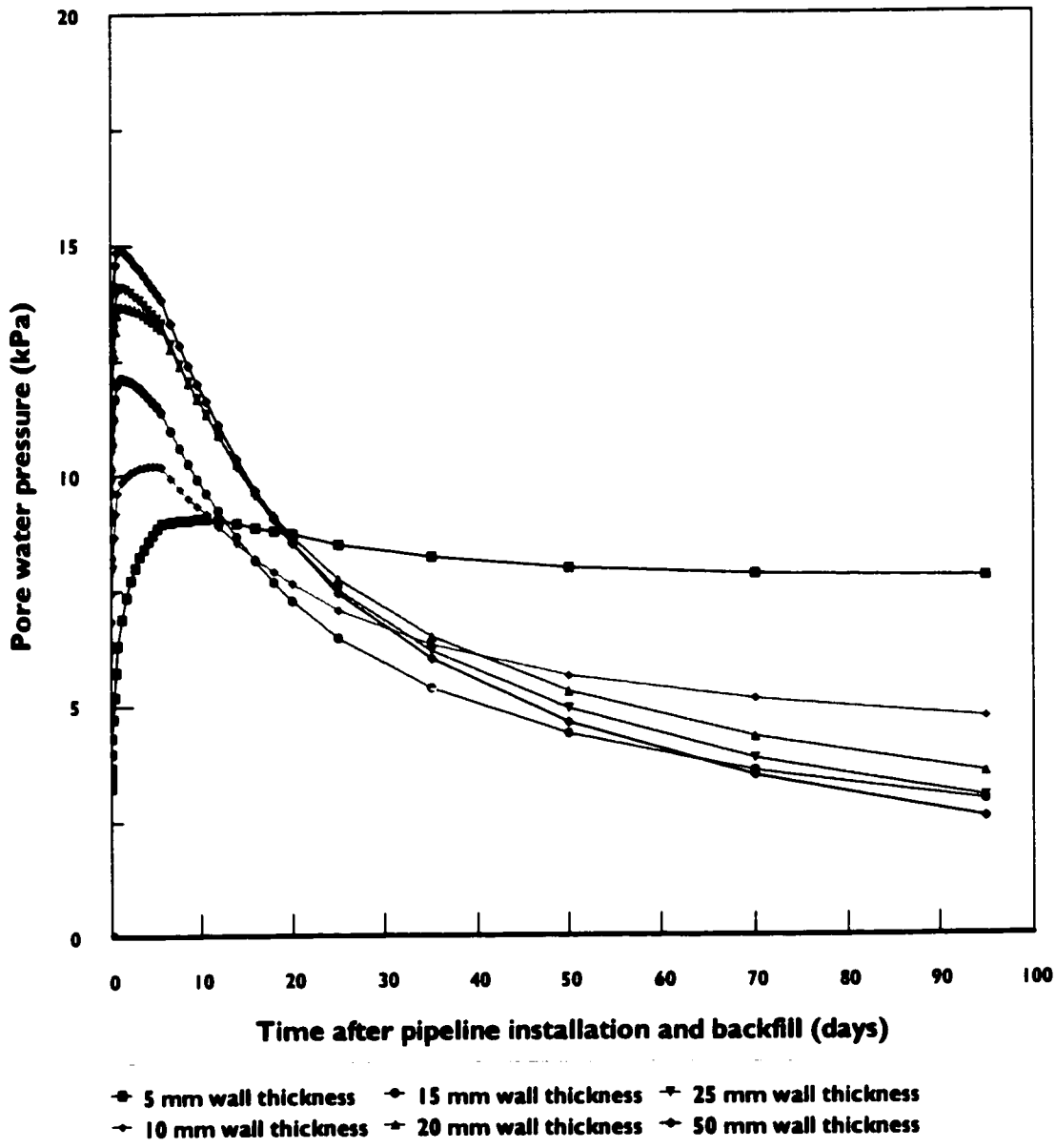

Figure 7-5: Pore water pressure at the pipeline crown

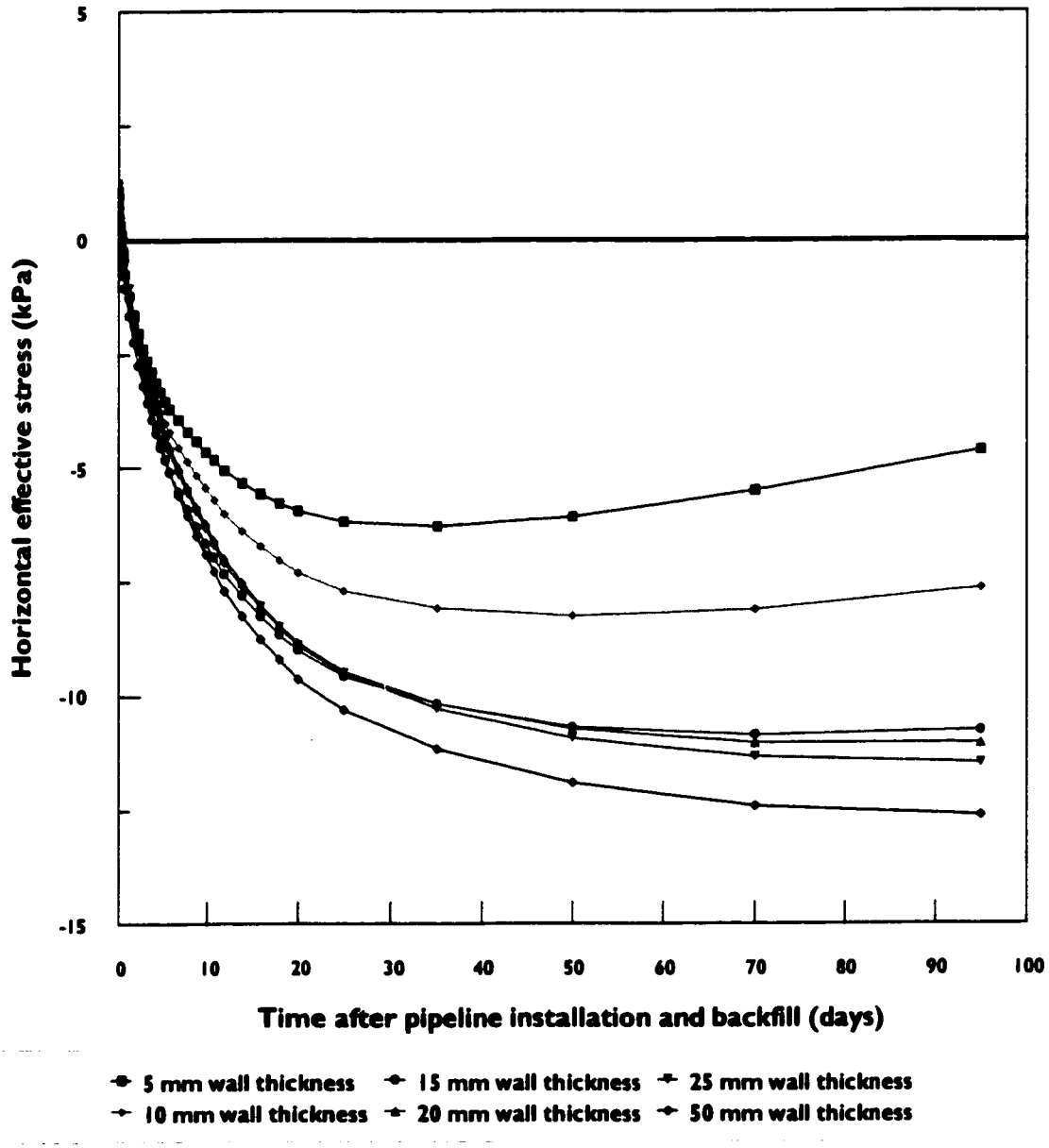

Figure 7-6: Horizontal effective stress at the lateral pipe springline

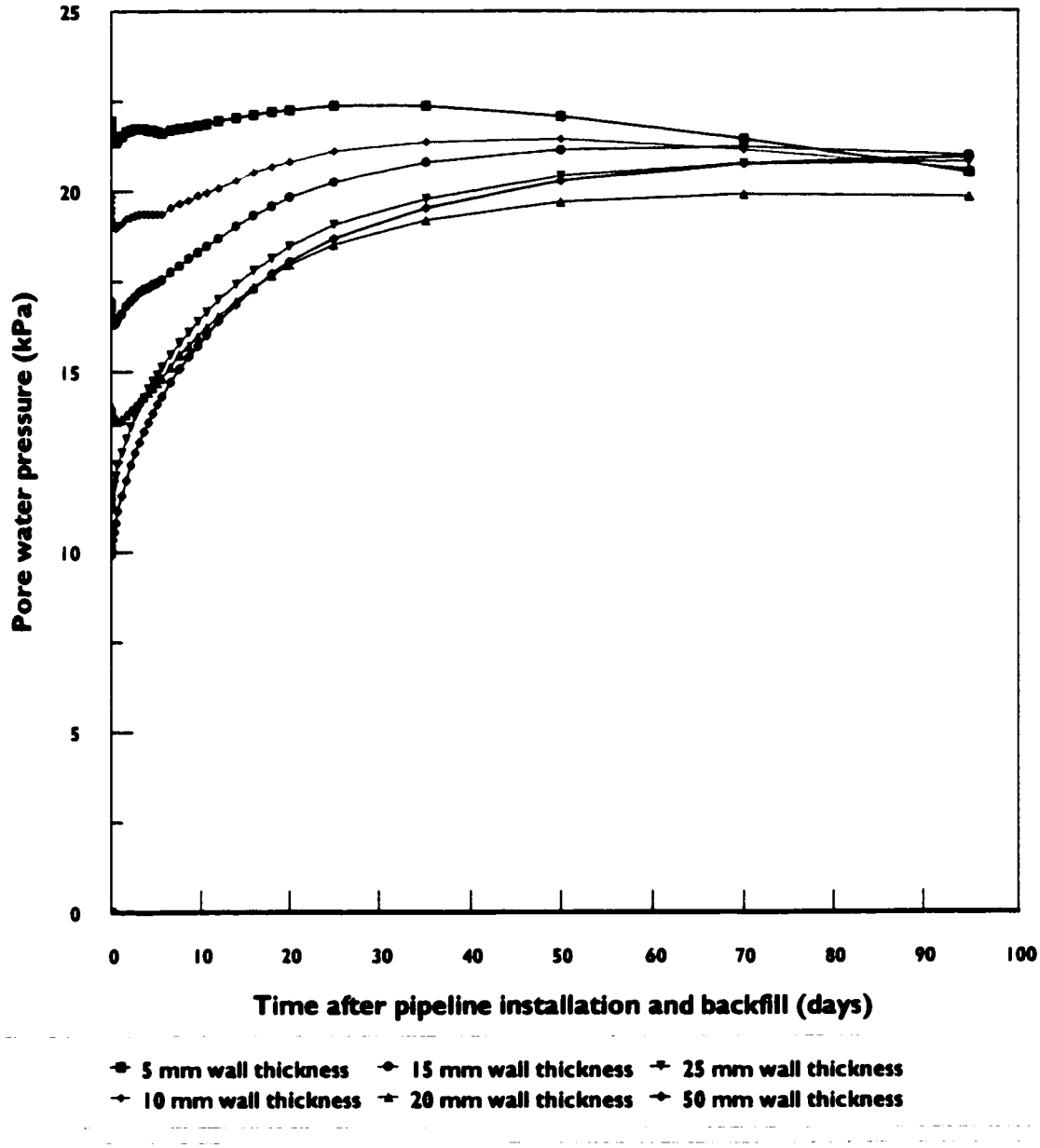

Figure 7-7: Pore water pressure at the lateral pipe springline

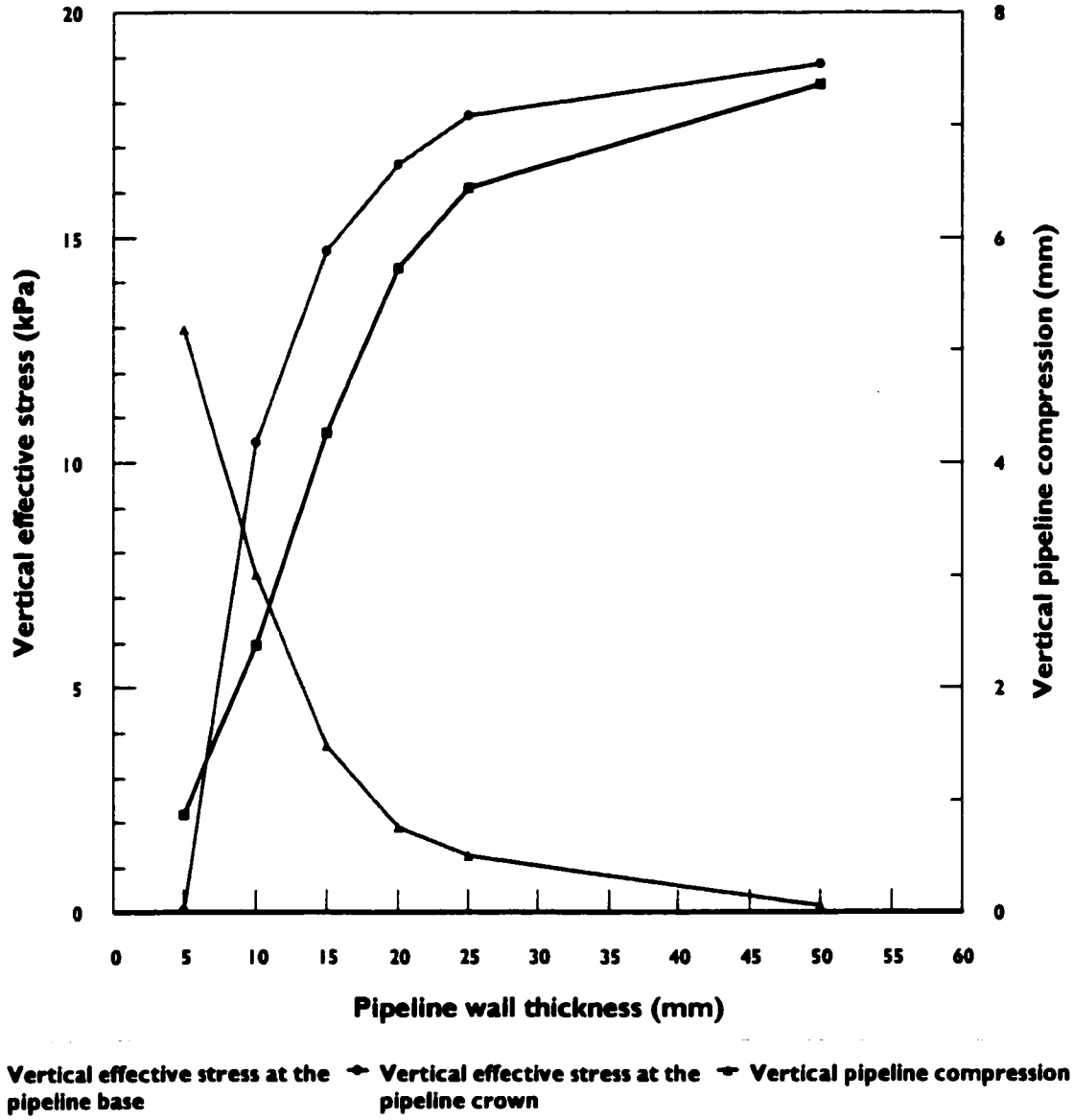

Figure 7-8: Effect of pipeline wall thickness (Vertical effective stress and pipeline compression)

CHAPTER 8

CONCLUSIONS AND RECOMMENDATIONS FOR FURTHER RESEARCH

CHAPTER 8

CONCLUSIONS AND RECOMMENDATIONS FOR FURTHER RESEARCH

8.1. CONCLUSIONS

In general, this research showed the capability of numerical analyses in simulating long term effects of construction activities and its adaptation to the various conditions that may be encountered in pipeline construction. The study also demonstrated the use of finite element analysis in establishing simple design guidelines based on complex soil/pipeline interaction and time dependant behavior.

The main objective of this research was to develop a better understanding of the mechanics involved in soil/pipeline interaction in overconsolidated soils with low hydraulic conductivity. The delayed effect of trench excavation in overconsolidated clay soils and the effects of sloping ground, backfill compaction, and pipeline stiffness were modeled. The results indicate that the reaction of the soil mass to the trench excavation continued for as long as four years after backfilling.

The investigation revealed that a trench excavation would trigger a release (unloading) of locked-in K_o lateral stresses. The unloading process in the vicinity of the trench walls is almost immediate; however, a delayed reaction from the unloading of the soil mass further away from the trench could continue for years, even if the trench is immediately backfilled. The prolonged unloading of the soil mass creates a lateral thrust on the backfill material. This thrust peaks in the upper half of the trench which causes a squeezing force in the backfill, acting downward on the pipeline. This squeezing effect creates a continuous generation of pore water pressure which counteracts the natural dissipation with time causing an apparent delay in pore water pressure dissipation.

This investigation also showed that in a v-shaped depression, the lateral unloading due to the excavation of the trench does not directly affect the soil mass above the trough level. This soil mass in the side slopes acts as a damper by absorbing the deformation energy of the underlying

soil subjected to lateral unloading. This is manifested by smaller lateral displacement of soil into the trench and faster pore water pressure dissipation in the backfill, associated with higher ground slopes. As a result, a higher total stress acts at the base and crown of the pipeline with level ground and smaller ground slopes causing more deformation in the pipeline section than with steep ground slopes. A higher effective stress is computed at the base and crown of the pipeline with sloping ground due to slower pore water pressure dissipation.

A surcharge-type compaction for a reasonable duration is found to reduce damaging stresses at the base and crown of the pipeline, during and after surcharge loading. This is particularly important when the integrity of the pipeline cross-section is of concern. The size and duration of the surcharge for different pipeline layouts and soil conditions can be optimized through further parametric studies. This implies that a somewhat higher embankment over the filled trench, in this case, may not result in more damaging stresses on the pipeline than a simple filling of the trench. Somewhat higher lateral stresses against the trench wall caused by a surcharge over the backfill would help counteract the effect of delayed K_o unloading.

Another important conclusion from the analyses is that a less rigid pipeline section would carry less of the weight of overlying fill material and will cause more of the load to be carried by the fill material on either side of the pipeline. This results in higher lateral pressure on the pipeline section and slower dissipation of pore water pressure around the pipeline.

8.2. RECOMMENDATIONS FOR FURTHER RESEARCH

Although this study investigated the effect of several variables on soil/pipeline interaction, it still considered one type of soil and backfill material, one level of overconsolidation, and other fixed parameters such as the shape of the pipeline section and the trench layout.

The study provides a qualitative understanding of the soil/pipeline interaction and lays tracks for many potential studies to establish design guidelines which are free from excessive simplifications and assumptions. One potential subject for further investigation is a similar study for a range of soils, including granular soils and clays with different sensitivity. With sufficient parametric studies conducted in the same manner, comprehensive design guidelines can be established, which consider realistic field parameters and long term conditions.

REFERENCES

REFERENCES

Cowherd, D. C., and I. J. Corda, 1994. Lessons Learned from Culvert Failures and Nonfailures. Transportation Research record 1431, TRB, National Research Council, Washington, D.C., pp. 13-21.

Crawford, James R, 1998. M.A.Sc. Thesis, Backfill Pressures Within a Reinstated Trench, University of Ottawa, Ottawa, ON.

Duncan, J.M., Byrne, Peter, and Wong, Kai S, 1978. Strength, stress-strain and bulk modulus parameters for finite element analyses of stress and movement in soil masses. Rport No. UCB/GT/78-02, College of Engineering, Office of the Research Services, University of California, Berkeley, California.

Heger, F. J., and E. T. Selig, 1994. Rigid Pipe Distress in High Embankments over Soft Soil Strata. Transportation Research record 1431, TRB, National Research Council, Washington, D.C., pp. 46-52.

Hill, J. J., and F.J. Laumann, 1994. Overstressed Precast Concrete Pipe Arch and Its Redesign. Transportation Research record 1431, TRB, National Research Council, Washington, D.C., pp. 41-45.

Kay, J. N., S. J. Hain, and C. S. Chang, 1982. Design Method for Concrete Pipe Under High Fills. Transportation Research record 878, TRB, National Research Council, Washington, D.C., pp. 29-33.

Leonards, G. A., and C. H. Juang, 1985. Predicting Performance of Buried Metal Pipe Arches. Transportation Research record 1008, TRB, National Research Council, Washington, D.C., pp. 53-57.

Leonards, G. A., C. H. Juang, T. H. Wu, and R. E. Stetkar, 1985. Predicting Performance of Buried Metal Conduits. Transportation Research record 1008, TRB, National Research Council, Washington, D.C., pp. 42-52.

McGrath, T. J., and E.T. Selig, 1994. Backfill Placement Methods Lead to Flexible Pipe Distortion. Transportation Research record 1431, TRB, National Research Council, Washington, D.C., pp. 27-32.

Moser, A. P., R. R. Bishop, O. K. Shupe, and D. R. Bair, 1985. Deflection and Strains in Buried FRP Pipes Subjected to Various Installation Conditions. Transportation Research record 1008, TRB, National Research Council, Washington, D.C., pp. 109-116.

Paulin, Michael J., Phillips, Ryan, and Boivin, Raymond, 1995. Centrifuge Modelling of Lateral Pipeline/Soil Interaction. *In* Proceedings of the 14th International Conference on Offshore Mechanics and Arctic Engineering, ASME, Copenhagen, Denmark, June 18-22, pp.107-123

Paulin, Michael J., Phillips, Ryan, and Boivin, Raymond, 1996. An Experimental Investigation Into Lateral Pipeline/Soil Interaction. *In* Proceedings of the 15th International Conference on Offshore Mechanics and Arctic Engineering, ASME, Florence, Italy, pp.313-323

Paulin, Michael J., 1998. Ph. D Thesis, an investigation into pipelines subjected to lateral soil loading, Memorial University of Newfoundland, St. John's, Newfoundland.

Poorooshasb, F., M. J. Paulin, M. Rizkalla, and J.I. Clark, 1994. Centrifuge Modeling of Laterally Loaded Pipelines. Transportation Research record 1431, TRB, National Research Council, Washington, D.C., pp. 33-40.

Quigley, Donald W., and Duncan, J.M., 1978. Earth pressures on conduits and retaining walls. Rport No. UCB/GT/78-06, College of Engineering, University of California, Berkeley, California.

Rude, L. C., 1983. Computer Modeling of the Cross Canyon Culvert. Transportation Research record 903, TRB, National Research Council, Washington, D.C., pp. 109-114.

Seed, R. B., and J. R. Raines, 1988. Failure of Flexible Long-Span Culverts Under Exceptional Live Loads. Transportation Research record 1191, TRB, National Research Council, Washington, D.C., pp. 22-29.

Selig, E. T., and T. J. McGrath, 1994. Pipe Failure Caused by Improper Groundwater Control. Transportation Research record 1431, TRB, National Research Council, Washington, D.C., pp. 22-26.

Selig, E. T., M. C. McVay, and C. S. Chang, 1982. Finite-Element Modeling of Buried Concrete Pipe Installations. Transportation Research record 878, TRB, National Research Council, Washington, D.C., pp. 17-23.

Sharp, K. D., L. R. Anderson, A. P. Moser, and R. R. Bishop, 1985. Finite Element Analysis applied to the Response of Buried FRP Pipe Under Various Installation Conditions. Transportation Research record 1008, TRB, National Research Council, Washington, D.C., pp. 63-72.

SIGMA/W software manual, 1997. Geo-Slope International, 1400 Ford Tower, 633-6th Ave SW, Calgary, Alberta, Canada.

Som, Nithindra Nath, 1968. Ph. D Thesis on the effect of stress path on the deformation and consolidation of London Clay, University of London (Imperial Colledge of Science and Technology).

Spangler, M.G., 1962. Culverts and Conduits in Foundation Engineering. Edited By G.A. Leonards, McGraw-Hill Book Co., Inc., New York, pp. 965-999.

Tadros, M. K., J. V. Benak, A. M. Abdel-Karim, and K.A. Bexten, 1989. Field Testing of a Concrete Box culvert. Transportation Research record 1231, TRB, National Research Council, Washington, D.C., pp. 49-55.

Watkins, R. K., R. C. Reeve, and J. B. Goddard, 1983. Effect of Heavy Loads on Buried Corrugated Polyethylene Pipe. Transportation Research record 903, TRB, National Research Council, Washington, D.C., pp. 99-108.